Flow Properties of Moine Thrust Zone Mylonites in Northern Assynt, NW Scotland

Benjamin Louis Roth

Thesis submitted to the faculty of the Virginia Polytechnic Institute and State University in partial fulfillment of the requirements for the degree of

Master of Science
In
Geosciences

Committee:
Richard D. Law
James A. Spotila
Robert J. Tracy

December 7, 2010
Blacksburg, VA

Keywords: Moine Thrust Zone, mylonites, strain, vorticity, piezometry

Flow Properties of Moine Thrust Zone Mylonites in Northern Assynt, NW Scotland

Benjamin L Roth

Abstract

Quartz-rich mylonites present along the Moine Thrust Zone are well suited for the application of various analytical techniques designed for investigating the flow processes by which rock deformation occurred. These analytical techniques were applied to a suite of samples from the footwall and hangingwall of the Moine thrust exposed along the Allt Pol a' Mhadaich stream located in the northern part of the Assynt window. Vorticity analyses were performed to determine the relative contributions of pure and simple shear deformation within the penetratively deforming thrust sheets. Integration of vorticity data with 3D strain analyses demonstrated that sub-vertical shortening perpendicular to the flow plane, accompanied by thrust transport parallel extension, occurred during mylonitization, and was driven by emplacement of the overlying Moine nappe. Quartz c-axis fabrics in the mylonites are characterized by well-defined asymmetric Type-1 cross girdles in which internal and external skeletal asymmetries are indicative of a top-to-the-WNW shear sense, compatible with regional thrusting. These c-axis fabrics were also used to estimate deformation temperatures. Differential flow stresses associated with mylonitization were estimated from the grain size of dynamically recrystallized quartz. Deformation temperature and flow stress data were then incorporated into a dislocation creep flow law for quartz to estimate strain rates. Finally, along strike variation in these flow properties at the base of the Moine nappe to the north and south of the APM section were investigated and results from the APM section compared with previously published studies of mylonites exposed in eastern Assynt that occupy similar structural positions.

This thesis is dedicated to my parents,

Ronald and Veronica Roth

and to the individuals who brought me in to this world.

ACKNOWLEDGEMENTS

On September 1, 1985, I was born to a 14 year old mother and 16 year old father. We have never met, outside of those first few hours of my life spent in the hospital, and little information is known about who they are. I can only imagine the hardships that they endured, and the difficult decisions that were faced prior to my being born. After birth, I was immediately put up for adoption, where I was fortunate to not have a long wait. In December 1985, I was welcomed to the home of Ron and Ronnie Roth as their son.

I would like to thank my parents first and foremost. It is because of them that I am where I am at right now. Through their love and devotion, they raised me to be the best person I can be, and have given me all of the tools to be successful in my personal life. They believed in me, and supported me in all aspects of life and growing up, and for this I am eternally grateful. I love you both, and thank you for every opportunity you have given me.

I also wish to thank my advisor, Rick Law, for taking me on as a Masters student. I am forever indebted to him for the knowledge and opportunities he has given me. He has been nothing less than a true mentor and colleague. Our Friday night therapy sessions with him and his wife Clare at the Underground in Blacksburg were pivotal in keeping my mental state on an even keel through the progression of the project. I consider Rick and Clare to be very close friends and wish them nothing but the best in the future. In every aspect of my life, I will always remember that, "standards must be maintained."

My good friend and colleague, Ryan Thigpen, took me under his wing at the beginning of my project and even though was in the midst of finishing his PhD, always had time to answer a question, share a beer, and most importantly remind me of the pecking order in the office. He was, and still is, a great mentor and some one I will continue to look up to in the future. To say that I'm a better person because of him might be a bit of a stretch, but he and his wife Summer are some of my dearest friends and I am truly honored to be a part of the team.

Among all of my friends, Jim Schiffbauer has probably bore the greatest burden of friendship. Our relationship started while he was the T.A. for the undergraduate course I was taking at Virginia Tech, and was only strengthened when walking in to class one morning, we realized that we both drove Jeep Wranglers. Some might say it was love at first sight, fate, or just two dudes at the right place at the right time. Regardless of how it started, he has been there for the best and worst times and always helped me through. I look forward to sharing many more laughs, burritos, and Coors Lights in the future. Thanks for everything Jim.

Finally, I would like to thank the rest of my friends – Ashley Holmes, Matt Nash, The Phil Mothena, Don Stahr, Troy Dexter, John Wyatt, Matt Francsis and everyone else who has been there to share a laugh or a beer. You have all played a serious role in keeping my mental state intact and your friendships are extremely valued.

List of Figures

List of Tables

Chapter 1: Introduction

The primary focus of the research presented in this thesis is the examination of deformation microstructures in mylonites exposed in the Assynt District of the Moine thrust zone, NW Scotland. These mylonites are located in the uppermost part of the Glencoul thrust sheet, and are cut by the Aisninin imbricate fault system that roofs in to the overlying Moine thrust. Flow associated with development of these mylonites occurred as a result of ductile thrusting at the base of the Moine nappe during the late Scandian phase of Caledonian mountain building at c. 430 Ma.. The following chapters describe a laboratory-based study in which a range of analytical techniques were integrated to quantify the flow parameters associated with generation of these mylonites.

Chapter 2 "*Geologic background"* and Chapter 3 *"Deformation microstructures"* serve as a general introduction to the geology of this section of the Moine Thrust Zone, and the deformation mechanisms responsible for mylonite generation. The Allt Pol a' Mhadaich (APM) stream has exposed an approximately 100m deep section into the Aisinnin imbricates in the footwall of the Moine thrust. A total of 15 oriented samples were collected along this section of Lewisian gneiss, Cambrian Basal Quartzite and Pipe Rock, while two samples of Moine schist were collected from the base of the overlying Moine nappe. A series of microstructural analyses, based on the presence of relic detrital quartz grains, recrystallized quartz grains and rigid clasts of feldspar and epidote were completed and are described in the following chapters.

In Chapter 4 *"3D strain analysis, quartz crystal fabrics, and their implications for deformation history"* detrital grains imaged in thin sections cut from the Cambrian Basal Quartzite and Pipe Rock were used as strain markers and analyzed using the Rf/Phi technique. 2D strain data collected on mutually perpendicular thin sections were combined to estimate 3D strains. The resulting strain data indicate that plastic deformation associated with mylonitization occured within the general flattening field, near to plane strain conditions. Quartz c-axis fabrics measured optically on detrital grains are all characterized by asymmetric Type-1 skeletons on which both internal and external fabric parameters indicate a top-to-the-WNW

shear sense, in agreement with the sense of over-thrusting indicate by thrust geometries. These c-axis fabrics are have been used for determining deformation temperatures and are also used as input data for several methods of vorticity analysis outlined in Chapter 5.

In Chapter 5, *"Vorticity of flow, vertical thinning, and transport parallel extension"* data for quantifying flow vorticities associated with mylonitization in the APM stream section samples are reported. These vorticity values provide an estimate of the relative contributions of pure versus simple shear during mylonitization. Results of the vorticity analyses are then used in conjunction with 3D strain data (Chapter 4) to estimate the amounts of shortening (perpendicular to the inferred flow plane) as well as transport parallel extension associated with penetrative deformation of the Cambrian quartzites.

In Chapter 6, *"Quartz piezometry and strain rates"* variation in dynamically recrystallized grain size with structural position is investigated in the APM samples using the linear intercept method. These quartz grain size data were then used to estimate flow stresses (differential stress) associated with mylonitization using two piezometers, as well as examining the validity of using 2D (raw) versus 3D (corrected) grain size data in estimating flow stresses using the different piezometers. By incorporating estimated deformation temperatures (Chapter 4) and flow stresses into a dislocation creep flow law, strain rates associated with mylonitization were then calculated using a wide range of experimentally derived flow parameters.

In Chapter 7 *"Comparison with the Stack of Glencoul and analyses along strike"* flow data obtained in Chapters 4-6 from the APM stream section samples were compared with previously published data from mylonites located along strike at the Stack of Glencoul that occupy a slightly higher structural position in the local series of mylonitic thrust sheets. These two locations displayed a marked difference in microstructural styles and associated flow parameters. Flow vorticities and stresses at the base of the overlying Moine nappe were also estimated using a suite of samples collected along strike from 6 km to the north of the APM stream section, southwards through the APM section to the Stack of Glencoul. Finally, the various

flow parameter data derived in Chapters 3-7 are integrated in to a structural model for evolution of the mylonitic thrust sheets.

Chapter 2: Geologic background

Abstract

The Allt Pol a'Mhadaich stream has exposed approximately 100m of Cambrian quartzite in the footwall of the Moine thrust. The Basal Quartzite and Pipe Rock members of the Eriboll Formation are well exposed and structurally overly the unconformable contact with the sheared Lewisian basement gneiss at the base of this section. The contact of the Moine thrust plane is subject to interpretation (Geological Survey 1923, BGS 2007) due to the presence of an unexposed sheet of mylonites of probable Moine protolith. Dense sampling of this section indicates that the foliation is dipping to the ESE, with observed lineations also trending to the ESE, which corresponds with the regional WNW movement along the Moine thrust.

Introduction

The geologic framework of NW Scotland is composed of two fundamental tectonic units, the Hebridean and Northern Highlands terrrains, that were juxtaposed during the Grampian and Scandian phases (475-460 and 435-425 Ma, respectively) of the Caledonian Orogeny (see reviews by Park et al. 2002; Strachan et al. 2002). The Grampian event was produced by collision between an island arc and the margin of Laurentia (Hebridean Terrain), resulting in obduction of ophiolites and regional metamorphism (Dewey & Shackleton, 1984). Direct evidence for Grampian age deformation and metamorphism in the extreme NW edge of the Northern Highlands terrrain is limited. Development of major ductile thrusts in the Caledonian orogenic wedge in the Northern Highlands, located to the ESE of the Hebridean Terrain, is believed to have been a dominantly Scandian event produced by collision between what is now NW Scotland (Northern Highland Terrain) and the Laurentian margin and Baltica (Coward, 1990; Dewey & Mange, 1999; Dewey & Strachan, 2003).

The Moine thrust zone forms the NW margin of the Caledonian orogenic belt on mainland Scotland (Peach et al. 1907). The foreland to the thrust zone (Hebridean terrane) is composed of Lewisian basement rocks (Archaean to Palaeo-proterozoic crystalline gneiss), unconformably overlain by Torridonian (Neoproterozoic) sandstones in the west and Cambrian-Ordovician shelf sedimentary rocks to the east. The Torridonian sandstones are thought to have

been deposited in rift valleys within the heart of Rodinia, near the Grenville orogenic belt. The Cambrian-Ordovician sediments are made up, in ascending order, of the Eriboll Formation (Basal Quartzite, Pipe-Rock), An-t-Sron Formation (shale, siltstone, and sandstone), and Durness Limestone. This succession formed as a Laurentian passive margin shelf sequence bordering the Iapetus Ocean (Park et al, 2002 and references therein).

The Northern Highland terrane is bounded to the NW by the Moine thrust zone and to the SE by the Great Glen fault, and is dominated by the Moine Supergroup which is characterized by variably metamorphosed psammites, semipelites, and pelites (see reviews by Strachan et al. 2002, 2010). The Moine sediments are thought to have developed through erosion of the *c.* 1.1-1.0 Ga Grenville orogenic belt associated with assembly of the supercontinent Rodinia (Dalziel & Soper 2001). These Neoproterozoic metasedimentary rocks were thrust over the Hebridean terrane during closure of the Iapetus Ocean when three crustal blocks converged: Laurentia, Baltica, and Avalonia (Soper & Hutton 1984; Pickering et al. 1988; Soper et al. 1992).

Study area - historical background

The main focus area for this study is a vertical transect through mylonitic Cambrian quartzites located in the footwall to the Moine thrust. The transect is located at the northern end of the Assynt half window through the Moine thrust zone (Fig. 2.1) and is structurally located within the upper part of the Glencoul thrust sheet (GTS), at the top of the thrust zone, and lies beneath Moine metasedimentary rocks of the overlying Moine nappe. The transect is well exposed in the Allt Pol a' Mhadaich (APM) stream section located approximately 650m to the southwest of Loch Strath nan Aisinnin (fig. 2.1). The GTS dominates the northern part of the Assynt window, taking its name from the type locality at Loch Glencoul (Peach et al. 1888; 1907; Geological Survey 1923 - Special Assynt Sheet). The GTS in northern Assynt is composed of a basal sheet of Lewisian basement gneisses overlain by Cambro-Ordovician sedimentary rocks (Geological Survey 1923, Butler 1984, 1988, 2004). The APM stream section has cut through the footwall of the Moine thrust (NC 31500,

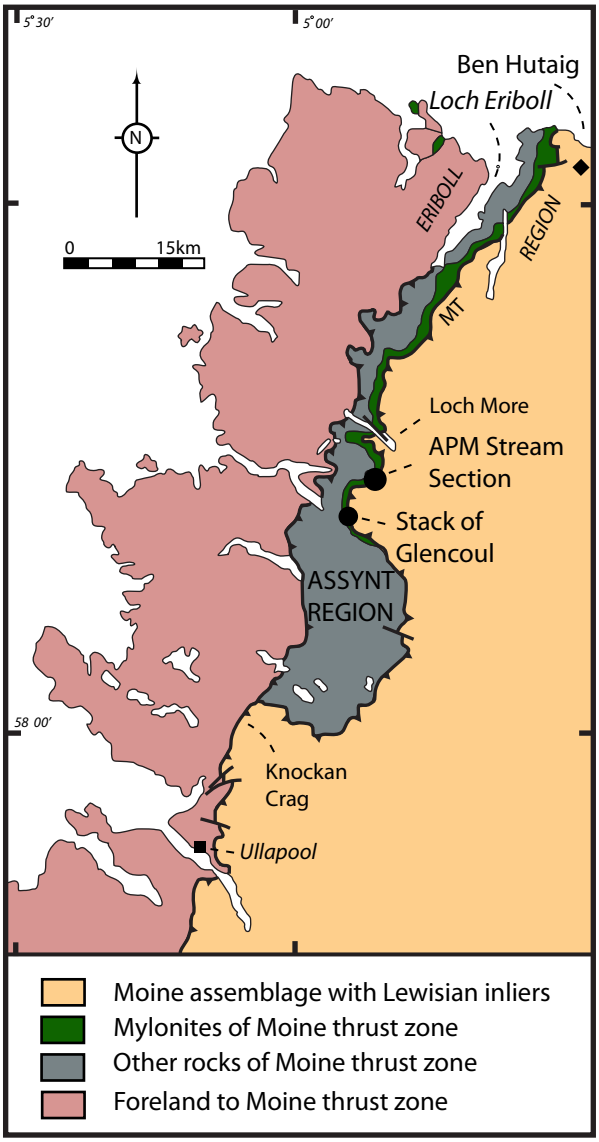

Figure 2.1 Simplified geologic map of northwest Scotland showing position of the Moine thrust zone extending from the north coast southwards to Ullapool and Loch Broom. Position of the Allt Pol a' Mhadaich (APM) stream section in the northern part of the Assynt Region is indicated.

32450) exposing these Cambro-Ordovician quartzites down to their contact with the Lewisian gneiss at the base of the stream section (NC 31536, 32433).

Original mapping of this area by C.T. Clough, H.M. Cadell and C.H. Dinham in 1886 and 1913 (Geological Survey of Great Britain; unpublished 6 inch to the mile clean copy sheet - Sutherland LI) shows the APM stream section running SSE to NNW from a gently dipping band of mylonite (μ) of probable Moine protolith that separates overlying Moine metasedimentary rocks (to the SE) from Cambrian sedimentary rocks (to the NW), and cutting progressively down in to underlying Pipe Rock and then Basal (*False Bedded*) Quartzite of the Cambrian succession, and finally into Lewisian gneiss underlying the Basal Quartzite. The Cambrian quartzite and Lewisian gneiss exposed in the APM stream section belong structurally to the "Aisinnan Imbricates" recognized by the Geological Survey in the upper part of the Glencoul thrust sheet (Peach et al. 1888, 1907). The contact between Basal Quartzite and Lewisian gneiss was shown as an unconformity on the original Geological Survey maps (see also Peach et al. 1888, p. 416). Shearing of pipes (*Skolithos*) was indicated in the Pipe Rock by annotated notes on this 6 inch clean copy sheet (see also Peach et al. 1888, p. 433; Peach et al.

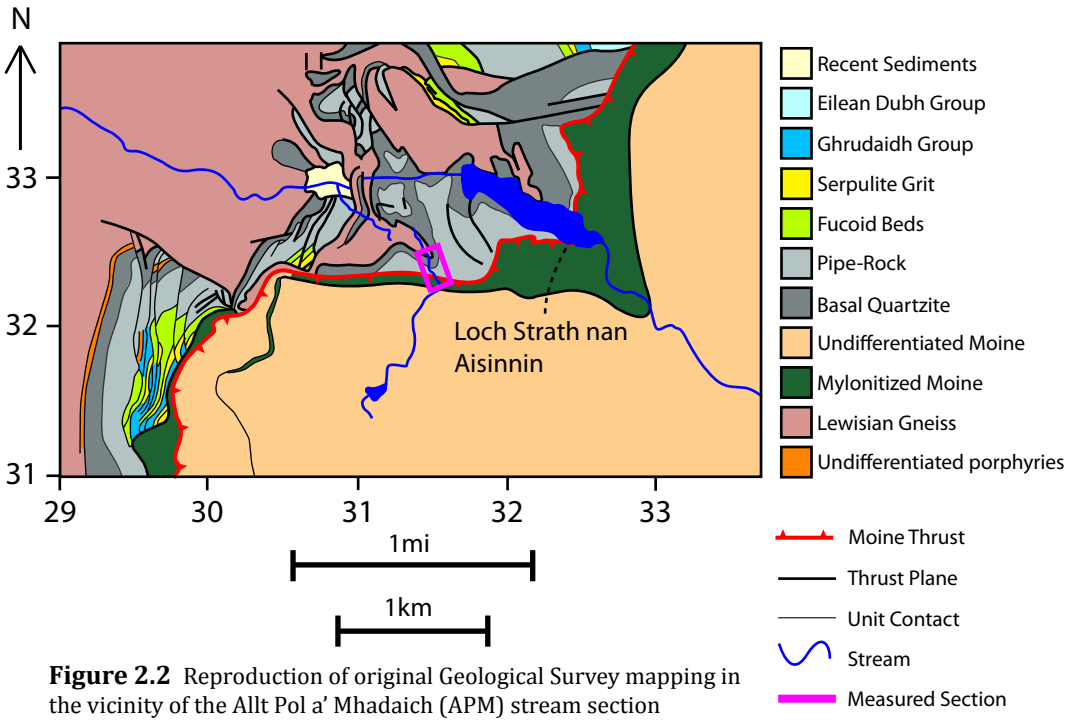

Figure 2.2 Reproduction of original Geological Survey mapping in the vicinity of the Allt Pol a' Mhadaich (APM) stream section (Geological Survey 1923, 1931). Dashed purple box shows position of the APM stream section. Position of Moine thrust (taken to be at base of mapped mylonite sheet) is indicated by red line; see text for discussion on positioning of Moine thrust.

1907, p. 499). This original interpretation of mapped structural relationships is followed on both the Geological Survey's first edition of the one inch to the mile Assynt Special Sheet (Geological Survey 1923) and the one inch to the mile Altnahara Sheet (Sheet 108, Geological Survey 1931), and is reproduced here in Figure 2.2.

The area between the Glencoul thrust and Loch More was remapped by Butler (1984) and later by the British Geological Survey in the early 2000s, with results being incorporated on to a new 1:50, 000 scale version of the Assynt Special Sheet (BGS 2007). A greater degree of structural complexity in the area around the APM stream section is indicated on the new Assynt Special Sheet with repetition of the Basal Quartzite - Pipe Rock succession by imbricate thrusting and a thrust being placed along the contact between the Basal Quartzite and underlying Lewisian gneiss. In addition, the sheet of mylonites (μ) of unspecified protolith separating Moine from Cambrian rocks on the original maps was subdivided in to map units of mylonite derived from Cambrian quartzite (μErs) and mylonitic gneiss (μOL)

probably derived from the Lewisian. Interestingly, this structural sub-unit of mylonitic Lewisian was shown outcropping around the eastern part of Loch Strath nan Aisinnan on the original 1886 clean copy survey sheets, but was not explicitly separated from mylonites of other possible protolith in the subsequent one inch to the mile sheets, (Geological Survey 1923, 1931). The BGS (2007) reinterpretation of the area surrounding the APM stream section is shown in Figure 2.3. On the original BGS maps the position of the Moine thrust plane is placed at the base of this sheet of mylonites (see also discussion by Law and Johnson 2010, p. 474). In contrast, on the new Assynt Special Sheet (BGS 2007) the Moine thrust is placed at the top of the mylonite sheet. In this new BGS interpretation, the base of the mylonite sheet would correspond to an un-named thrust. This un-named thrust may mark the lateral equivalent of the Lochan Riabhach thrust recognized by Holdsworth et al. (2006, 2009) in the Eriboll region to the north (see also discussion by Thigpen et al.

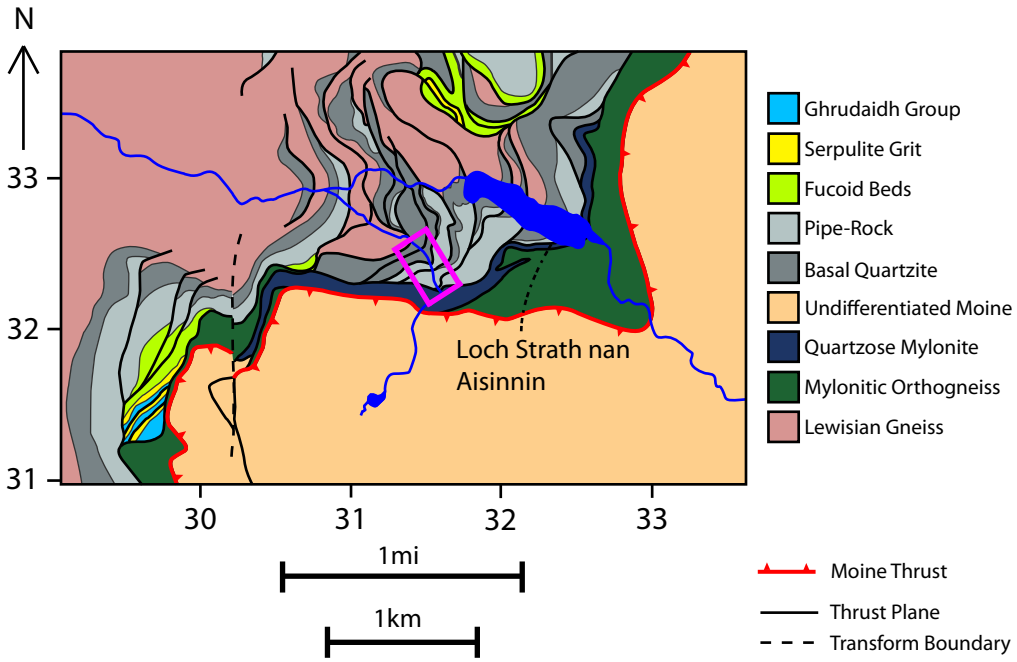

Figure 2.3 Reproduction of revised Geological Survey mapping in the vicinity of the Allt Pol a' Mhadaich (APM) stream section as shown on the 2007 Assynt Special Sheet (BGS 2007). Purple box shows position of the APM stream section. Position of Moine thrust (taken to be at the top of the mapped mylonite sheet) is indicated by red line; see text for discussion on positioning of Moine thrust. Note: the mylonite separating Cambrian quartzites from overlying Moine rocks is divided in to units derived from Lewisian gneiss and Cambrian quartzite.

2010b). Structural distances quoted in this thesis for the APM stream section (Table 2.1) are calculated with respect to the base of the mapped mylonite sheet.

Study area - details of measured section

A total of 15 samples of Lewisian gneiss, Cambrian quartzite and Moine metasedimentary rocks were collected from the APM stream section by R.D. Law and R. Thigpen in 2002 - 2007. Ordinance Survey grid coordinates and structural distances of samples above/below the Moine thrust (base of mapped mylonite sheet) are listed in Table 2.1 and field measurements are summarized in Figure 2.5. A NNW-SSE striking cross-section based on this fieldwork, and drawn along the length of the APM stream section, is shown in Figure 2.4., while field measurements of foliations and lineations are summarized in Table 2.1 and Figure 2.5. The position of this section, relative to the original and revised BGS maps is also shown in Figures 2.2 and 2.3, respectively. Note that this section is oblique to both the regional WNW thrust transport direction and to the dip direction of the quartzites; hence calculated apparent dips are shown. The section extends from the Lewisian gneiss up through the Cambrian quartzites in to the Moine metasedimentary rocks.

Sample	Ordinance Survey Coordinates	Distance from BGS (1923) MTP (m)	Foliation strike	Foliation Dip	Lineation plunge & trend
M.2	NC 31714 32103	+51.6	068	02 SE	0 to 110
M.1	NC 31500 32450	+44.4	064	24 SE	16 to 104
Q.1	NC 31500 32450	-7.6	097	34 S	0 to 100
Q.2	NC 31500 32450	-20.0	100	24 S	02 to 104
Q.3	NC 31500 32450	-27.1	090	20 S	15 to 104
Q.4	NC 31500 32450	-31.6	000	15 S	14 to 100
Q.5	NC 31500 32450	-34.2	000	24 S	24 to 090
Q.6	NC 31500 32450	-45.3	045	16 SE	12 to 090
Q.7	NC 31531 32410	-46.7	030	20 SE	14 to 088
Q.8	NC 31531 32410	-55.6	054	18 SE	16 to 100
Q.9	NC 31539 32408	-67.6	030	36 SE	32 to 104
Q.10	NC 31542 32415	-77.8	020	26 SE	26 to 120
Q.11	NC 31500 32450	-88.9	140	16 NE	10 to 096
Q.12	NC 31500 32450	-91.6	002	20 SE	20 to 108
L.1	NC 31536 32433	-93.3	176	20 SE	14 to 096

Table 2.1 Grid coordinates and foliation/lineation data for each sample in the APM stream section. Samples are listed based on structural position (cf. Fig. 2.4). Distances for samples are listed as structurally above (+) and below (-) the Moine thrust plane (Geolocial Survey 1923).

Along the line of this cross section, no exposures were found of the sheet(s) of mylonitic rocks mapped as a distinct structural unit (separating Cambrian from Moine rocks) on both the original and revised BGS maps, although the position of this inferred structural unit is marked by a bench-like topographic feature. No individual faults were identified in the APM stream section; however, observed variations in both strike and dip of foliation (Fig. 2.5, Table 2.1) may indicate relatively small- scale imbrication of the Cambrian quartzites.

The contact between the Lewisian gneiss and overlying Basal Quartzite is well exposed in the APM stream section beneath the main waterfall (Fig. 2.4; samples L.1 and Q.12). The contact is parallel to mylonitic foliation associated with crystal plastic deformation and dynamic recrystallization of quartz in both the gneiss and quartzite. This pervasive foliation extends up structural section through the entire exposed sequence of Cambrian quartzite (both Basal Quartzite and Pipe Rock) and is accompanied by a transport parallel mineral stretching lineation lying on the foliation (Fig. 2.5). Thus, although the contact between Lewisian gneiss and overlying Basal Quartzite is intensely sheared, it may represent a modified unconformity as depicted on the original Geological Survey maps (Geological Survey 1923, 1931), rather than a discreet thrust fault as indicated on the revised Assynt Special Sheet (BGS 2007).

The exposed sequence of Cambrian quartzites within the APM stream section were not distinguished as being mylonitically deformed on either the original or revised Geological Survey maps (Geological Survey 1923, 1931, & BGS 2007) although, as previously described, an overlying (unexposed) sheet of mylonitic rocks was interpreted to lie along the topographic bench at the top of the stream section, separating the Cambrian quartzites from the overlying Moine Schists (Figs. 2.2 and 2.3). This is surprising given that both on the original 6 inch to the mile clean copy sheets, and in the published descriptions of this stream section (probably by C.T. Clough), attention was drawn to both intense shearing of the Pipe Rock and transport-parallel stretching of pebbles in the Basal Quartzite (Peach et al. 1888, p. 433; Peach et al. 1907, p. 499; Read 1931, p. 23).

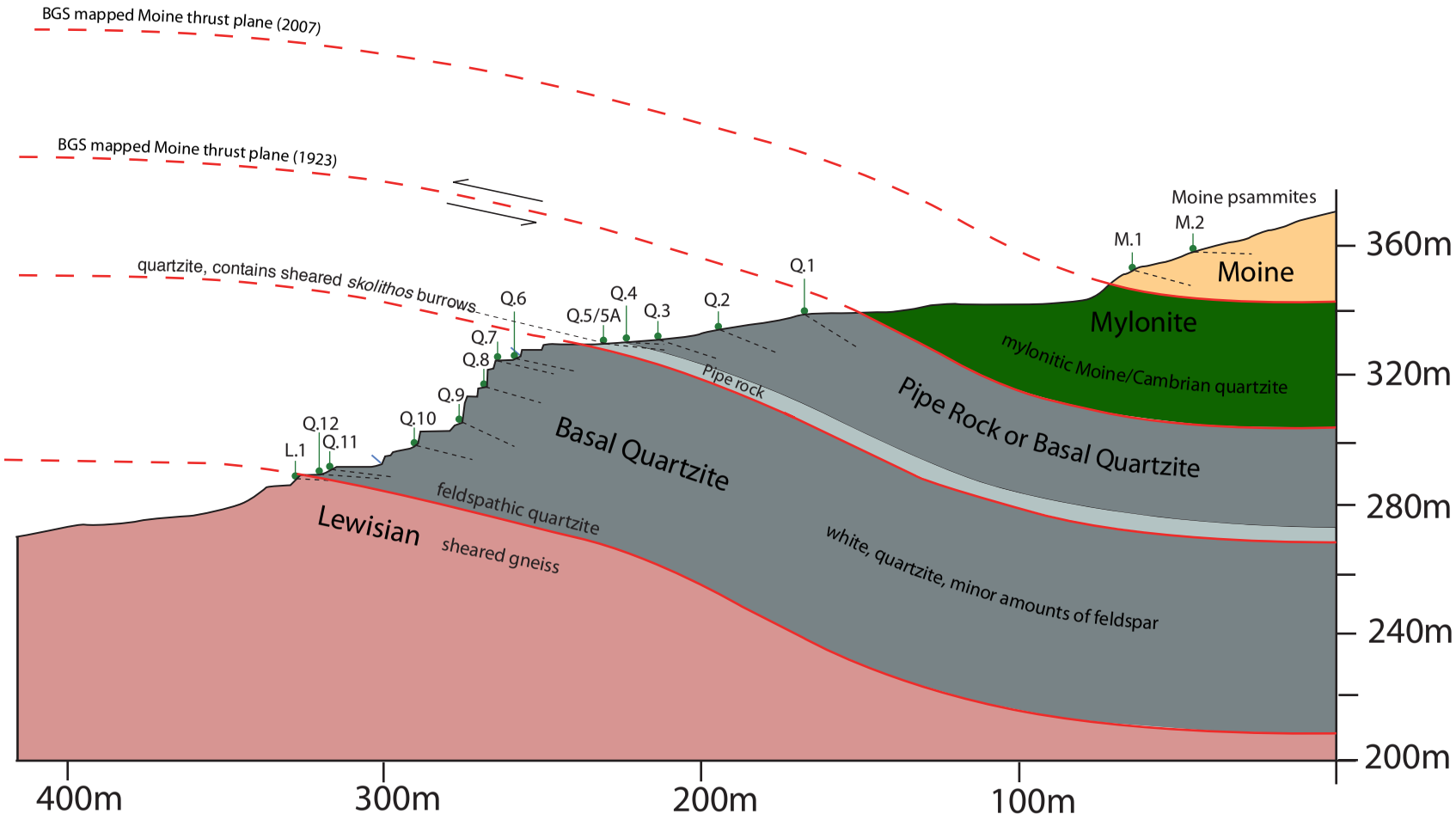

Figure 2.4 Cross section drawn along the Allt Pol a' Mhadaich (APM) stream section. Locations of samples from Moine psammites and pelites (M1 and M2), Cambrian quartzites (Q.1 - Q.12) and Lewisian gneiss (L.1) are indicated. Position of Moine thrust is dependent on whether mylonite sheet is of Moine or Cambrian quartzite protolith (mylonite in thrust sheet are not exposed in vicinity of APM stream section). Notes: 1) section is drawn oblique to thrust transport direction and local dip; see text for discussion, and 2) Cambrian quartzite above exposure of Pipe Rock are interpreted as Basal Quartzite on Geological Survey's revised Assynet Special sheet (BGS 2007) with an imbricate thrust placing Basal Quartzite on top of Pipe Rock.

The exposed section of Cambrian quartzites contains a variable amount of feldspar, with the greatest concentration generally seen in the Basal Quartzites near the contact with the underlying Lewisian gneiss (Fig. 2.4). Only one horizon of Pipe Rock was identified in the exposed section (Fig. 2.4, samples Q.5 and Q.5A), and along this horizon the *Skolithos* burrows have been sheared over in to the mylonitic foliation lying parallel to the ESE trending mineral stretching lineation. This horizon of Pipe Rock is located near the center of the exposed section of Cambrian quartzite; no *Skolithos* burrows have been found in the overlying quartzites (Fig. 2.4). It is unclear if the overlying non-burrowed quartzites should also be assigned to the Pipe Rock (as shown on the original Survey maps; Fig. 2.2) or if they belong to the Basal Quartzite and have been thrust over the Pipe Rock (as would be consistent with the imbricate faulting indicated on the revised Assynt Special Sheet; Fig. 2.3). The thickness of the Basal Quartzite underlying the Pipe Rock horizon is estimated at approximately 50m, while the exposed Pipe Rock horizon itself is only a few meters thick. The thickness of the overlying quartzites is estimated at approximately 30-35m, giving a total thickness for the exposed section of Cambrian quartzite of approximately 85-90m. Non-mylonitic Basal Quartzite in the Assynt Region has a measured stratigraphic thickness of 75-125m (BGS 2007).

Assuming that the mylonitic quartzites located between the underlying Lewisian gneiss and overlying Pipe Rock horizon (Fig. 2.4) represent the entire Basal Quartzite succession, the measured thickness of 50m in the APM stream section would indicate a sub-vertical shortening of approximately 33- 60% associated with penetrative mylonitization during thrusting. These estimates of thinning associated with mylonitization are in good agreement with early observations by the Geological Survey (Peach et al. 1888, p. 434) that Cambrian quartzites near Loch Strath nan Aisinnin (*Asinteach*) have been *"reduced to a third of their original straigraphic thickness"*. All Cambrian quartzite samples collected have proved suitable for strain and vorticity analyses, enabling independent assessment of these shortening estimates (see Chapters 4 and 5).

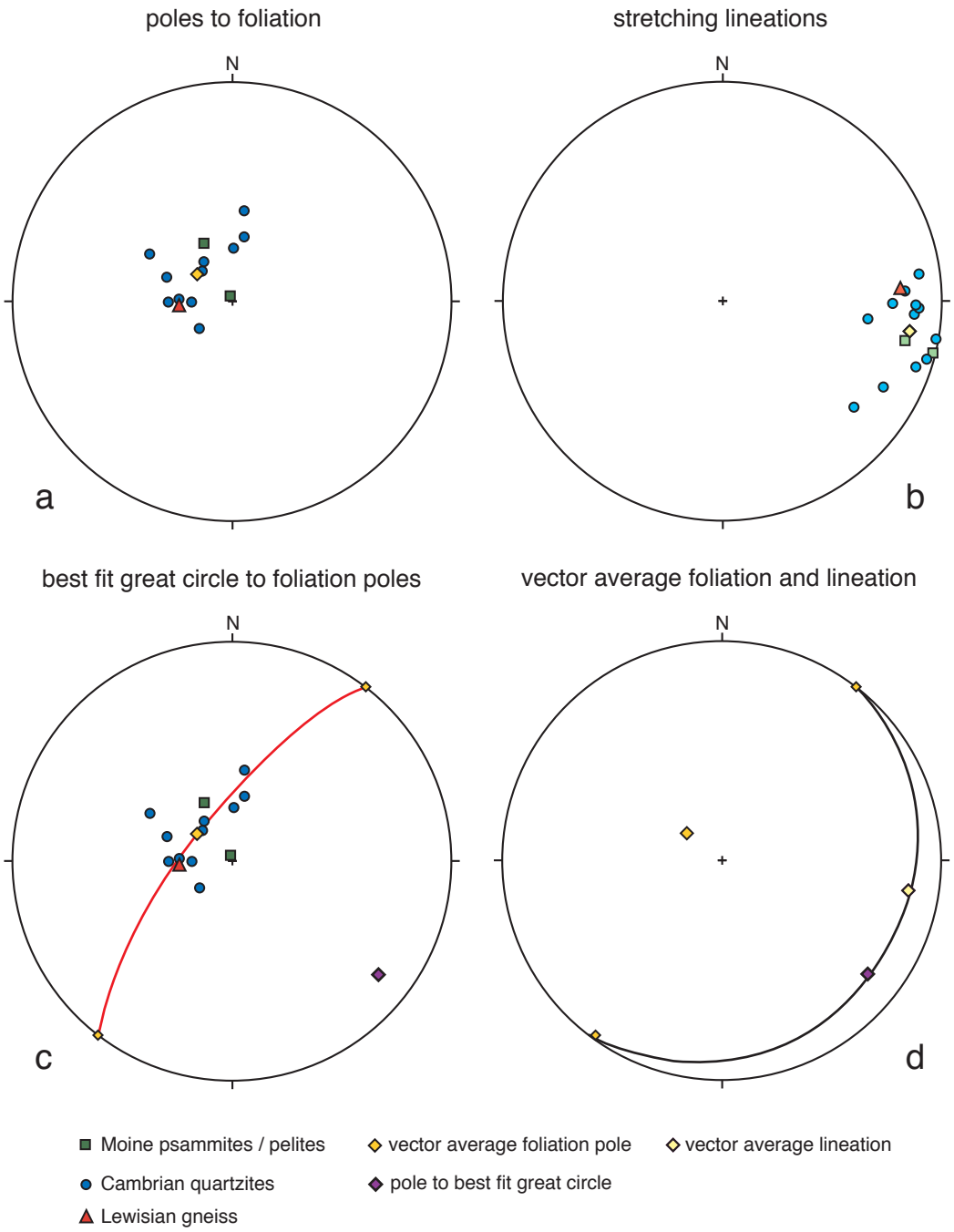

Figure 2.5 Structural data for Allt Pol a' Mhadaich (APM) stream section. (a) Poles to mylonitic foliation in the Moine, Cambrian quartzites and Lewisian gneiss samples and (b) stretching lineations. (c) Best fit great circle (and corresponding potential fold axis) to the population of poles to observed foliation plotted in (a). (d) Vector averageof foliation and stretching lineations, indicating a general ESE dip for foliation, and stretching lineations trending at ~100.

Outcrops of Moine pelites and psammites are present in the upper reaches of the stream section (sample M.1) and in small crags (sample M.2) overlooking the bench-like ground along which the Geological Survey mapped their mylonite sheet (Fig. 2.2). Moine samples M.1 and M.2 both proved suitable for vorticity analysis although only M.2 could be used for piezometry analyses due to the abundance of mica present in sample M.1. In both samples, strain analysis could not be conducted due to the lack of strain markers – such as relict detrital grains preserved in the underlying Cambrian quartzites.

References Cited:

BRITISH GEOLOGICAL SURVEY 2007. Assynt, Special Sheet, Bedrock, 1:50 000 Geology Series: Keyworth, Nottingham, British Geological Survey.

BUTLER, R.W.H. 1984. Structure evolution of the Moine thrust belt between Loch More and Glendhu, Sutherland. *Scottish Journal of Geology*, **20**, 161-179.

BUTLER, R.W.H. 1988. Excursion 9: The thrust belt in northern Assynt. In: Allison, I., May, F., & Strachan, R.A. (*eds*) *An Excursion Guide to the Moine Geology of the Scottish Highlands*. Scottish Academic Press on belhalf of Edinburgh Geological Society and the Geological Society of Glasgow, Edinburgh, pp. 176-188.

BUTLER, R.W.H. 2004. The nature of roof thrusts in the Moine thrust belt, NW Scotland: implications for the structural evolution of thrust belts. *Journal of the Geological Society, London,* **161,** 849-859.

COWARD, M.P. 1990. The Precambrian, Caledonian, and Variscan framework to NW Europe. *In:* Hardman, R.F.P. & Brooks, J. (eds) *Tectonic Events Responsible for Britian's Oil and Gas Reserves.* Geological Society of London, Special Publications, **55**, 1-34.

DALZIEL, I.W. & SOPER, N.J. 2001. Neoproterozoic extension on the Scottish Promontory of Laurentia; paleogeographic and tectonic implications. *Journal of Geology***, 109**, 299-317.

DEWEY, J.F. & SHACKLETON, R.J. 1984. A model for the evolution of the Grampian tract in the early Caledonides and Appalachians. *Nature*, **312**, 115-120.

DEWEY, J.F. & MANGE, M. 1999. Petrography of Ordovician and Silurian sediments in the western Irish Caledonides: tracers of a short-lived Ordovician continent-arc collision orogeny and the evolution of the Laurentian-Appalachian-Caledonian margin. *In:* MacNiociall, C. & Ryan, P.D. (eds) *Continental Tectonics.* Geological Society, London, Special Publications, **164**, 55-107.

DEWEY, J.F. & STRACHAN, R.A. 2003. Changing Silurian-Devonian relative plate motion in the Caledonides: Sinistral transpression to sinistral transtension. *Journal of the Geological Society, London*, **151**, 615-628.

GEOLOGICAL SURVEY OF GREAT BRITAIN (SCOTLAND), 1923. Geological Map of the Assynt District at 1:63,360. Geological Survey of Great Britain, Scotland.

GEOLOGICAL SURVEY OF GREAT BRITAIN (SCOTLAND), 1931. Altnaharra Sheet at 1:63,360. Geological Survey of Great Britain, Scotland.

HOLDSWORTH, R.E., ALSOP, G.I., & STRACHAN, R.A. 2007. Tectonic stratigraphy and structural continuity of the northernmost Moine thrust zone and Moine Nappe, Scottish Caledonides. Geological Society, London, Special Publications, **272**, 121-142.

HOLDSWORTH, R.E., STRACHAN, R.A., ALSOP, G.I., GRANT, C.J., & WILSON, R.W. 2006. Thrust sequences and the significance of low-angle, out-of-sequence faults in the northernmost Moine Nappe and Moine thrust zone, NW Scotland. *Journal of the Geological Society of London*, **163**, 801-814.

LAW, R.D. & JOHNSON, M.R.W. 2010. Microstructures and crystal fabrics of the Moine thrust zone and Moine Nappe; history of research and changing tectonic interpretations. *In:* Law, R.D., Butler, R.W.H., Holdsworth, R., Krabbendam, M. & Strachan, R. (eds) *Continental Tectonics and Mountain Building - The Legacy of Peach and Horne*. Geological Society, London, Special Publications, 443-503.

PARK, R.G., STEWART, A.D. & WRIGHT, D.T. 2002. The Hebridean Terrane. *In:* Trewin, N.H. (ed) *The Geology of Scotland.* Geological Society, London, 45-80.

PEACH, B.N., HORNE, J., GUNN, W., CLOUGH, C.T., HINXMAN, L.W. & CADELL, H.M. 1888. Report on recent work of the Geological Survey in the N.W. Highlands of Scotland, based on field notes and maps of Messers. B.N. Peach, J. Horne, W. Gunn, C.T. Clough, L. Hinxman, and H.M. Cadell. *Quarterly Journal of the Geological Society, London*, **64**, 378-441.

PEACH, B.N., HORNE, J., GUNN, W., CLOUGH, C.T., HINXMAN, L.W. & TEALL, J.J.H. 1907. *The Geological Structure of the North-West Highlands of Scotland.* Memoir of the Geological Survey of Great Britain.

PICKERING, K.T., BASSETT, M.G., & SIVETER, D.J. 1988. Late Ordovician-Early Silurian destruction of the Iapetus Ocean; Newfoundland, British Isles and Scandanavia; a discussion. *Transactions of the Royal Society of Edinburg: Earth Sciences*, **79**, 361-382.

READ, H.H. 1931. *The Geology of Central Sutherland (Sheets 108 and 109)*. British Geological Survey Memoir, 238pp.

SOPER, N.J. & HUTTON, D.H.W. 1984. Late Caledonian sinistral displacements in Britain; implications for a trhee-plate collision model. *Tectonics*, **3**, 781-794.

SOPER, N.J., STRACHAN, R.A., HOLDSWORTH, R.E., GAYER, R.A., & GREILING, R.O. 1992. Sinistral transpression and the Silurian closure of Iapetus. *Journal of the Geological Society of London,* **149**, 871-880.

STRACHAN, R.A., SMITH, M., HARRIS, A.L. & FETTES, D.J. 2002. The Northern Highland and Grampian Terranes. *In:* Trewin, N.H. (ed) *The Geology of Scotland.* The Geological Society, London, 81-147.

STRACHAN, R.A., HOLDSWORTH, R.E., KRABBENDAM, M. & ALSOP, G.I. 2010. The Moine Supergroup of NW Scotland; insights into the analysis of polyorogenic supracrustal sequences. Geological Society, London, Special Publications, **335**, 233-254.

THIGPEN, J.R., LAW, R.D., LLOYD, G.E., & BROWN, S.J. 2010. Deformation temperatures, vorticity of flow, and strain in the Moine thrust zone and Moine nappe: Reassessing the tectonic evolution of the Scandian foreland – hinterland transition zone. *Journal of Structural Geology*, **32**, 920-940.

Chapter 3: Deformation Microstructures

Abstract

Deformation microstructures within the plastically deformed and dynamically recrystallized mylonitic Cambrian quartzites were observed in thin section throughout the APM stream section. C- and A-sections displayed elongate plastically deformed detrital quartz grains to be used in strain analysis (Chapter 4). Rigid grains (feldspars and opaque minerals) are also present and serve as the foundation for one method of vorticity analysis (Chapter 5). Shear sense indicators are also present and suggest a top-to-the-WNW sense of motion, compatible with the regional thrusting of the Moine thrust. Dynamic recrystallization has occurred primarily by means of sub-grain rotation, though some instances of grain boundary migration were noted. The production of preferably aligned recrystallized grain fabrics also indicate a top-to-the-WNW shear sense, and are used in conjunction with quartz c-axis fabric analysis (Chapter 4) in a second method of vorticity analysis.

Introduction

This study of flow properties associated with mylonitization of Moine psammites and underlying Cambrian quartzites is based on the microstructures in these plastically deformed and dynamically recrystallized rocks. Flow-related macroscopic and microscopic structures were first described from the Moine thrust zone by Callaway (1883, 1884) and Bonney (1883) at the Stack of Glencoul (Fig. 2.1), who noted the flattening of detrital quartz grains and the sheared *skolithos* burrows in Cambrian quartzites seen in outcrop. Closely similar macro- and micro-structures to those described by Callaway and Bonney are also present in samples taken from the APM stream section although, as noted in Chapter 2, mylonitic Cambrian quartzites in the APM section belong to a structurally lower thust sheet than the mylonites exposed at the Stack. Work by John Christie in the 1950's for his PhD dissertation at Edinburgh University (Christie 1956) set the foundation for future microstructural studies in the Assynt region. Christie recognized that: 1) ribbon-like quartz grains in the mylonitic Cambrian quartzites were due to high strain plastic deformation (Christie, 1963), 2) small, equant quartz grains in the

mylonites were produced by dynamic recrystallization rather than by fracture processes (Christie et al., 1954; Christie, 1960; Carter et al., 1964) and, 3) that the high degree of quartz crystallographic preferred orientations in the mylonites was due to plastic deformation and dynamic recrystallization (Christie, 1963).

APM section - Moine psammites and pelites

Two samples (M1 and M2) of Moine pelite/psammite were collected from above the APM stream section (Fig. 2.4). These samples are located at the base of the Moine nappe and are structurally separated from the underlying Cambrian quartzites of the stream section by a 40 m thick sheet of mylonite that may be of either Moine (Geological Survey 1923) or Cambrian quartzite (BGS 2007) protolith. No exposure within this mylonite sheet (as mapped by BGS) have been found near the APM stream section. As discussed in Chapter 2, if this mylonite sheet is of Moine protolith then the Moine thrust (sensu-stricto) should be placed along the base of the sheet (Geological Survey 1923). In contrast, if the mylonite sheet is of Cambrian quartzite protolith then the Moine thrust should be placed along the upper surface of the sheet (BGS 2007) while an un-named thrust, possibly corresponding to the Lochan Riabach thrust recognized to the north at Loch Eriboll (Holdsworth 2006, 2007) may be placed along the lower surface of the mylonite sheet (Thigpen et al. 2010 a and b).

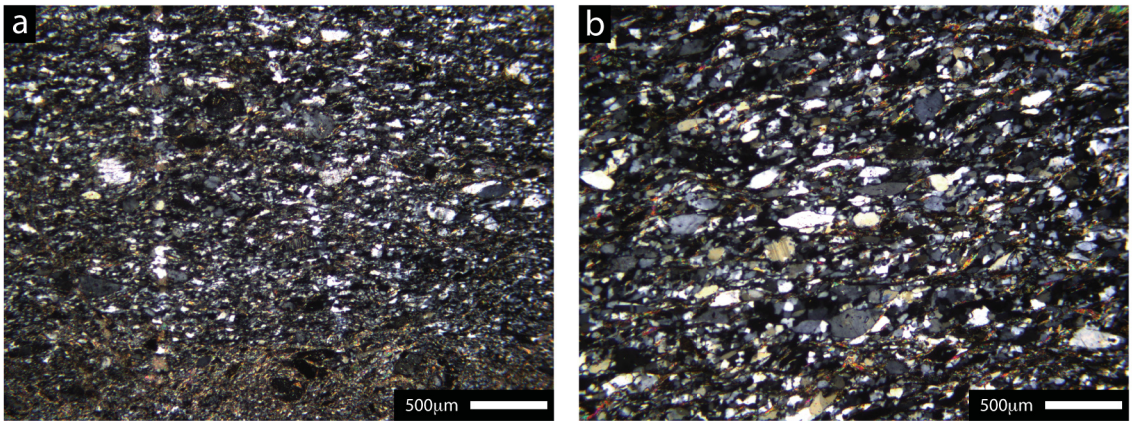

Figure 3.1 Micrographs from Moine pelite M.1 (a) and psammite M.2 (b). Thin sections cut perpendicular to foliation and parallel to lineation. Foliation is defined by mica laths set in a matrix of dynamically recrystallized quartz (50 micron grain size). Feldspar clasts are more obvious in psammite (b).

For samples M1 and M2 (and all other Moine samples subsequently analyzed along strike to the north and south - see Chapter 7) thin sections were cut perpendicular to foliation and parallel to lineation (Fig. 3.1). Quartz is totally recrystallized in these samples and, in contrast to the underlying Cambrian quartzites of the APM stream section, no relict detrital quartz grains - that might be used as strain markers - have been preserved. Observed microstructures indicate that dynamic recrystallization of quartz was dominantly by grain boundary migration (Regime 3 of Hirth & Tullis 1992) in the Moine samples, although there is some local microstructural evidence for transitional sub-grain rotation to grain boundary migration recrystallization. Recrystallized quartz grains (50μm grain size) in the Moine psammites are significantly larger than in the underlying Cambrian quartzites.

Feldspar, epidote, opaque mineral and garnet clasts are present in the Moine psammites and pelites, locally making up 30-50% of the total grain content. Mica laths and recrystallized quartz grains in the surrounding matrix anastomose around these clasts that have clearly behaved in a more rigid manner. Overgrowths of interlayered white mica and chlorite are present on many of these clasts. Overgrowths of pleochroic fox-red biotite on small garnet clasts are recorded in sample M.2 suggesting higher deformation temperatures. Very similar pristine overgrowth of pleochroic red biotite on garnet clasts have been reported by Bailey (1955, pp. 114-117) from the base of the Moine nappe in the Loch More area, to the north of the APM stream section (see also Read 1931, pp. 46-50). These overgrowths define sigma-shaped wings that are consistent with a top to the WNW shear sense. Shear bands (extensional crenulation cleavages) in the more micaceous units also indicate a top to the WNW shear sense.

Adopting the microstructural thermometer proposed by Stipp et al. (2002), microstructures indicating transitional sub-grain rotation to grain boundary migration recrystallization of quartz would indicate deformation temperatures of c. 495-530 °C in the psammites at the base of the Moine nappe. Higher deformation temperatures would be indicated if recrystallization was exclusively by grain

boundary migration. Based on opening angles in quartz c-axis fabrics measured on recrystallized grains, Thigpen et al. (2010b) have estimated deformation temperatures of 520° - 580°C for Moine psammites collected along strike at the base of the Moine nappe between Loch More and eastern Assynt.

APM section - Cambrian quartzites

For all samples collected from the APM stream section, thin sections were cut perpendicular to foliation and parallel to lineation (XZ sections). Ribbon-like relict detrital quartz grains were observed in all Cambrian quartzites from the APM stream section. These relict grains display undulose extinction, deformation bands, and sub-basal deformation lamellae. The aspect ratios of the relict detrital grains range from about 5:1 to 14:1.

No convincing correlation has been established between the average aspect ratio of relict detrital grains and the structural position of individual samples relative to mapped thrust faults (Geological Survey 1923, BGS 2007) at the top of the APM stream section (Figs 2.2, 2.3, and 2.4). Mylonitic foliation in thin sections cut perpendicular to foliation and parallel to lineation is defined by alignment of the long axes of plastically deformed detrital grains (Fig. 3.2a, c, e & g). These grains are used for strain analysis in Chapter 4. The degree of recrystallization observed in thin section stays relatively constant at 10-20% throughout the Cambrian quartzite section (Fig. 3.2e, g), increasing to about 40-50% in quartzites (samples Q.1 and Q.2, Fig. 3.2a, c) located closest to the overlying thrust plane(s).

In samples where suitable detrital grain strain markers were present, thin sections were also cut perpendicular to both foliation and lineation (YZ sections). The relict detrital quartz grains in these sections have less variable aspect ratios than in the XZ sections ranging only from about 3:1 to 5.5:1. Once again, no correlation was found between detrital grain aspect ratios and distance beneath the overlying thrust plane(s). The degree of recrystallization is similar to that observed in XZ sections, ranging from about 10-20% with a minor increase observed in sample Q.1 at the top of the APM section. However, a striking difference between the XZ and YZ sections is that the flattened relict grains in the YZ sections lack the

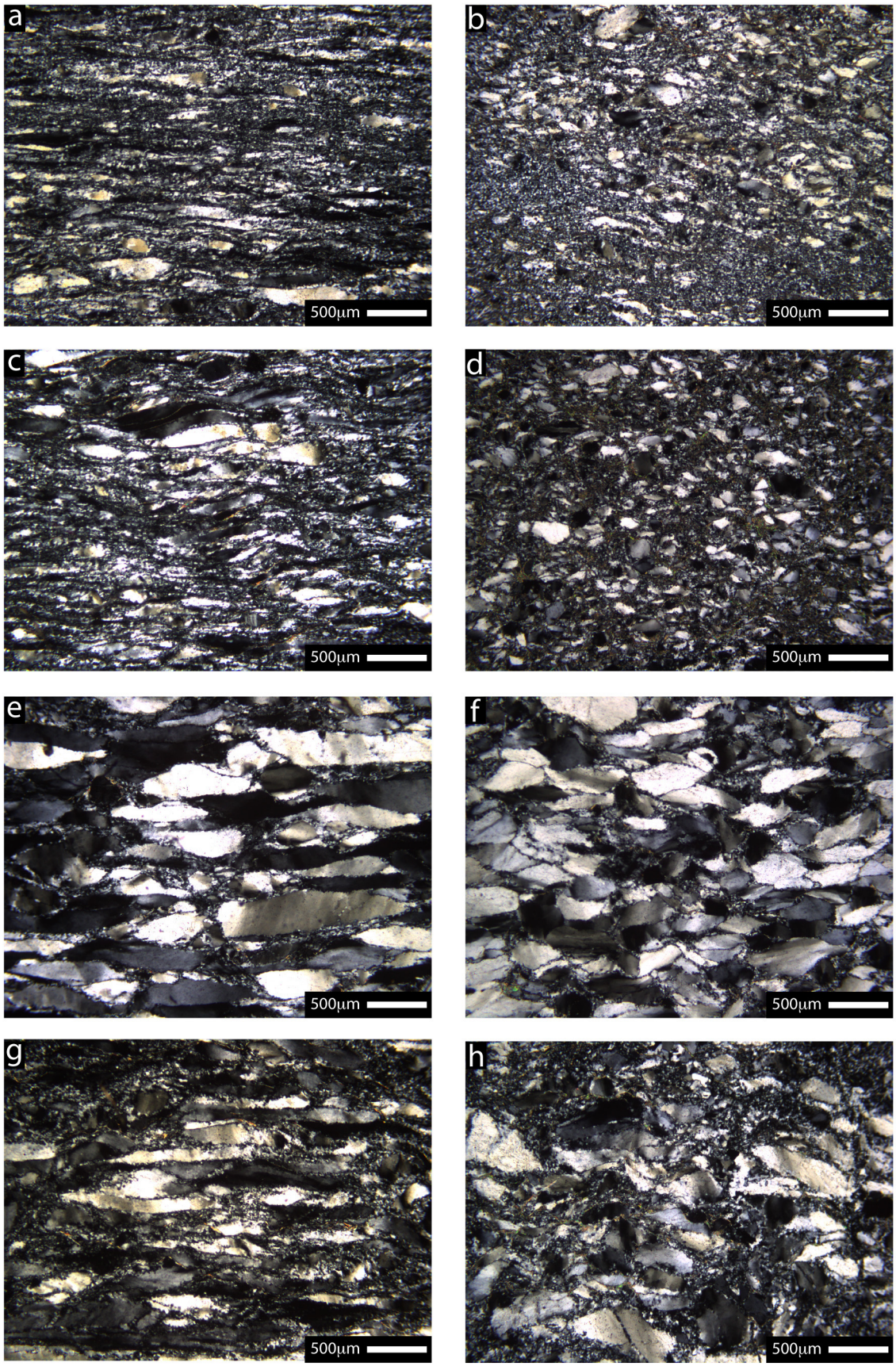
a
500µm
b
500µm
c
500µm
d
500µm
e
500µm
f
500µm
g
500µm
h
500µm

Figure 3.2 Micrographs from Cambrian quartzites of the APM stream section; all micrographs are from sections cut perpendicular to foliation and were taken using a 4x objective. Images in the left column are from XZ sections (cut parallel to lineation) with the corresponding YZ plane sections (perpendicular to lineation) shown in the right column. The micrographs are arranged in pairs and are shown with increasing distance from the contact with the Moine thrust plane (as defined on the original Assynt special sheet): (a, b) sample Q.1, (c, d) sample Q.5, (e, f) sample Q.7, and (g, h) sample Q.11. The images from the XZ plane show the deformed relict detrital grains and their preferred orientation parallel to foliation. This alignment is less clearly defined in the YZ sections where the relict detrital grains appear less deformed and have a lower degree of shape preferred orientation. An increase in degree of recrystallization (10-20% to 40-50%) is recorded moving up structural section. The deformed relic grains in Q.7 and Q.11 (e-f and g-h) indicate that a general flattening strain is dominant in these samples, while deformation is closer to plane strain in samples Q.1 and Q.5 (a-b and c-d) (cf. strain analysis data in Fig. 4.2).

preferred foliation-parallel alignment observed in the XZ sections. Contrasting microstructures observed in XZ and YZ thin sections from four Cambrian quartzites, arranged in order of descending structural position, are shown in Figure 3.2 (b, d, f, & h).

In some cases, the relict grains used as strain markers in the Cambrian quartzites exhibit core-mantle structures with subgrains defining the outer margins (mantles) of the relic grains (Fig. 3.3a). The presence of recrystallization along the margins of the relict grains can lead to an overestimation of the true aspect ratio (Dayan 1981, p. 228-232) of the relic grains, thereby giving a false impression of the amount of grain flattening.

In the Cambrian quartzites from the APM stream section, the grain size of dynamically recrystallized grains, that form a matrix around the detrital grains, ranges from about 20-30μm. According to Stipp & Tullis (2003) such grain sizes

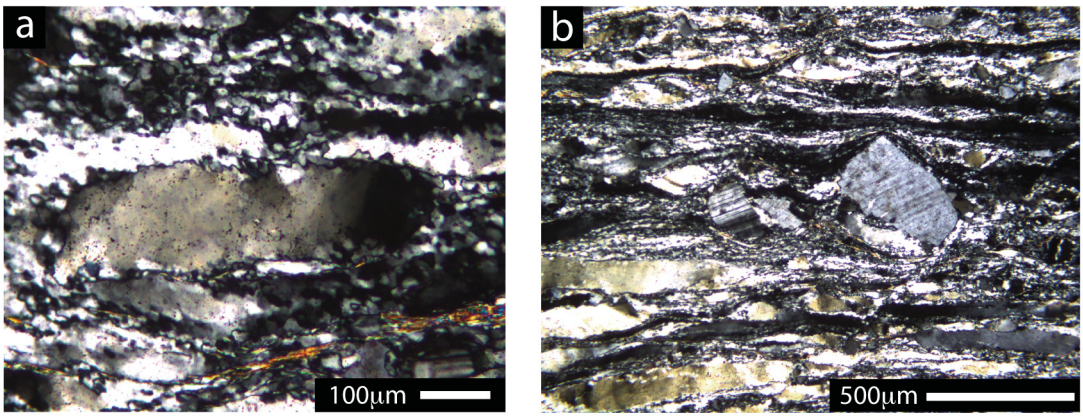

Figure 3.3 XZ sections of Cambrian quartzite viewed to NNE. (a) Micrograph of a relic detrital grain taken at 10x magnification from Cambrian quartzite sample Q.6; a mantle of subgrains and recrystallized grains is present on the margin of the deformed relic grain. (b) Micrograph taken at 4x magnification from sample Q.9; rigid plagioclase feldspar clasts surrounded by inter-banded relic detrital grains and foliation-parallel domains of recrystallized quartz , Note pressure cap defined by intensely deformed ribbon quartz above feldspar clast.

should be associated with dynamic recrystallization dominated by grain boundary migration (Regime 3 recrystallization of Hirth & Tullis 1992). However, the microstructures in the Cambrian quartzites indicate a dominance of recrystallization by sub-grain rotation (Regime 2 of Hirth & Tullis 1992). Adopting the microstructural thermometer of Stipp et al. (2002) these microstructures would indicates a deformation temperature of 420° - 480 °C (Stipp et al. 2002). The upper greenschist facies temperature range inferred from the sub-grain rotation microstructures in the Cambrian quartzites is in agreement with deformation temperatures indicated by opening angles in the c-axis fabrics from these samples; see Chapter 4.

Clasts of feldspar and opaque minerals are present within the Cambrian quartzites of the APM stream section, but represent <10% of the total grain fraction. These minerals have not deformed plastically, but have instead acted as rigid clasts around which the relict detrital quartz grains and the domains of recrystallized quartz anastomose (Figure 3.3b).

The Cambrian quartzites locally display in XZ thin sections an alignment of the long axes of elongate dynamically recrystallized grains (S_b) that is oblique to the mylonitic foliation (S_a). In all cases examined the sense of obliquity is consistent with a top to the WNW shear sense. This shear sense indicator is illustrated in Figure 3.4a where the mylonitic foliation is shown in red and the oblique grain shapes are outlined in green. The angle between the S_a and S_b fabrics ranges from 20°-45°. These oblique grain shape fabrics are used as input data for one method of vorticity analysis discussed in Chapter 5.

Other shear sense indicators recorded in the Cambrian quartzites of the APM stream section include asymmetric cross-girdle quartz c-axis fabrics (Chapter 4) and weakly developed shear bands. All quartz crystallographic fabrics measured in the quartzites are consistent with a top to the WNW shear sense. In the majority of quartzite samples the shear bands are consistent with the top to the WNW shear sense associated with thrusting (Fig. 3.4b). In several samples, however, shear bands indicating a top down to the ESE (i.e. normal) sense of shearing were also

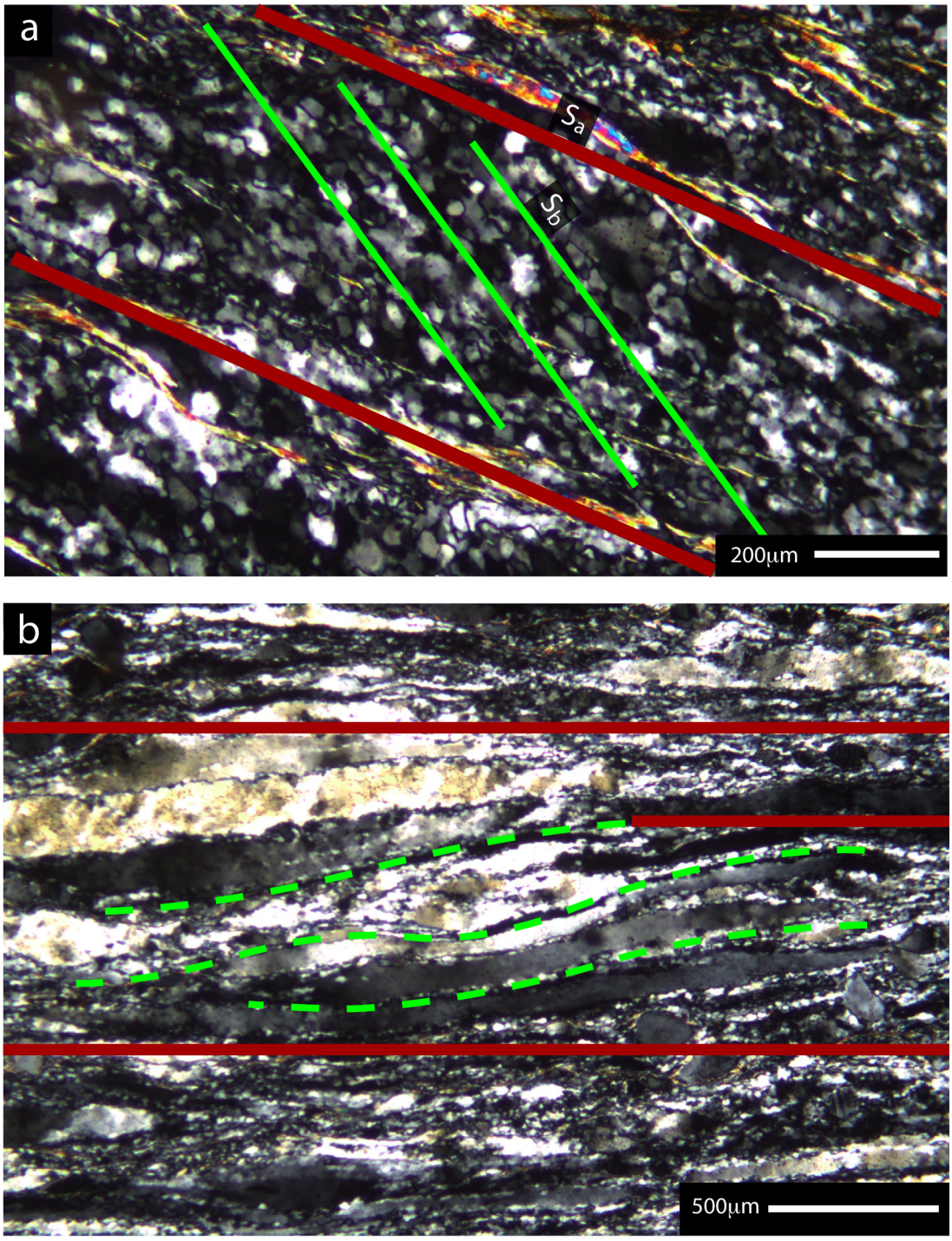

Figure 3.4 XZ sections of Cambrian quartzite (sample Q.10) viewed to NNE. (a) Domains of dynamically recrystallized quartz with grain long axes (Sb) aligned oblique to mylonitic foliation (Sa). (b) Ribbon grains and weakly developed shear band, typical of those observed throughout the APM stream section. Foliation orientation indicated by red lines in both micrographs; oblique grain shape alignment indicated by green lines in (a); shear band orientation indicated by broken green lines in (b). Top to the WNW shear sense indicated by microstructures in both micrographs.

recorded. These shear bands were primarily observed toward the top of the APM stream section, notably in samples Q.3 and Q.4, where their combined presence with top to the WNW shear bands could indicate an increasing component of pure-shear deformation.

References Cited:

BAILEY, E. B. 1955. Moine tectonics and metamorphism in Skye. *Transactions of the Edinburgh Geological Society*, **16**, 93-166.

BONNEY, T.G. 1883. Notes on a series of rocks collected by C. Callaway.*Quarterly Journal of the Geological Society, London,* **39**, 414-422.

BRITISH GEOLOGICAL SURVEY 2007. Assynt, Scotland Special Sheet, Bedrock, 1:50 000 Geology Series: Keyworth, Nottingham, British Geological Survey.

CALLAWAY, C. 1983. The age of the newer gneissic rocks of the northern Highlands. *Quarterly Journal of the Geological Society of London*, **39**, 355-414.

CALLAWAY, C. 1884. Notes on progressive metamorphism. *Geological Magazine*, **1**, 218-224.

CARTER, N.L., CHRISTIE, J.M., & GRIGGS, D.T. 1964. Experimental deformation and recrystallization of quartz. *Journal of Geology,* **72**, 687-733.

CHRISTIE, J.M., MCINTYRE, D.B. & WEISS, L.E. 1954. Appendix to McIntire, D.B. The Moine thrust - its discovery, age and tectonic significance. *Proceedings of the Geologists' Association*, **65**, 219-220.

CHRISTIE, J.M. 1956. *The Moine Thrust Zone in the Assynt Region.* Unpublished PhD Thesis, University of Edinburgh.

CHRISTIE, J.M. 1960. Mylonitic rocks of the Moine thrust-zone in the Assynt region, north-west Scotland. *Transactions of the Edinburgh Geological Society*, **18**, 79-93.

CHRISTIE, J.M. 1963. The Moine thrust zone in the Assynt region, northwest Scotland. *University of California Publications in Geological Sciences,* **40**, 345-440.

DAYAN, H. 1981. *Deformation studies of the folded mylonites of the Moine Thrust, Eriboll District, Northwest Scotland* [Ph.D. thesis]: University of Leeds.

GEOLOGICAL SURVEY OF GREAT BRITAIN (SCOTLAND), 1923. Geological Map of the Assynt District at 1:63,360. Geological Survey of Great Britain, Scotland.

HIRTH, G. & TULLIS, J. 1992. Dislocation creep regimes in quartz aggregates. *Journal of Structural Geology,* **14**, 145-159.

HOLDSWORTH, R.E., STRACHAN, R.A., ALSOP, G.I., GRANT, C.J. & WILSON, R.W. 2006. Thrust sequences and the significance of low-angle, out-of-sequence faults in the northernmost Moine Nappe and Moine thrust zone, NW Scotland. *Journal of the Geological Society of London,* **163**, 801-814.

HOLDSWORTH, R.E., ALSOP, G.I., & STRACHAN, R.A. 2007. Tectonic stratigraphy and structural continuity of the northernmost Moine thrust zone and Moine Nappe, Scottish Caledonides. Geological Society, London, Special Publications, **272**, 121-142.

READ, H.H. 1931. *The Geology of Central Sutherland (Sheets 108 and 109).* British Geological Survey Memoir, 238pp.

STIPP, M., STUNITZ, H., HEILBRONNER, R. & SCHMID, S. 2002. Dynamic recrystallization of quartz: correlation between natural and experimental conditions. In: De Meer, S., Drury, M.R., De Bresser, J.H.P. & Pennock, G.M. (eds) *Deformation Mechanisms, Rheology and Tectonics: Current Status and Future Perspectives.* Geological Society, London, Special Publications, **200**,171-190.

STIPP, M. & TULLIS, J. 2003. The recrystallized grain size piezometer for quartz. *Geophysical Research Letters,* **30**, 5.

THIGPEN, J.R., LAW, R.D., LLOYD, G.E., BROWN, S.J., & COOK, B. 2010a. Deformation temperatures, vorticity,of flow and strain symmetry in the Loch Eriboll mylonites, NW Scotland; implications for the kinematic and structural evolution of the northernmost Moine thrust zone. *In:* Law, R.D., Butler, R.W.H., Holdsworth, R., Krabbendam, M. & Strachan, R. (eds) *Continental Tectonics and Mountain Building - The Legacy of Peach and Horne*. Geological Society, London, Special Publications, **335**, 623-662.

THIGPEN, J.R., LAW, R.D., LLOYD, G.E., & BROWN, S.J. 2010b. Deformation temperatures, vorticity of flow, and strain in the Moine thrust zone and Moine nappe: Reassessing the tectonic evolution of the Scandian foreland – hinterland transition zone. *Journal of Structural Geology*, **32**, 920-940.

Chapter 4: 3D strain analysis, quartz crystal fabrics, and their implications for deformation history

Abstract

3D strain analyses were performed on mylonites derived from Cambrian quartzites and exposed in the APM stream section of northern Assynt. These exposures belong to the Aisinnan imbricates located in the upper part of the Glencoul thrust sheet. Strain analyses involved Rf/phi analysis of relic detrital quartz grains and data were manipulated using several software packages. The resulting strain values indicate that deformation took place within the general flattening field, but under close to plane strain conditions. Quartz c-axis fabrics measured on detrital grains are characterized by well-defined asymmetric Type-1 cross girdle fabrics. The internal and external asymmetries observed in these fabrics indicate a top-to-the-WNW shear sense, which is compatible with regional thrusting along the Moine thrust zone. The c-axis fabrics also provide a potential method for estimating deformation temperatures and provide input data for several methods of vorticity analysis that will be described in Chapter 5.

Introduction

Understanding the 3-dimensional strain of a region can provide valuable information on both local and regional deformational histories. Figure 4.1 illustrates the potential spectrum of 3D strains that can occur under varying deformation conditions. This version of the classic "Flinn" diagram is based on Lode's parameter υ, where constrictional, flattening and plane strains are represented by υ values of -1, +1 and 0, respectively. Assuming zero volume loss, plane strain deformation may develop under simple shear, pure shear or general shear conditions.

As described in Chapter 2, Cambrian quartzites of the APM stream section are plastically deformed and variably recrystallized. Following similar studies in other parts of the Moine thrust zone (e.g. Dayan 1981; Strine & Wojtal 2004; Law et al. 2010), the relict plastically deformed detrital grains in these mylonitic quartzites

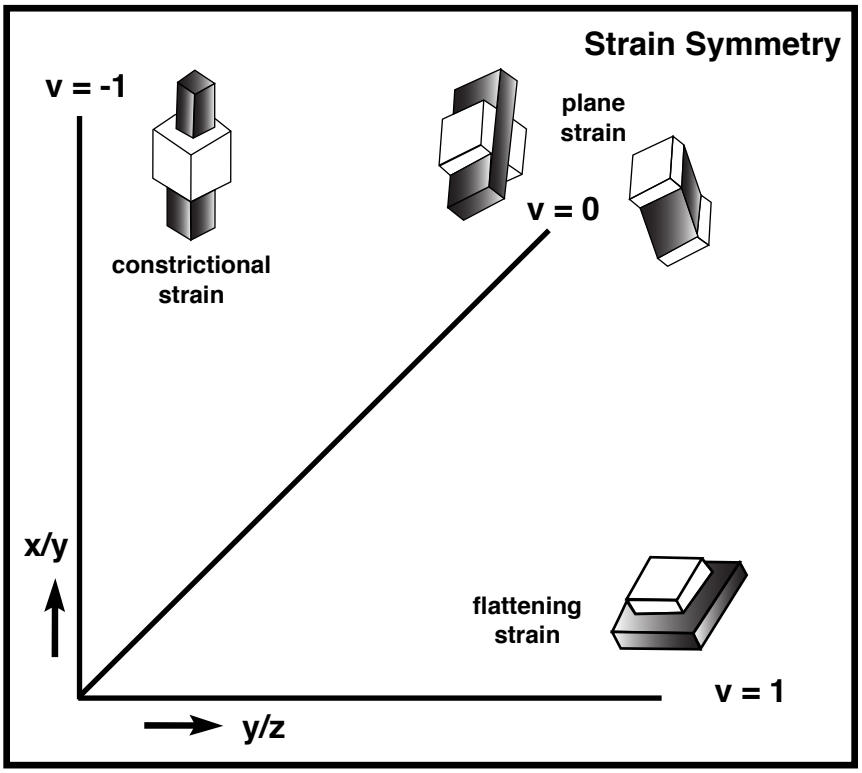

Figure 4.1. Schematic Flinn plot illustrating different types of 3D strain; strain magnitude increases outward from the origin. In each example an original cube is deformed in to a new shape; examples include flattening strains (denoted by Lodes Unit υ=+1 which plots along the base line); constriction (Lodes Unit υ=-1 which plots along the vertical axis) and plane strain (Lodes Unit υ=0, which plots along the 45° line and involves no stretching parallel to the intermediate principal axis of the associated strain ellipsoid). For plane strain examples of coaxial deformation (pure shear) and non-coaxial deformation (simple shear or general shear) are shown. Adapted from Hobbs et al. (1976).

may be used as potential strain markers, although the potential influence of dynamic recrystallization on relict detrital grain shape must be kept in mind when employing relic detrital grain shapes as strain markers (see discussion by Dayan 1981; Law et al. 2010). Within the APM stream section, mylonitic Moine metasedimenatry rocks in the hangingwall to the Moine thrust are unsuitable for strain analysis due to more pervasive dynamic recrystallization of quartz that has overprinted and destroyed original detrital grain shapes.

Mylonitic foliation in both the Cambrian quartzites and overlying Moine metasedimentary rocks of the APM stream section dips gently (vector average of 22°) towards the ESE (Fig. 2.5 and Table 2.1). Color banding (presumably indicating bedding), where present, appears to be parallel to foliation. A weak-moderately developed mineral lineation is present on the foliation planes and plunges gently

towards the ESE (Fig. 2.5 and Table 2.1) parallel to the regionally inferred thrust transport direction (Peach et al. 1888, 1907).

In this chapter, analysis of 3D strain is conducted to help quantify (assuming constant volume deformation) the amount of sub-vertical shortening perpendicular to foliation, and the amount of within-foliation stretching parallel and perpendicular to the mineral lineation. Quartz c-axis fabrics measured on detrital grains in the mylonites are also described in this Chapter and used to estimate deformation temperatures. In Chapter 5, skeletal asymmetry data from these fabrics, in combination with microstructural and strain data, are used to first estimate flow vorticities and then quantify both shortening perpendicular to the gently dipping thrust system and stretching parallel to tectonic transport.

2D and 3D Strain Analysis

For each quartzite sample from the APM stream section, 2D strain analyses were performed on at least one thin section cut perpendicular to foliation and parallel to the lineation. In the majority of samples (eight out of twelve) two mutually perpendicular oriented thin-sections were cut: i) perpendicular to foliation and parallel to lineation, ii) perpendicular to lineation/foliation. These thin-sections will be referred to as C and A sections, respectively. Although the 2D strain data from these mutually perpendicular section planes can be numerically combined to estimate the best-fit 3D strain ellipsoid, it should be kept in mind that data from a third section plane is needed to verify compatibility between the 2D data and the estimated strain ellipsoid. In exposures of the mylonitic Cambrian quartzites at Loch Eriboll (Dayan 1981) and the Stack of Glencoul (Law et al. 2010) this has previously been accomplished by preparing foliation-parallel thin-sections. However, in the samples from the APM stream section the blocks used for preparing foliation-parallel sections progressively cleaved along foliation during sample preparation making it impossible to produce thin sections of this orientation.

2D strain analyses were performed on the C and A sections using Rf/Phi analysis of the deformed detrital grain shapes. The Rf/Phi technique was first described by Ramsay (1967) and later refined by Dunnet (1969) and Lisle (1977, 1985), and is applicable to suites of deformed elliptical markers in which

deformation has modified the shape (ratio Rf of long to short principal axes) and orientation Phi (relative to sample reference frame) of initially elliptical markers. This method is summarized in Figure 4.2. The technique is most simply applied when the suite of original elliptical markers had a random alignment of their long axes before deformation, but can be adapted for cases where there was an original (e.g. sedimentary) preferred alignment (see reviews by Dunnet & Siddans 1971, Lisle 1985). For individual relic detrital grains in the A and C thin-sections the positions of principal axes were estimated visually in the petrographic microscope and their lengths measured using a micrometer. The orientation (Phi) of the principal long axis for individual grains was recorded relative to foliation defined by trails of mica and secondary mineral phases in thin section. The orientation of foliation itself was determined by taking multiple orientations using the rotating stage on the microscope and finding the average angle of foliation to be used as a base reference line.

All appropriate detrital grain shapes present in individual thin sections were measured. However, due to variation in degree of dynamic recrystallization, the total number of relict detrital grain shapes appropriate for meaningful strain analysis varied from sample to sample. Within the suite of quartzites analyzed the minimum number of suitable markers measured in a given thin section was 141 grains, while the majority of thin sections contained >250 suitable relic grains. Borradaile (1984) has previously estimated that 50-75 such markers should be sufficient for confidently determining 2D strain values.

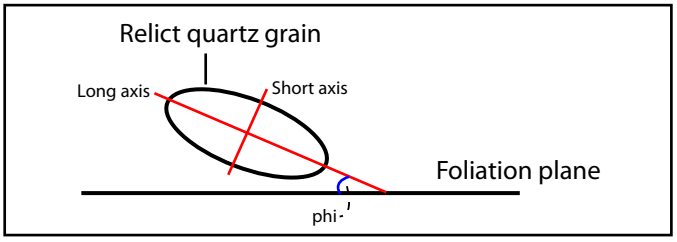

Figure 4.2 Parameters used to define the shape and orientation of a deformed elliptical marker in the Rf/Phi method of strain analysis. The markers used in this study are relict detrital quartz grains imaged in the plane of a thin section, where the shape of the grain is expressed as the ratio of the long to short axes, and the orientation of the grain is expressed as the angle, phi, between the long axis and the foliation plane.

For each thin section the measured Rf and Phi data were analyzed using two computer programs (Mulchrone & Meere 2001; Chew 2003) based on the Rf/Phi technique. Both programs yield estimates of 2D strain ratio (Rs) and orientation of

a

Sample	X	Y	Z	Rxz	Ryz	Rxy	lnRxz	lnRyz	lnRxy	Flinn k	Nadai Es	Lodes V	K
Q.1	2.224	1.137	0.395	5.625	2.875	1.957	1.727	1.056	0.702	0.599	1.205	0.172	0.707
Q.2	--	--	--	6.800	--	--	--	--	--	--	--	--	--
Q.3	2.232	1.159	0.388	5.775	3.000	1.925	1.754	1.099	0.608	0.408	1.236	0.295	0.545
Q.4	--	--	--	6.125	--	--	--	--	--	--	--	--	--
Q.5	2.336	1.045	0.419	5.700	2.550	2.235	1.740	0.936	0.741	0.708	1.189	0.116	0.792
Q.6	2.003	1.234	0.405	4.950	3.050	1.623	1.599	1.115	0.507	0.339	1.148	0.361	0.469
Q.7	1.915	1.241	0.421	4.550	2.950	1.542	1.515	1.082	0.411	0.261	1.091	0.449	0.380
Q.8	2.324	1.407	0.306	7.600	4.600	1.652	2.028	1.526	0.489	0.197	1.414	0.492	0.341
Q.9	--	--	--	9.950	--	--	--	--	--	--	--	--	--
Q.10	--	--	--	6.000	--	--	--	--	--	--	--	--	--
Q.11	1.938	1.265	0.408	4.750	3.100	1.532	1.558	1.131	0.395	0.230	1.120	0.483	0.349
Q.12	2.390	1.110	0.380	6.350	2.950	2.153	1.848	1.082	0.763	0.545	1.348	0.194	0.675

b

Sample	X	Y	Z	Rxz	Ryz	Rxy	lnRxz	lnRyz	lnRxy	Flinn k	Nadai Es	Lodes V	K
Q.1	2.224	1.102	0.406	5.450	2.700	2.019	1.696	0.993	0.702	0.599	1.205	0.172	0.707
Q.2	--	--	--	7.250	--	--	--	--	--	--	--	--	--
Q.3	2.174	1.184	0.388	5.600	3.050	1.836	1.723	1.115	0.608	0.408	1.236	0.295	0.545
Q.4	--	--	--	6.500	--	--	--	--	--	--	--	--	--
Q.5	2.239	1.067	0.419	5.350	2.550	2.098	1.677	0.936	0.741	0.708	1.189	0.116	0.792
Q.6	2.012	1.211	0.411	4.900	2.950	1.661	1.589	1.082	0.507	0.339	1.148	0.361	0.469
Q.7	1.886	1.251	0.424	4.450	2.950	1.508	1.493	1.082	0.411	0.261	1.091	0.449	0.380
Q.8	2.236	1.371	0.326	6.850	4.200	1.631	1.924	1.435	0.489	0.197	1.414	0.492	0.341
Q.9	--	--	--	9.400	--	--	--	--	--	--	--	--	--
Q.10	--	--	--	6.600	--	--	--	--	--	--	--	--	--
Q.11	1.897	1.278	0.412	4.600	3.100	1.484	1.526	1.131	0.395	0.230	1.120	0.483	0.349
Q.12	2.430	1.130	0.360	6.650	3.100	2.145	1.895	1.131	0.763	0.545	1.348	0.194	0.675

Table 4.1. Strain data from mylonitic Cambrian quartzites exposed in the APM stream section; samples are arranged in descending order of structural position beneath the Moine thrust plane (cf. Fig. 2.4) as defined on the original Assynt Special Sheet (Geologic Survey1923). a) data based on the 2D strain estimates obtained using the Chew (2003) program, b) data based on the 2D strain estimates obtained using the Mulchrone & Meere (2001) program. Stretches (X, Y and Z) parallel to the three principal axes of the estimated strain ellipsoid assume zero volume loss during deformation; note that in four samples only 'C' sections were used and hence 3D strains could not be estimated. For each data set, 3D strain parameters (k, Es, υ and K) were calculated using the Holcombe Strain Calculator. The value K is a modification of the Flinn k values based on a relationship of the Lode's υ parameter. K is used for plotting on the Log Flinn plot (Figure 4.4).

the calculated strain ellipse. Within observational error, principal axes of the calculated strain ellipse were found to be parallel and perpendicular to the visually estimated average foliation trace in each thin section. Calculated Rs values from these analyses are given in Tables 4.1 a & b. For the thin sections analyzed it was found that the two methods give slightly different Rs values. For the C sections Rs values of 4.5 – 7.6 and 4.4 – 6.8 were estimated using the Chew (2003) and Mulchrone & Meere (2001) programs, respectively; with arithmetic means of 5.6 and 5.5. For the A sections Rs values of 2.5 – 4.6 and 2.5 – 4.2 were estimated using the Chew and Mulchrone programs, respectively, with arithmetic means of 3.134 and 3.075.

While each program is based on the same basic Rf/Phi technique, the design of the Chew (2003) Excel macro enables the user to vary the range of potential Rs values that may be compatible with the input strain data, and through a series of iterations find the "best fit" Rs value. This is accomplished through '*Chi-squared*' statistical tests and determining the minimum X^2 value. In contrast, the Mulchrone & Meere (2001) program only provides a single estimated Rs value. However, the difference in Rs values estimated by the two programs for a given thin section were found to be minimal (cf. Tables 4.1a and 4.1b) and, as will be discussed below, lead to closely similar 3D strain estimates for individual samples.

If 2D strain data is collected on principal planes of the 3D strain ellipsoid then there should be a simple algebraic relationship between Rs values of the form: $R_{XY} = R_{XZ}/R_{YZ}$. As outlined above, for the APM stream section quartzites we were unable to prepare foliation-parallel thin sections that one might expect to be at least sub-parallel to the XY plane of the strain ellipsoid. Therefore we were unable to directly verify that our sections were cut parallel to principal sections through the strain ellipsoid using this predicted numerical relationship. However, our 2D analyses on all A and C sections did indicate that within observational error the average foliation was oriented parallel to a principal plane of the 2D strain ellipse - and hence a principal plane of the strain ellipsoid. Additionally, our quartz c-axis fabrics (discussed later in this chapter) confirm that the mineral lineation lying on the mylonitic foliation is oriented parallel to the maximum principal extension direction (X) of the strain ellipsoid in all analyzed samples. Therefore, we are confident that within observational error our C and A sections have been cut parallel to the R_{XZ} and R_{YZ} sections, respectively, of the strain ellipsoid.

Stretches parallel to the three principal axes of the strain ellipsoid were calculated for each sample in which 2D strain data were available from C and A sections. For these calculations, which assume constant volume deformation, the program *Strain Calculator*, developed by Rod Holcombe (University of Queensland) and available as freeware, was used. This program was also used to calculate the shape of the strain ellipsoid (which can be expressed by either the Flinn parameter

K, or Lode's Unit υ) and magnitude of 3D strain (expressed by the Nadai strain parameter Es). K, υ and Es results indicated by the Holcombe program were cross-checked and verified by hand calculation for all individual samples. Results based on 2D strain estimates indicated by the Chew (2003) and Mulchrone & Meere (2001) programs are shown in Tables 4.1a and 4.1b, respectively.

When plotted on the Hsu strain diagram (Figure 4.3), the mylonitic quartzites all fall within the general flattening field, with the estimated Lode's Unit υ ranging between about +0.1 and +0.55 for both sets of 2D strain data. Stretches along the X (parallel to the thrust transport direction) and Y (parallel to orogenic strike) principal axes of the estimated strain ellipsoids range between 90-140% and 10-40% respectively, while shortening along the Z axis (perpendicular to the gently dipping mylonitic foliation) is estimated at 55-65%. These estimates all assume constant volume deformation. If the estimated non-plane strain deformation is real then this presents obvious space problems in terms of accommodating along strike stretching. Comparison of our 3D strain data with lines of plane strain deformation

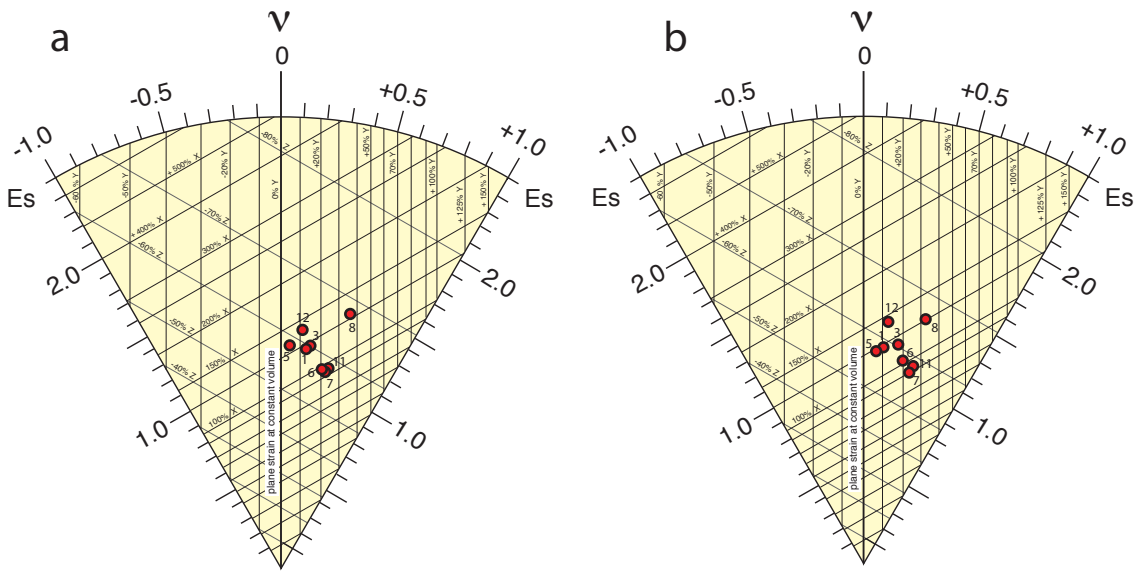

Figure 4.3 Hsu natural strain plots for mylonitic Cambrian quartzites from the APM stream section using 2D data from a) the Chew (2003) and, b) the Mulchrone & Meere (2001) programs, respectively. All data plot within the general flattening field, as expressed by Lode's parameter υ. 3D strain magnitudes (expressed by Es) increase linearly outwards from the origin of the plots. Assuming constant volume deformation, stretches (extensions) of 90-140% and 10-40% are indicated parallel to tectonic transport direction and along orogenic strike, respectively, accompanied by 55-65% shortening perpendicular to gently dipping mylonitic foliation.

at different volume losses (Ramsay & Wood 1973) indicates that a 20-50% volume loss would be needed to explain our data in terms of a plane strain deformation with no stretching along orogenic strike (Figure 4.4). This seems unlikely given the apparent dominance, at least under the optical microscope, of crystal plastic deformation (constant volume deformation).

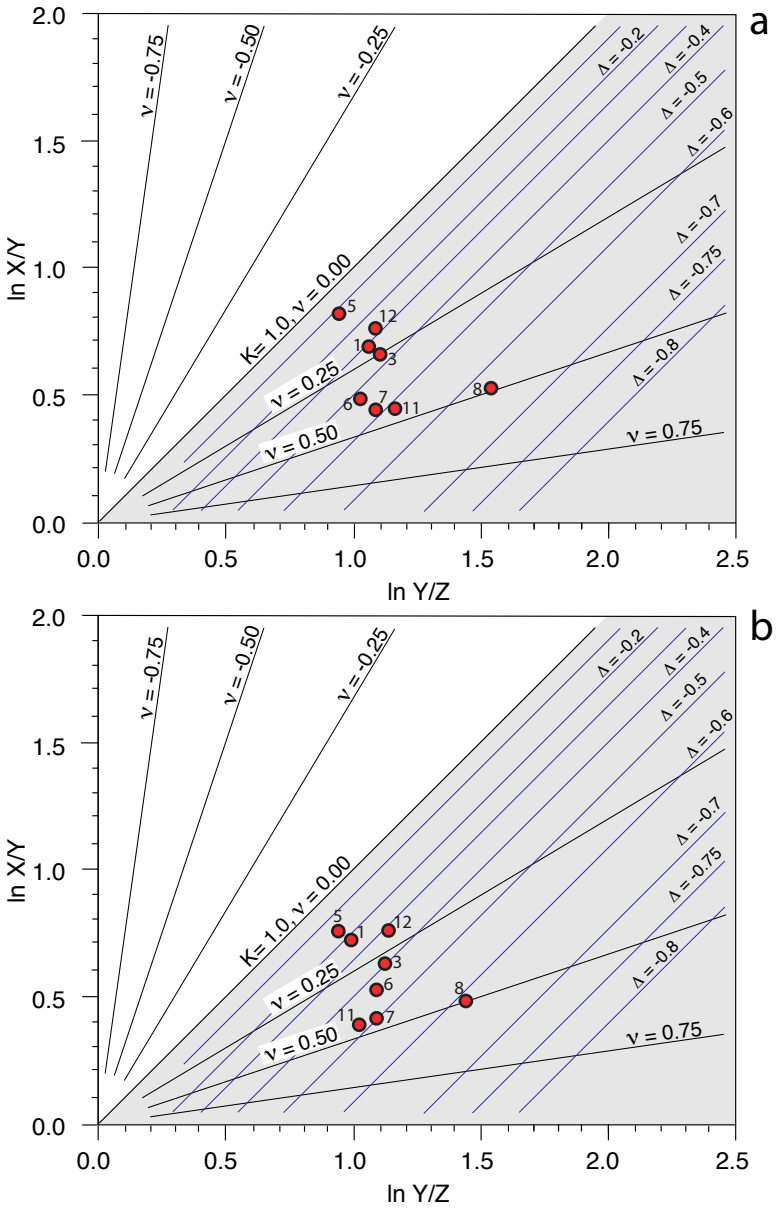

Figure 4.4 Log Flinn for mylonitic Cambrian quartzites from the APM stream section using 2D data from a) the Chew (2003) and, b) the Mulchrone & Meere (2001) programs, respectively. All data plot within the general flattening field, as expressed by Lode's parameter υ. and Flinn's parameter K. Lines of plane strain deformation for different volume loses (Δ) are taken from Ramsay & Wood (1973). Volume losses of 20-60% are required for estimated 3D strains to develop under plane strain conditions with zero finite stretch along orogenic strike.

Within the APM stream section no convincing correlation has been established within the suite of 12 mylonitic quartzites between strain magnitude and structural distance beneath the overlying thrust. Indeed, the highest magnitude strain (Es ~ 1.4) was measured in sample Q.8 located in the center of the mylonitic Basal Quartzites at 35m above the Lewisian gneiss. A similar lack of correlation between estimated strain magnitude and distance beneath the Moine thrust plane has previously been reported by Law et al. (2010) at the Stack of Glencoul, approximately 6km along strike to the south of the APM stream section. However, important caveats need to be placed on using relic detrital grain shapes as strain markers in these quartzites. Inclusion of ribbon grains that might be formed from foliation-parallel deformation bands or diffusive mass transfer along dilating foliation planes (vein fills) in the data sets could lead to an over-estimation of Rs values. We note, however, that the Rf/Phi programs appear to minimize the influence of these anomalously elongate grains in calculating Rs. Similarly, dynamic recrystallization around the margins of an elongate parent (e.g. detrital) grain, producing even a constant width mantle of new grains, will significantly alter the aspect ratio of the core parent grain (Dayan 1981) leading to an over-estimation of Rs value. In contrast, strain partitioning between the detrital grains and their surrounding matrix of smaller dynamically recrystallized grains may result in underestimating the bulk Rs value if only strain in the relict detrital grains is taken in to account.

Crystal Fabrics

Quartz c-axis fabrics in samples from the APM stream section were measured on C plane thin-sections using an optical microscope and universal stage. In the Moine samples (hanging wall to the Moine thrust) fabrics were measured using dynamically recrystallized quartz grains, while in the footwall Cambrian quartzites fabrics were measured in all 12 samples using plastically deformed detrital quartz grains. All crystal fabrics are displayed (Figure 4.5) on lower-hemisphere Schmidt equal area projections where the plane of projection is oriented perpendicular to foliation and parallel to the ESE plunging stretching lineation; each fabric diagram is viewed towards the NNE. The original u-stage data were collected and converted to

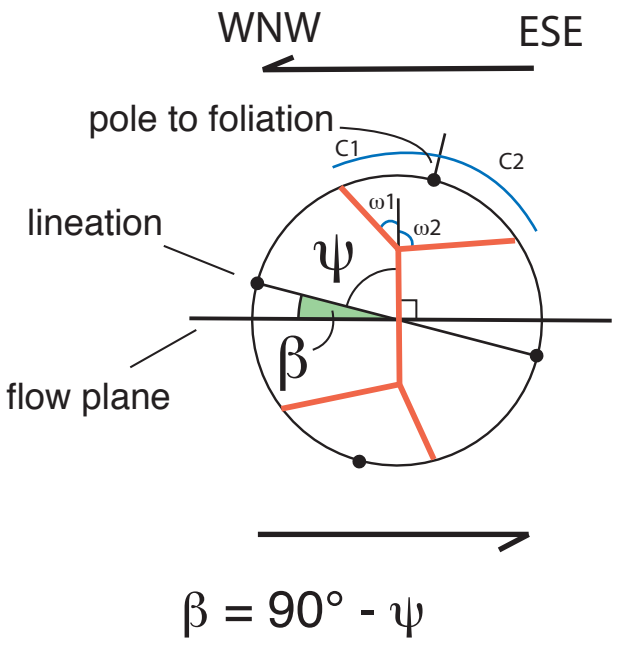

Figure 4.5 Parameters used to characterize external and internal asymmetry in quartz c-axis fabrics. External skeletal fabric asymmetry characterized by ψ, C1 and C2; internal fabric asymmetry characterized by ω1 and ω2. The C1 and C2 angles are measured in the projection plane from the leading and trailing fabric edges, respectively, to the foliation pole. The ω1 and ω2 values are based on the angle at which the central segment of the cross girdle fabric intersects the leading and trailing edges, respectively, of the fabric skeleton. The flow plane is determined by drawing a line perpendicular to the central segment of the cross girdle. The acute angle (β) between the inferred flow plane and the foliation is used in several methods of vorticity analysis - see Chapter 5. Skeletal fabric also demonstrates how fabric asymmetry may be used as a shear sense indicator.

sample coordinates using an Excel Macro developed by Dr. Sean Mulcahy as part of his PhD research at the University of California at Davis. These data were then plotted and contoured using the program STEREONET developed by Professor Neil Mancktelow at ETH, Zurich, running in the Macintosh *'Classic'* operating system. The ranges in orientation of shear bands (denoted by bars with arrows) and alignment (Sb) of elongate dynamically recrystallized quartz grains oriented oblique to foliation, where observed in C plane thin-section, are indicated on the fabric diagrams (Figs. 4.6 & 4.7).

Under appropriate circumstances quartz c-axis fabrics can be used for addressing a range of structural/tectonic problems (see reviews by Schmid & Casey 1986; Law 1990, Passchier & Trouw 2005) including: i) qualitatively determining shape of the strain ellipsoid (e.g. flattening, plane strain); ii) qualitative assessment of whether deformation was dominantly coaxial or non-coaxial (asymmetric versus symmetric fabrics); iii) determining bulk shear senses (asymmetric fabrics) in plastically deformed rocks; iv) as input data for several techniques for quantitative determination of flow vorticities (see Chapter 5); v) determining deformation temperatures. Internal fabric symmetry parameters (ψ and complimentary angle β; numerical difference between C2 and C1) and external symmetry fabric

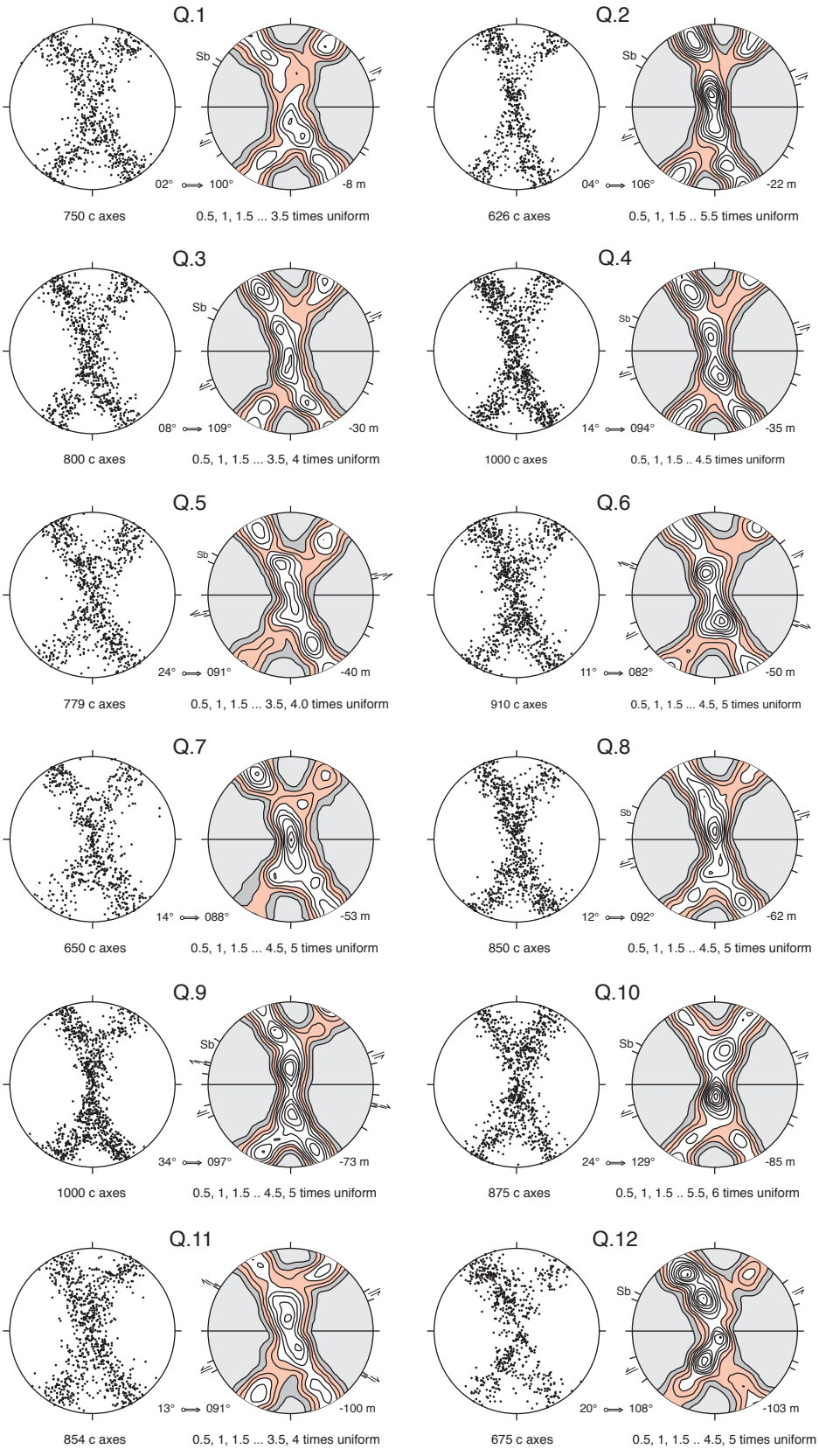
Q.1
Sb
02° ⟹ 100°
-8 m
750 c axes
0.5, 1, 1.5 ... 3.5 times uniform
Q.2
Sb
04° ⟹ 106°
-22 m
626 c axes
0.5, 1, 1.5 .. 5.5 times uniform
Q.3
Sb
08° ⟹ 109°
-30 m
800 c axes
0.5, 1, 1.5 ... 3.5, 4 times uniform
Q.4
Sb
14° ⟹ 094°
-35 m
1000 c axes
0.5, 1, 1.5 .. 4.5 times uniform
Q.5
Sb
24° ⟹ 091°
-40 m
779 c axes
0.5, 1, 1.5 ... 3.5, 4.0 times uniform
Q.6
11° ⟹ 082°
-50 m
910 c axes
0.5, 1, 1.5 ... 4.5, 5 times uniform
Q.7
14° ⟹ 088°
-53 m
650 c axes
0.5, 1, 1.5 ... 4.5, 5 times uniform
Q.8
Sb
12° ⟹ 092°
-62 m
850 c axes
0.5, 1, 1.5 .. 4.5, 5 times uniform
Q.9
Sb
34° ⟹ 097°
-73 m
1000 c axes
0.5, 1, 1.5 .. 4.5, 5 times uniform
Q.10
Sb
24° ⟹ 129°
-85 m
875 c axes
0.5, 1, 1.5 .. 5.5, 6 times uniform
Q.11
13° ⟹ 091°
-100 m
854 c axes
0.5, 1, 1.5 ... 3.5, 4 times uniform
Q.12
Sb
20° ⟹ 108°
-103 m
675 c axes
0.5, 1, 1.5 .. 4.5, 5 times uniform

Figure 4.6 On previous page, optically measured quartz c-axis fabrics from relict detrital grains in mylonitic Cambrian quartzites from the APM stream section. Fabrics are contoured in multiples of 0.5 times uniform distribution. Less than 0.5, 0.5-1.0, 1.0-2.0 and >2.0 times uniform density distribution indicated by light gray, dark grey, pink and white ornaments, respectively. All fabrics are viewed towards the north and are shown on projection planes oriented perpendicular to foliation (horizontal bars) and parallel to mineral lineation. Plunge and trend of lineation for each sample indicated. Orientation ranges of shear bands and elongate dynamically recrystallized grains (Sb) also indicated. For structural position of individual samples see Fig. 2.4.

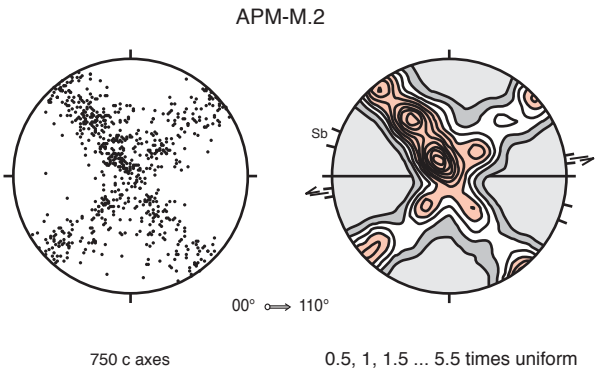

Figure. 4.7 Optically measured quartz c-axis fabric from dynamically recrystallized quartz grains in mylonitic Moine psammite from the APM stream section. See Fig. 4.6 for explanation of plotting convention followed.

parameters (numerical difference between ω2 and ω1) employed in our analyses are summarized in Figure 4.5. These fabric parameters were determined visually for each sample by drawing fabric skeletons on superimposed contour and point diagrams. Minimum, maximum and best-fit (β) values for external symmetry parameter β were also visually determined for each fabric (Table 4.2) and, in combination with strain and microstructural data, will be used to quantify flow vorticities in Chapter 5. Measured values of skeletal fabric parameters for individual samples are summarized in Table 4.2.

All mylonitic Cambrian quartzites from the APM stream section are characterized by well-developed Type-1 (Lister 1977) cross girdle c-axis fabrics (Figure 4.6) in which the central segment of the cross-girdle fabric intersects the foliation at right angles to the mineral lineation. By analogy with both numerical simulations and analog modeling of fabric development (e.g. Lister & Williams 1979; Lister & Hobbs 1980; Jessell & Lister 1990; Herwegh & Handy 1996) this geometric relationship between crystal and grain shape fabrics strongly indicates that the mineral lineation has developed parallel to the maximum principal axis of the associated strain ellipsoid - see above sections on strain analysis.

In all quartzite samples both internal and external skeletal symmetry fabric parameters are consistent with a top to the WNW shear sense, although the C2-C1 external fabric parameter only indicates a small asymmetry in comparison with the

Sample	C1	C2	C1+C2	βbf	βmax	βmin	ω1	ω2	Temp°C
M.2	37	47	84	31	36	27	0	90	680
Q.1	29	30	59	14	18	11	13	43	470
Q.2	21	30	51	11	15	7	5	48	405
Q.3	26	27	53	11	15	8	11	28	420
Q.4	25	27	52	12	17	6	7	22	410
Q.5	26	33	59	13	18	10	7	48	470
Q.6	26	31	57	15	19	10	7	50	450
Q.7	27	28	55	11	15	9	8	42	440
Q.8	24	30	54	11	15	7	10	31	430
Q.9	23	26	49	5	8	3	10	26	400
Q.10	25	28	53	8	13	4	9	30	420
Q.11	27	30	57	14	19	10	11	44	450
Q.12	27	31	57	13	17	11	11	54	460

Table 4.2 Internal and external fabric asymmetry parameters for mylonitic Moine psammites (sample M-2) and Cambrian quartzites (Q1-Q12) in the APM stream section; explanation of parameters given in Fig. 4.5. Deformation temperatures inferred from quartz c-axis fabric opening angles (C1+C2), using the Kruhl (1998) fabric thermometer, are also shown. Samples arranged in order of structural position - see Fig. 2.4

other external (β) and internal (ω2 - ω1) parameters (Table 4.2). The sample of mylonitic Moine (M2) collected at the top of the stream section is also characterized by an asymmetric cross-girdle fabric (Fig. 4.7) in which all external and internal fabric asymmetry parameters (Table 4.2) are consistent with a top to the WNW shear sense. However, the degree of asymmetry for all internal and external skeletal parameters in sample M.2 is greater than in the underlying Cambrian quartzites.

Opening angles (C1 + C2) for cross-girdle c-axis fabrics measured on individual mylonitic quartzite samples using detrital grains range between 49° and 59°. Kruhl (1998) has observed an approximately linear correlation between previously reported quartz c-axis fabric opening angles and deformation temperatures in a wide range of tectonic environments, and has proposed that fabric opening angle may be used as a deformation thermometer, assuming that deformation temperature is the primary factor controlling opening angle. Using the Kruhl (1998) thermometer - as adapted by Morgan and Law (2004), the 49°-59° range in opening angles measured on the detrital quartz grain fabrics would indicate deformation temperatures of c. 395-470 °C. These temperature estimates are in broad agreement with deformation temperatures indicated by quartz recrystallization microstructures in these mylonites using the microstructural thermometer proposed by Stipp et al. (2002) - see Chapter 6.

No convincing correlation between opening angle/inferred deformation temperature and structural position has been observed in these mylonitic Cambrian quartzites (cf. Figs. 4.6, 4.7 and Table 4.2). These estimated deformation temperatures are broadly compatible with greenschist facies conditions traditionally thought to characterize penetrative (crystal plastic) deformation in the immediate hanging wall and footwall of the Moine thrust, although Johnson et al. (1985) have previously argued, based on illite crystallinity data, that deformation at least in the Assynt region occurred under lower greenschist (c. 300-400 °C) rather than upper greenschist (c. 400-500 °C) conditions. It must be kept in mind, however, that in addition to deformation temperature, fabric opening angles may increase with increasing hydrolytic weakening or decreasing strain rate (see discussions by Lister & Dornsiepen 1981, Morgan & Law 2004).

Given the lack of diagnostic mineral assemblages in the APM stream section, a thermometer that is independent of strain rate and potential hydrolytic weakening is clearly needed here. Although beyond the scope of our present study, the Ti in quartz thermometer (see reviews by Kohn & Northrup 2009, Thomas et al. 2010) may offer a way forward, although the relatively low temperatures associated with deformation adjacent to the Moine thrust plane would make application of this thermometer problematic due to the very low expected concentrations of Ti in quartz under greenschist facies conditions (Thomas et al. 2010, their figure 8).

In contrast to opening angles of 49-59° measured in the mylonitic Cambrian quartzites, an opening angle of 84° was measured in sample M2 (Type 2 cross-girdle fabric) from the mylonitic Moine meta-sedimentary rocks at the top of the APM stream section (Table 4.2). Taking the Kruhl (1998) thermometer at face value, this opening angle would indicate a deformation temperature of c. 670 °C which is clearly incompatible with deformation under greenschist facies conditions. The anomalously large opening angle could be explained by focused hydrolytic weakening within these rocks located in the immediate hanging wall to the Moine thrust. We do note, however, that this sample of Moine psammite contains relic garnet clasts with wings of brick-red pleochroic biotite aligned parallel to the mylonitic foliation (see Chapter 3). The sense of asymmetry of the biotite wings on

the garnet clasts is consistent with a top to the WNW shear sense. Although it could be argued that the garnet grains are either detrital or related to an earlier (e.g. Grampian) phase of metamorphism, the presence of locally pristine pleochroic biotite that has demonstrably developed during thrust-related mylonitization would indicate an absolute minimum of upper greenschist facies conditions for these tectonites. Similar microstructural observations at this structural level have previously been made by Read (1931, pp. 46-50) and Bailey (1955, pp. 114-117) from mylonites in the Ben Hee - Loch More area along strike to the north of the APM stream section - see also discussion by Law & Johnson (2010, pp. 483).

Summary

1. 3D strain analysis of the mylonitic Cambrian quartzites exposed in the APM stream section indicate deformation within the general flattening field, with a maximum principal stretching of 90-140% parallel to the WNW thrust transport direction. The analysis also indicates a moderate stretching of 10-40% along orogenic strike as well as a sub-vertical shortening of 55-65% perpendicular to the gently dipping mylonitic foliation. These strain estimates assume a constant volume deformation. A volume loss of 20-50% would be required to explain the calculated strains in terms of a plane strain deformation, with no stretching along orogenic strike.
2. Optical microscopy indicates that the mylonitic Cambrian quartzites and overlying Moine psammites are characterized by well-developed, asymmetrical Type-2 (Moine) and Type-1 (Cambrian quartzite) cross girdle c-axis fabrics. In each sample, the asymmetry is indicative of a top-to-the-WNW shear sense, which is compatible with the known transport direction for the Moine thrust zone. Qualitatively the asymmetric fabrics indicate a non-coaxial flow in the footwall (Aisinnan imbricates) and hanging wall to the Moine thrust, although internal skeletal parameters ($\omega 2$-$\omega 1$) are more asymmetric than external parameters (C2-C1), and Moine mylonites above the thrust plane exhibit greater fabric asymmetries than mylonitic quartzites beneath the thrust.

3. Estimated deformation temperature for the footwall mylonitic Cambrian quartzites range from 395-470 °C using the Kruhl (1998) thermometer and opening angles taken from quartz c-axis fabrics measured on plastically deformed detrital grains. Similar deformation temperatures are indicated by quartz recrystallization microstructures in these tectonites (see Chapter 6) using the microstructural thermometer proposed by Stipp et al. (2002). These inferred deformation temperatures are broadly compatible with the traditional assumption that mylonitization along the leading edge of the Moine nappe occured under greenschist facies conditions, although our microstructural and fabric data would indicate upper, rather than lower, greenschist facies conditions, as has commonly been assumed from the local presence of chlorite in these mylonites.
4. Significantly higher deformation temperatures are indicated by fabric opening angles in the overlying mylonitic Moine psammites of the APM stream section. The higher opening angles in these hangingwall mylonites could, alternatively be explained by focused hydrolytic weakening, but the local presence of pristine pleochroic brick-red garnet, which is demonstrably synchronous with top to the WNW shearing and mylonite formation, may also indicate significantly higher deformation temperatures.

References Cited:

BAILEY, E. B. 1955. Moine tectonics and metamorphism in Skye. *Transactions of the Edinburgh Geological Society*, **16**, 93-166.

BORRADAILE, G.J., 1984. Strain analysis of passive elliptical markers: success of de-straining methods. *Journal of Structural Geology,* **6**, 433–437.

CHEW, D.M. 2003. An Excel spreadsheet for finite strain analysis using the R_f/phi technique. *Computers & Geosciences*, **29**, 795-799.

DAYAN, H. 1981. *Deformation studies of the folded mylonites of the Moine Thrust, Eriboll District, Northwest Scotland* [Ph.D. thesis]: University of Leeds.

DUNNET, D. 1969. A technique of finite strain analysis using elliptical particles. *Tectonophysics*, **7**, 117-136.

DUNNET, D. & SIDDANS, A.W.B. 1971. Non-random sedimentary fabrics and their modification by strain. *Tectonophysics*, **12**, 307-325.

HERWEGH, M. & HANDY, M.R. 1996. The evolution of high-temperature mylonitic microfabrics; evidence from simple shearing of a quartz analogue (norcamphor). *Journal of Structural Geology*, **18**, 689-710.

HOBBS, B.E., MEANS, W.D., & WILLIAMS, P.F. 1976. An outline of structural geology. John Wiley & Sons, Inc., New York, NY. 571 pp.

JESSEL, M.W. & LISTER, G.S. 1990. A simulation of temperature dependence of quartz fabrics. In: Knipe, R.J. & Rutter, E.H. (eds), *Deformation Mechanisms, Rheology and Tectonics.* Geological Society of London, Special Publications, **54**, 353-362.

JOHNSON, M.R.W., Kelley, S.P., Oliver, G.J.H., Winter, D.A., 1985. Thermal effects and timing of thrusting in the Moine thrust zone. *Journal of the Geological Society of London*, **142**, 863–874.

KOHN, M.J., NORTHRUP, C.J., 2009. Taking mylonites' temperatures. *Geology,* **37**, 47-50

KRUHL, J.H., 1998, Reply: Prism- and basal-plane parallel subgrain boundaries in quartz: a microstructural geothermobarometer. *Journal of Metamorphic Geology*, **16**, 142-146.

LAW, R.D., 1990. Crystallographic fabrics: a selective review of their applications to research in structural geology. *In:* Knipe, R.J., Rutter, E.H. (eds) *Deformation Mechanisms, Rheology and Tectonics*. Geological Society, London, Special Publications, **54**, 335-352.

LAW, R.D. & JOHNSON, M.R.W. 2010. Microstructures and crystal fabrics of the Moine thrust zone and Moine Nappe; history of research and changing tectonic interpretations. *In:* Law, R.D., Butler, R.W.H., Holdsworth, R., Krabbendam, M. & Strachan, R. (eds) *Continental Tectonics and Mountain Building - The Legacy of Peach and Horne*. Geological Society, London, Special Publications, **335**, 443-503.

LAW, R.D., MAINPRICE, D.H., CASEY, M., LLOYD, G.E., KNIPE, R.J., COOK, B., & THIGPEN, J.R., 2010. Moine thrust zone mylonites at the stack of Glencoul I - microstructures, strain and influence of recrystallization on quartz crystal fabric development. *In:* Law, R.D., Butler, R.W.H., Holdsworth, R., Krabbendam, M., Strachan, R. (eds), *Continental Tectonics and Mountain Building – The Legacy of Peach and Horne*. Geological Society, London, Special Publications, **335**, 543-577.

LISLE, R.J. 1977. Estimation of the tectonic strain ratio from the mean shape of deformed elliptical markers. *Netherlands Journal of Geosciences*, **56**, 140-144.

LISLE, R.J. 1985. Geological strain analysis; a manual for the R_f/phi technique, Pergamon Press, 99 p.

LISTER, G.S. 1977. Discussion; crossed-girdle c-axis fabrics in quartzites plastically deformed by plane strain and progressive simple shear. *Tectonophysics*, **39**, 51-54.

LISTER, G.S. & WILLIAMS, P.F. 1979. Fabric development in shear zones; theoretical controls and observed phenomena. *Journal of Structural Geology*, **1**, 283-297.

LISTER, G.S. & HOBBS, B.E. 1980. The simulation of fabric development during plastic deformation and its application to quartzite: the influence of deformation history. *Journal of Structural Geology*, **2**, 355-371.

LISTER, G.S. & DORNSIEPEN, U.F. 1982. Fabric transitions in the Saxony granulite terrain. *Journal of Structural Geology*, **4**, 81-93.

MORGAN, S.S. & LAW, R.D. 2004. Unusual transition in quartzite dislocation creep regimes and crystal slip systems in the aureole of the Eureka Valley-Joshua Flat-Beer Creek Pluton, California: a case for anhydrous conditions created by decarbonation reactions. *Tectonophysics*, **384**, 209-231.

MULCHRONE, K.F. & MEERE, P.A. 2001. A Windows program for the analysis of tectonic strain using deformed elliptical markers. *Computers & Geosciences*, **27**, 1251-1255.

PASSCHIER, C.W. & TROUW, R.A.J., 2005. Micro-tectonics, Second Edition Springer, 366 pp.

PEACH, B.N., HORNE, J., GUNN, W., CLOUGH, C.T., HINXMAN, L.W. & CADELL, H.M. 1888. Report on recent work of the Geological Survey in the N.W. Highlands of Scotland, based on field notes and maps. *Quarterly Journal of the Geological Society, London*, **64**, 378-441.

PEACH, B.N., HORNE, J., GUNN, W., CLOUGH, C.T., HINXMAN, L.W. & TEALL, J.J.H. 1907. *The Geological Structure of the North-West Highlands of Scotland.* Memoir of the Geological Survey of Great Britain.

RAMSAY, J.G. 1967. A re-interpretation of the mechanics of the Ben Sgriol fold, Loch Hourn (northwest Scotland); a reply. *Tectonophysics,* **5**, 63-67.

RAMSAY, J.G. & WOOD, D.S. 1973. The geometric effects of volume change during deformation processes. *Tectonophysics*, **16**, 263-277.

READ, H.H. 1931. *The Geology of Central Sutherland (Sheets 108 and 109).* British Geological Survey Memoir, 238pp.

SCHMID, S.M. & CASEY, M. 1986. Complete fabric analysis of some commonly observed quartz c-axis patterns. In: Hobbs, B.E. & Heard, H.C. (eds) *Mineral and Rock Deformation Laboratory Studies: The Paterson Volume.* American Geophysical Union, Geophysical Monograph **36**, 263-286.

STIPP, M., STUNITZ, H., HEILBRONNER, R. & SCHMID, S. 2002. Dynamic recrystallization of quartz: correlation between natural and experimental conditions. In: De Meer, S., Drury, M.R., De Bresser, J.H.P. & Pennock, G.M. (eds) *Deformation Mechanisms, Rheology and Tectonics: Current Status and Future Perspectives.* Geological Society, London, Special Publications, **200**,171-190.

STRINE, M. & WOJTAL, S.F., 2004. Evidence for non-plane strain flattening along the Moine thrust, Loch Srath nan Aisinnin, North-West Scotland. *Journal of Structural Geology,* **26**, 1755–1772.

THOMAS, J.B., WATSON, E.B., SPEAR, F.S., SHEMELLA, P.T., NAYAK, S.K. & LANZIROTTI, A. 2010. TitaniQ under pressure: the effect of pressure and temperature on the solibility of Ti in quartz. *Contributions to Mineralogy and Petrology,* **160,** 743-759.

Chapter 5: Vorticity of flow, vertical thinning, and transport parallel extension

Abstract

This Chapter presents quantitative data from the APM stream section on flow vorticities associated with mylonitization in the hanging wall and footwall of the Moine Thrust. Independent estimates of flow vorticities were obtained using three analytical techniques. Estimated vorticity numbers (Wm), in general, range from approximately 0.75 - 0.90 (45-30% pure shear). For partially recrystallized Cambrian quartzites in the footwall to the Moine thrust, vorticity data was integrated with 3D strain data (Chapter 4) to estimate (assuming constant volume deformation) both shortening values perpendicular to the gently dipping flow plane, and extension values oriented parallel to the transport direction within the flow plane. Shortening estimates for individual quartzite samples ranged between 20-45%, while estimated transport-parallel extension values ranged between 20-50%.

Introduction

In this chapter, the mylonites exposed in the APM stream section are analyzed to determine flow vorticities associated with thrust-related deformation. 3D strain analyses reported in Chapter 4 indicate that deformation of the Cambrian quartzites located in the footwall of the Moine thrust, beneath the mylonite sheet mapped by the geological survey (Geological Survey 1923, BGS 2007), occurred in the general flattening field, with maximum principal stretching parallel to the WNW directed thrust transport. Strain analyses of the quartzites also indicate an intermediate principal stretch parallel to orogenic strike, and a maximum principal shortening perpendicular to the gently dipping foliation.

The plastically deformed Cambrian quartzites exposed in the APM stream section have proved suitable for three methods of vorticity analysis: Method 1 – the rigid grain (primarily feldspar and epidote clasts in matrix of dynamically recrystallized quartz) orientation method of Wallis et al (1993); Method 2 – the oblique dynamically recrystallized grain / quartz c-axis fabric method of Wallis (1992, 1995); and Method 3 – the Rxz strain ratio / quartz c-axis fabric method of Wallis (1992, 1995). Each of these methods uses data collected from thin sections cut perpendicular to foliation and parallel to the observed lineation in hand sample.

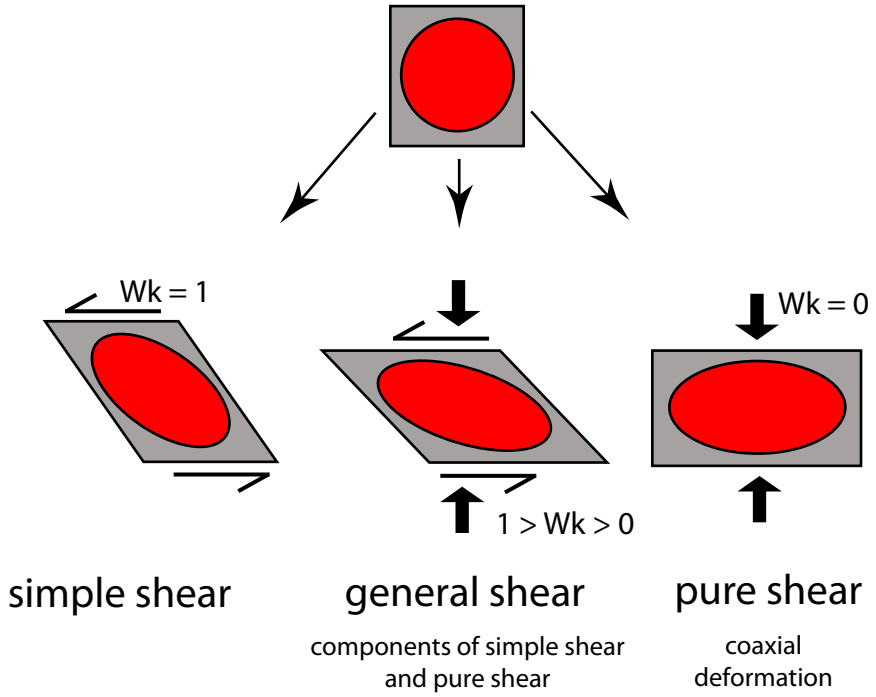

Figure 5.1 Spectrum of potential flow types for plane strain deformation. Wk values between 1 and 0 for general shear indicate varying contributions of simple and pure shear end members.

All three methods assume: a) steady state flow; b) that the vorticity vector is oriented perpendicular to the maximum and minimum principal axes of finite strain; and c) that flow was either orthorombic or monclinic, rather than triclinic (cf. Jiang 1998, Iacopini et al. 2007). Within the samples analyzed, the assumption of monoclinic or higher symmetry flow is strongly supported by the orientation of associated cross-girdle quartz c-axis fabrics (Chapter 4) with respect to sample coordinates, the fabric skeleton intersecting foliation parallel to the intermediate principal strain direction (Y).

For plane strain deformation, flow can be quantified in terms of the kinematic vorticity number, Wk (Means et al. 1980) that ranges between 1.0 (simple shear and 0.0, (pure shear) with general shear flows occurring under 1>Wk>0 conditions (Fig. 5.1). Equal contributions of pure and simple shear to a general flow are made at Wk = 0.71 (Law et al. 2004). In natural systems the vorticity of flow may vary with both position and time; see discussions by Fossen & Tikoff (1997, 1998) and Jiang (1998). Therefore, in natural deformation the flow is better

characterized by the mean kinematic vorticity number, Wm, where the vorticity of flow is envisaged as being integrated over space and time (Passchier, 1988). In cases of steady-state deformation, Wk=Wm. For the purposes of this study, vorticity data from the APM stream section are reported in terms of Wm.

Method 1 – Rigid Grains

The rigid grain method(s) is based on the assumption that rigid particles will rotate within a homogenously flowing matrix. The method employed in our analyses was first proposed by Wallis et al. (1993). The method assumes that no mechanical interaction occurs either between adjacent rigid grains, or between rigid grains and the plastically flowing matrix grains, as the rigid grains bodily rotate during progressive deformation. The pivotal step in this analytical method is determining a critical rigid grain aspect ratio (Rc) that separates grains with high aspect ratios (R > Rc) that have rotated to a stable preferred alignment during progressive deformation, from grains of lower aspect ration (R<Rc) that have continued to rotate and hence exhibit a random orientation (Fig. 5.2). Wallis et al. (1993) have proposed a simple relationship between vorticity number Wm and critical aspect ratio Rc (Fig. 5.2).

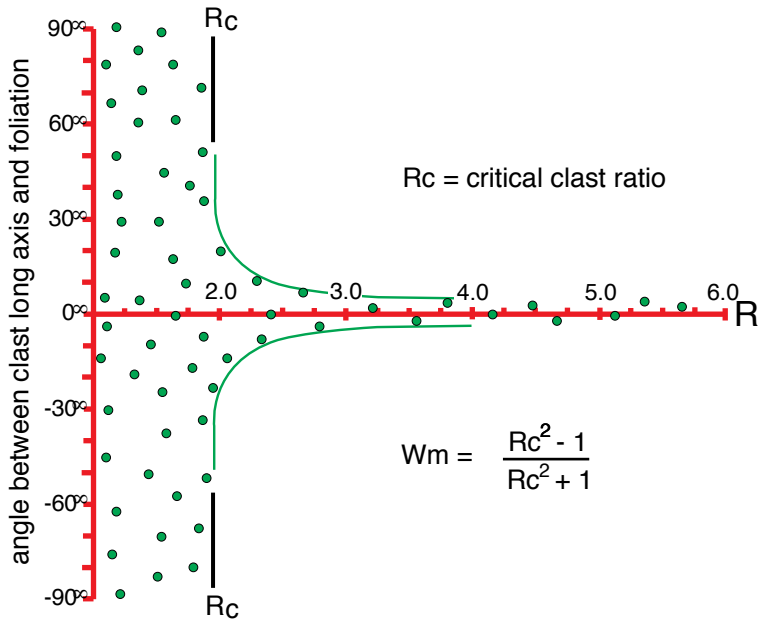

Figure 5.2 Schematic illustration of the Wallis et al. (1993) rigid grain plot; R - ratio of grain long / short axis. The Rc value represents the critical aspect ratio separating grains that infinitely rotate from grains that have rotated to a stable preferred alignment at a low angle to foliation. In the simplified case illustrated, Rc = 2.0, and infinitely rotating grain aspect ratios range between 1.0-2.0. The vorticity value, Wm, is determined by the relationship shown.

In the footwall Cambrian quartzites from the APM stream section, feldspar constitutes the most common type of rigid grain, while rigid grains of epidote and opaque minerals are recorded in some samples. Rigid grains of feldspar and opaque minerals are also present in the overlying Moine psammites, but in these hanging wall rocks rigid epidote grains are more abundant than in the footwall quartzites. In the footwall quartzites the rigid grains are embedded in a matrix of plastically flowing and dynamically recrystallized quartz with a minor amount of white-mica/chlorite. In the hanging wall Moine rocks the rigid grains are also embedded in a matrix of dynamically recrystallized quartz, but in these tectonites phyllosilicates (white mica, chlorite, biotite) make up a greater proportion of the matrix.

For each sample analyzed the aspect ratio (ratio of long to short axis) and orientation (with respect to foliation) of individual rigid grains were measured manually in thin sections cut perpendicular to foliation and parallel to lineation using an optical microscope and mechanical stage. Only rigid grains that were widely separated from their neighboring rigid grains were included in this analysis. Areas of the thin sections containing closely-spaced rigid grain were not included in the analyses as neighboring grains may have influenced each other's rotation history. Additionally, in some areas trails of rectangular feldspar fragments indicate that these clasts have been produced by break-up of larger parent grains along crystallographic cleavage planes, rather than acting as isolated rotating clasts throughout the deformation history.

Rigid grain plots for Cambrian quartzite and Moine samples from the APM section are shown in Figures 5.3 and 5.4, respectively; the plots are arranged in order of descending structural position (cf. Fig. 2.4) from sample M2 (Fig. 5.4) located at 50m above the Moine thrust (as defined by the Geological Survey 1923), to sample Q.12 (Fig. 5.3) at 90m beneath the thrust. In rigid grain plots for naturally deformed rocks there is commonly no unique and clear-cut Rc value separating randomly oriented clasts from higher aspect clasts with a strong preferred alignment. In such cases the range of Wm values consistent with the minimum and maximum Rc values (Rc_{min} and Rc_{max}) may be calculated (Law et al. 2004).

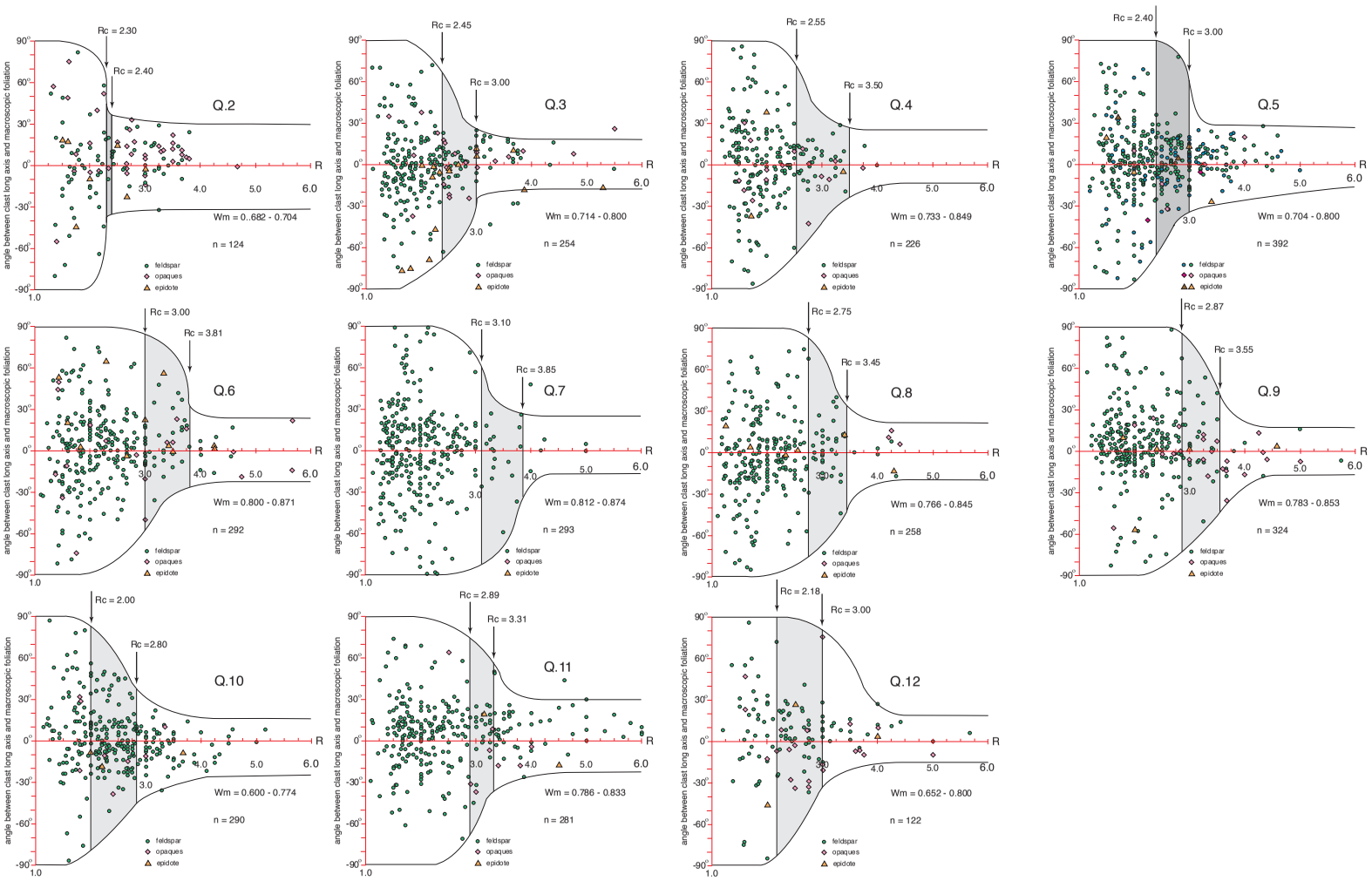
Q.2
Rc = 2.30
Rc = 2.40
Wm = 0..682 - 0.704
n = 124
Q.3
Rc = 2.45
Rc = 3.00
Wm = 0.714 - 0.800
n = 254
Q.4
Rc = 2.55
Rc = 3.50
Wm = 0.733 - 0.849
n = 226
Q.5
Rc = 2.40
Rc = 3.00
Wm = 0.704 - 0.800
n = 392
Q.6
Rc = 3.00
Rc = 3.81
Wm = 0.800 - 0.871
n = 292
Q.7
Rc = 3.10
Rc = 3.85
Wm = 0.812 - 0.874
n = 293
Q.8
Rc = 2.75
Rc = 3.45
Wm = 0.766 - 0.845
n = 258
Q.9
Rc = 2.87
Rc = 3.55
Wm = 0.783 - 0.853
n = 324
Q.10
Rc = 2.00
Rc =2.80
Wm = 0.600 - 0.774
n = 290
Q.11
Rc = 2.89
Rc = 3.31
Wm = 0.786 - 0.833
n = 281
Q.12
Rc = 2.18
Rc = 3.00
Wm = 0.652 - 0.800
n = 122
angle between clast long axis and macroscopic foliation
feldspar
opaques
epidote
R

Figure 5.3 On the previous page, rigid grain plots for Cambrian quartzites (Q2-12) of the APM stream section. The area marked in grey shows the range of uncertainty (Rc_{min} - Rc_{max}) in determining a critical aspect ratio (Rc) that may be used for estimating Wm values based on the equation in Figure 5.1.

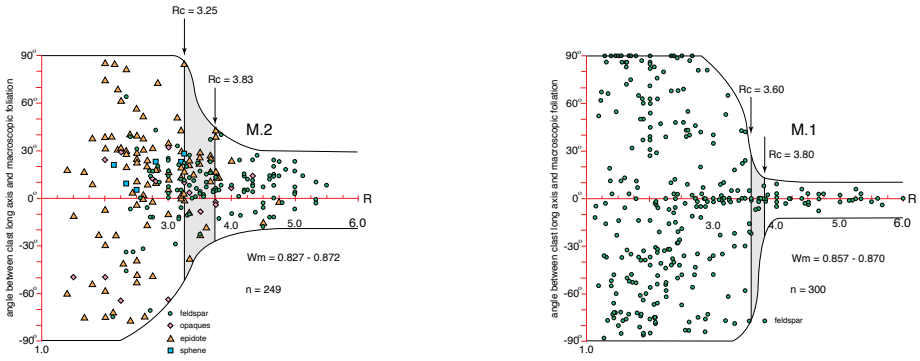

Figure 5.4 Rigid grain plots for mylonitic Moine psammites, samples M.2 & M.1. The area marked in grey shows the range of uncertainty (Rc_{min} - Rc_{max}) in determining the critical aspect ratio (Rc) used for estimating Wm values based on the equation in Figure 5.2.

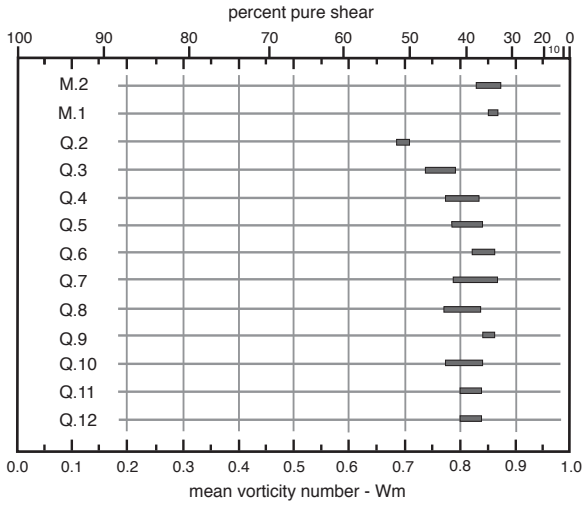

Figure 5.5 Bar charts indicating degree of uncertainty in estimating Wm using Method 1 rigid grain data. Wm estimates based on rigid grain data taken from two thin sections from each sample; see text for discussion. Samples from the APM stream section are arranged in descending order of structural position with Moine psammite M.2 and M.1 located above the thrust plane and Cambrian quartzites Q-2 - Q 12 located beneath the thrust. There is a slight apparent decrease in footwall vorticity values traced upwards towards the thrust. Above the thrust plane estimated vorticity values are higher. Data indicate that the footwall section was dominated by simple shear (55-65%) with pure shear becoming more important close to the thrust plane.

Estimated ranges in Wm values for the APM stream section samples are displayed as bar charts in Figure 5.5. The Wm values range between 0.775 - 0.85, indicating a general shear flow that was dominated by simple shear (55-65% simple shear component). Estimated vorticity values are essentially constant (Wm = 0.78-0.85) in the lower part of the measured section of Cambrian quartzites (samples Q.12 - Q.5) but progressively decrease slightly traced towards the overlying thrust plane in the upper part of the section (samples Q.4 - Q.2) with sample Q.2 located at approximately 20m below the thrust plane, having a Wm value of c. 0.7 (c. 50% simple shear). This is the reverse trend of what intuitively might be

expected approaching a thrust plane (cf. Law et al. 1986). In contrast, Moine samples M.1 and M.2 located 44-51m above the thrust plane yielded the highest estimated Wm values (0.83 - 0.87) indicating a dominance of simple shear in the immediate hangingwall to the thrust plane.

In order to determine a robust estimate of Rc, and hence Wm, using the rigid grain plot it is essential that clasts with an aspect ratio close to Rc that have a wide range of orientations (Fig. 5.2) are present in the thin section. In cases where only clasts with aspect ratios significantly less than Rc have a wide range of orientations, there is a greater uncertainty in determining Wm because of the greater numerical range of uncertainty in determining Rc min and Rc max (Fig. 5.6). This was a problem using a single thin section cut from some APM stream section samples. In order to more clearly define the likely range of Rc values a second thin section was cut and analyzed, when needed, from the same rock billet and analyzed, with grains of critical aspect ratio and orientation (high angle to foliation) preferentially being searched for. Rigid grain plots shown in Fig. 5.3 and bar charts for resultant Wm values shown in Fig. 5.5 include data from these additional thin sections. For comparison purposes bar charts for estimated Wm values using only Rc values

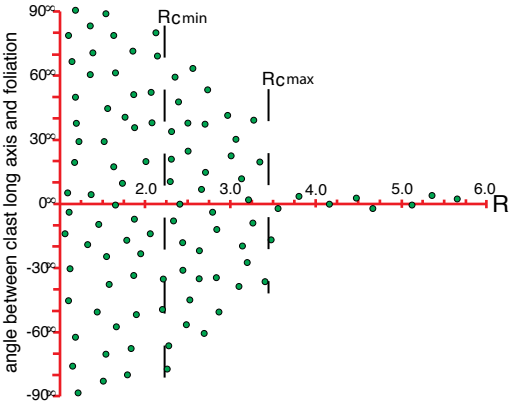

Figure 5.6 Schematic illustration of the Wallis (1993) rigid grain plot; adapted to illustrate the effect of uncertainty in determining Wm values in cases where only clasts with aspect ratios significantly less than Rc are present.

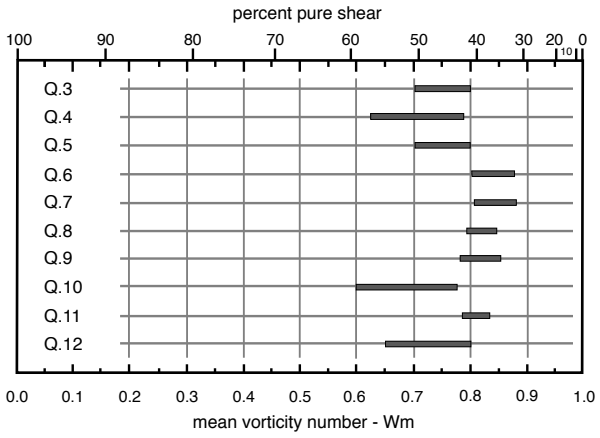

Figure 5.7 Bar charts showing Wm values estimated by Method 1 based on rigid grain data from a single thin section; i.e. before critical data from a second thin section were included in the analysis (cf. Fig. 5.4); see text for discussion. Use of data from a second thin section allowed Wm values to be estimated for sample Q.2. Data from the first thin section was insufficient to determine Rc and hence Wm. Sample M.2 did not require a second thin section due to the abundance of suitable rigid grain markers

estimated from rigid grains in a single thin section are shown in Figure 5.7. This practice of including additional critical data (where present) from a second thin section reduced the degree of uncertainty in estimating Wm values (samples Q.3, 4, 10 and 12; cf. length of bars in Figs. 5.5 and 5.7) and always resulted in an increase in estimated minimum Wm values.

Method 2 – Oblique grain shape alignment

This method of vorticity analysis was originally proposed by Wallis (1992, 1995) and is based on determining the acute angle between the flow plane and the instantaneous stretching axes (ISA). The method is summarized in Figure 5.8 and employs both the observed obliquity in thin section between foliation and elongate dynamically recrystallized quartz grains and skeletal analysis of associated Type 1 (Lister 1977) cross-girdle c-axis fabrics. As mentioned in the previous chapter, the orientation of the flow plane is determined by drawing a line perpendicular to the central segment of the cross-girdle fabric (Fig. 5.8a). The ISA is then determined by measuring the angles between the dynamically recrystallized grains (Sb) and the observed foliation in the XZ thin section (Fig. 5.8b). From this population of grains, the ISA is interpreted to be oriented parallel to the long axis of the dynamically recrystallized grain at the highest angle (θ max) of obliquity to foliation. From these crystal fabric and microstructural data, Wm can then be estimated (Fig. 5.8b).

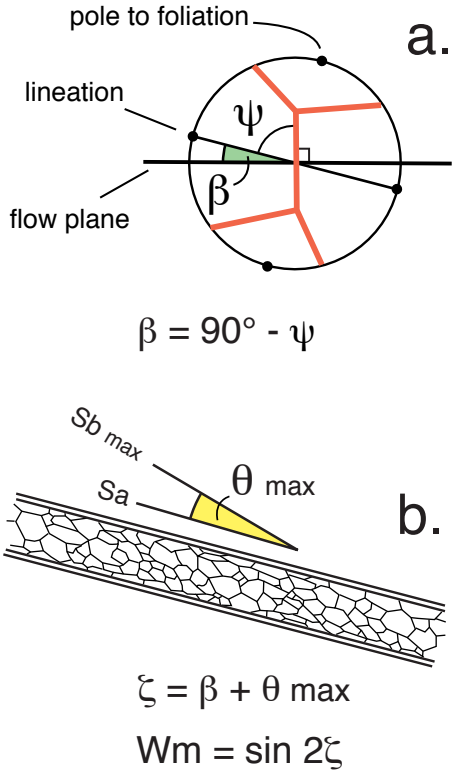

Figure 5.8 Summary of (a) crystal fabric and (b) microstructural input parameters used in Method 2 vorticity analysis; after Law (2010) and adapted from Wallis (1995) and Xypolias et al. (2001).

θ max was determined by measuring the angles between foliation and the long axes of adjacent elongate dynamically recrystallized quartz grains in XZ thin

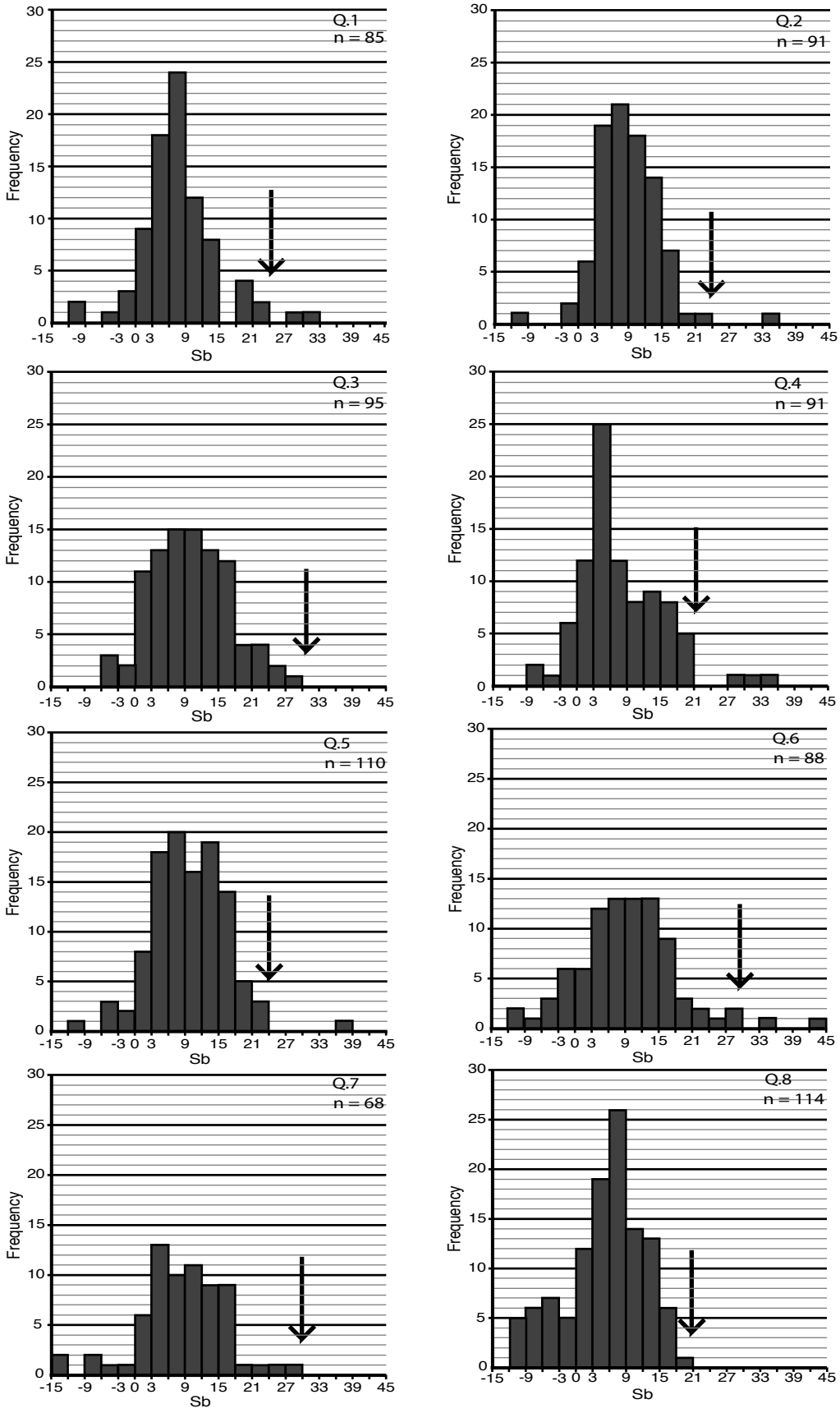
Q.1
n = 85
Q.2
n = 91
Q.3
n = 95
Q.4
n = 91
Q.5
n = 110
Q.6
n = 88
Q.7
n = 68
Q.8
n = 114
Frequency
Sb
0
5
10
15
20
25
30
-15 -9 -3 0 3 9 15 21 27 33 39 45

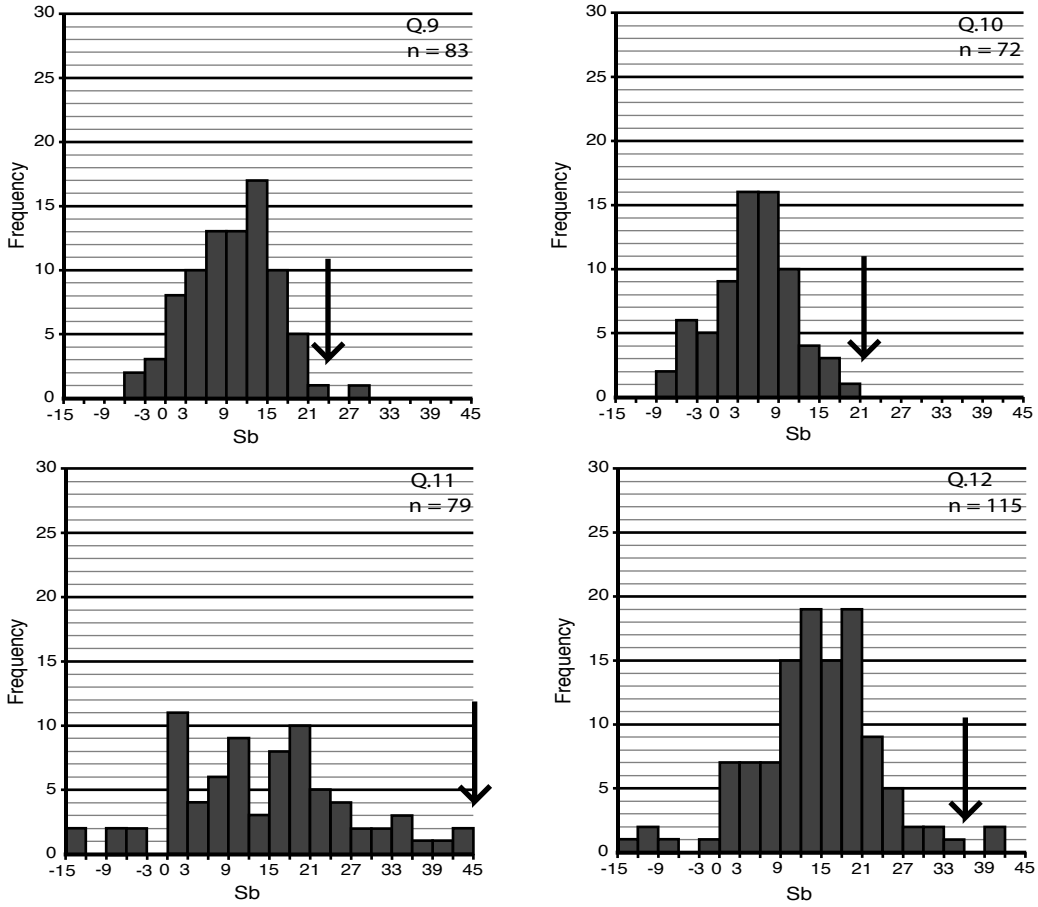

Figure 5.9 Histograms showing frequency distribution of obliquity between foliation and Sb fabrics in the APM stream section. The maximum angle of obliquity is interpreted to be the highest of the continuous Sb values. Outliers that are not continuous with the rest of the distribution are discounted. The range in Sb fabric obliquities is generally between 20-40°. These values are used for the Method 2 vorticity analysis based on the relationships proposed by Wallis (1992, 1995).

sections and plotting the data as histograms (Fig. 5.9). Plotting of the data reveals that there is frequently uncertainty in what θ value should be taken as θ max, as there are frequently a small number of grains forming outliers from the main population of grains at higher θ values. There is no generally accepted protocol for deciding which grain orientation should be taken as indicating θ max in such cases. Following several recent studies of this problem (e.g. Frassi et al. 2009; Langille et al. 2010; Law 2010; Xypolias et al. 2010; Xypolias 2010; but cf. Johnson et al. 2009) the maximum θ value indicated by the continuous population of grain orientations was used here.

This second method of vorticity analysis was found to be appropriate for the majority of the mylonitic Cambrian quartzites exposed in the APM stream section as

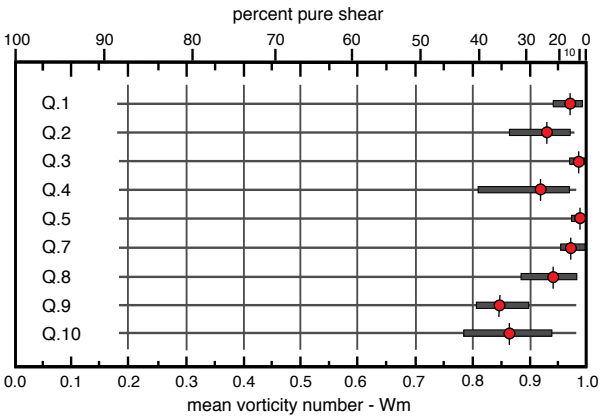

Figure 5.10 Bar charts indicating degree of uncertainty in estimating Wm values using combined crystal fabric and oblique dynamically recrystallized grain shape data (Method 2). APM stream section samples are arranged in descending order of structural position beneath the Moine thrust as defined by Geological Survey (1923). Red circles indicate Wm value that corresponds to the β best-fit value and gray bars indicate degree of uncertainty in estimating Wm max and Wm min values from visually estimated βmin and βmax values (Table 4.2). The Wm estimates from this method are generally higher than those from Method 1. Highest Wm values based on Method 2 are observed in the middle of the Cambrian quartzite section (samples Q.3, 5 and 7) and adjacent to the overlying thrust (sample Q.1).

these are almost ubiquitously characterized by well developed Type-1 cross girdle fabrics (described in Chapter 4) and the majority of quartzites also have an oblique alignment of dynamically recrystallized grains in XZ thin section. The estimated Wm values based on Method 2 analyses are shown in Figure 5.10, where the length of error bars represent the degree of uncertainty in Wm values, based on the β_{min} and β_{max} values determined from skeletal analysis of the quartz c-axis fabrics (see Table 4.2). Wm values based on visual best fit β values are indicated by red circles (Fig. 5.10) that may, or may not, coincide with the arithmetic average of Wmin and Wmax values for individual samples. Wm estimates for the mylonitic Cambrian quartzites using Method 2 range between 0.85 and 0.99 (65-90% simple shear). These Wm estimates are significantly higher than Wm values independently estimated using the rigid grain method. This is a common observation in many studies of naturally deformed quartzites (e.g. Law 2010; see discussion by Xypolias 2010) and may indicate either that the two methods are recording different parts of the flow history or that they are recording different minimum estimates of a true Wm value (e.g. Johnson et al. 2009, Stahr & Law in review).

A major caveat that must currently be placed on Method 2 analyses from the APM stream section is that only quartz-c-axis fabrics measured on plastically deformed detrital grains have so far been measured and used as input data. For rigorous estimation of Wm values using Method 2 the c-axis fabrics of the

dynamically recrystallized quartz grains in these mylonites must be measured and used as input data.

Method 3 – Rxz strain ratio/c-axis fabrics

This method was originally proposed by Wallis (1992, 1995) and for the APM stream section quartzites incorporates the β angle measured from quartz c-axis fabrics and Rxz strain ratio data based on the deformed relict quartz grains (see Chapter 4). Method 3 is summarized in Figure 5.11 and β angles used are best- fit, maximum and minimum β angles, as compiled in Table 4.2. Because two methods were used for determining Rxz strain ratios from, the Rf/phi data (Chew 2003 and Mulchrone & Meere 2001), two Wm values using the different sets of strain data are reported for each sample using this method.

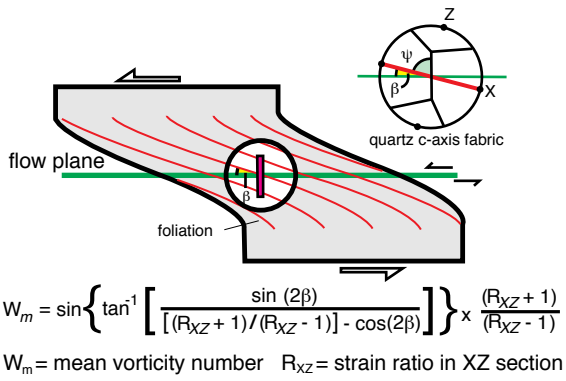

Figure 5.11 Schematic summary of Method 3 vorticity analysis adapted from Wallis (1995), where the β angle derived from quartz c-axis fabrics is used in conjunction with Rxz strain ratios to estimate Wm.

Vorticity estimates based on Method 3 are summarized in Figure 5.12. The length of error bars reflect the degree of uncertainty in Wm values based on the β_{min} and β_{max} values determined from skeletal analysis of the quartz c-axis fabrics (see Table 4.2). Wm values based on

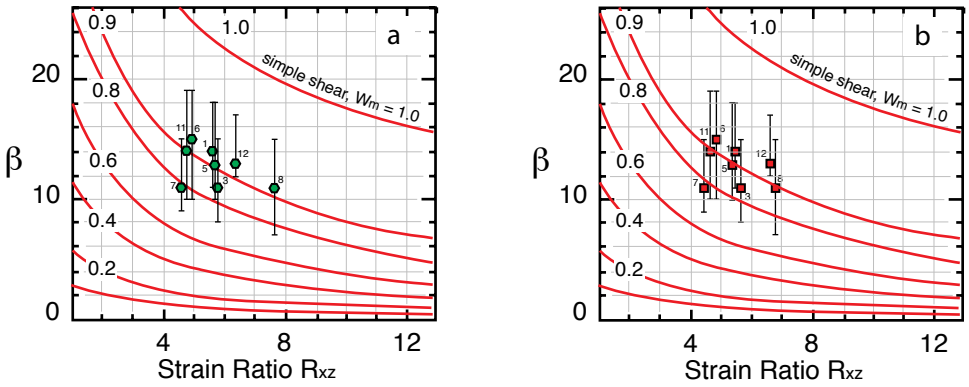

Figure 5.12 Vorticity numbers determined via Method 3 for Cambrian quartzites in the APM stream section. Strain data for (a) is taken from Table 4.1a and (b) from Table 4.1b, based on the Chew (2003) and Mulchrone & Meere (2001) strain analysis methods. These values are then coupled with β values from quartz c-axis fabrics (cf. Figure 4.6) measured by optical microscopy on detrital grains. Contours of equal vorticity number are indicated. The length of error bars represents the uncertainty associated with determining the β value from c-axis fabrics. Circles and squares indicate Wm values estimated from β best-fit value.

visual best-fit β values are indicated by circles in Figure 5.12. Comparison of Figures 5.12a and b indicates that this method of vorticity analysis is relatively insensitive to the small variation in strain values detected in the APM stream section, but is extremely sensitive to β values employed. This in turn is a reflection of the position that the APM stream section quartzites occupy in β - Rxz space (Fig. 5.12; see also general discussion by Grasemann et al. 1999, Law 2010). Estimated Wm values range between about 0.78 and 0.94 (60-75% simple shear). Figure 5.13 shows results from method 3 plotted as bar charts, with the samples listed relative to structural distance beneath the Moine thrust (as defined by Geological Survey 1923). The length of grey bars represent the error associated with determining the β value from c-axis fabric data and the red circles indicate the β best-fit value. In general, the Wm estimates fall between those of Method 1 and Method 2, showing no convincing correlation between vorticity number and distance beneath the thrust.

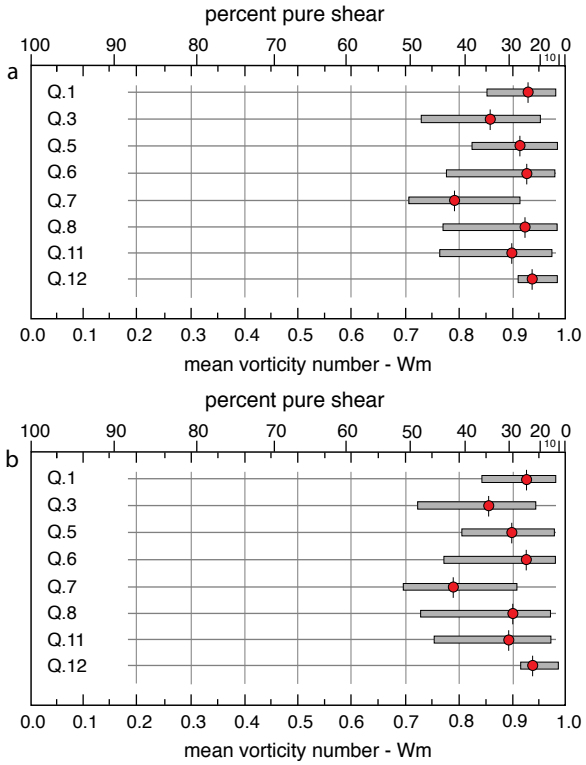

Figure 5.13 Bar charts indicating degree of uncertainty in estimating Wm values (Method 3) using combined crystal fabric and Rxz strain ratio data from (a) the Chew (2003) program and (b) Mulchrone & Meere(2001) program. Samples are arranged in descending order of structural position beneath the Moine thrust. Red circles represent Wm values calculated using the β best-fit angle; gray bars indicate degree of uncertainty in estimating Wm max and Wm min values from visually estimated βmin and βmax values, respectively. For each sample estimated Wm values are insensitive to differences in strain values. Wm estimates fall between those of Method 1 and Method 2, with no convincing correlation between vorticity number and distance beneath the thrust.

Comparison of vorticity methods

Data from the APM stream section indicate that the degree of uncertainty in estimating Wm using Method 3 is higher than in Methods 1 and 2 (compare length of bars for individual samples in Figures 5.4, 5.9 and 5.13) - at least when clasts of

critical aspect ratio/orientation are available for Method 1 analyses. This disparity of results is primarily a reflection of the difficulty in making a precise visual estimate of β values from even well-defined quartz fabric data, and the extreme sensitivity of Wm to variation in β values in Method 3 analyses (cf. lengths of Wm bars for samples Q.1, 5 and 6 in Figures 5.9, 5.12 and 5.13).

Wm estimates based on Method 1 are consistently lower for individual samples than estimates from Methods 2 and 3. Wm estimates from Method 1 are closer to Method 3 than Method 2 estimates. In some samples Method 2 analyses yield the highest Wm values (Q.5 and 7 in Figures 5.10 and 5.13) indicated by the three methods. This may be an artifact of using the sine function in Method 2 (Fig. 5.8b). Where the ζ value (Fig. 5.8) approaches 45° the resulting vorticity number will be closer to 1, basically indicating 100% simple shear deformation. Several samples from this study were not able to be included because the combined β and θ max angles were greater than 45°, contradicting the Means (1981) model for development of oblique grain shape fabrics.

Results from Methods 2 and 3 analyses do not indicate any convincing correlation between Wm value and structural position beneath the Moine thrust (as mapped by Geological Survey 1923), (Figs. 5.10 and 5.13). A weak correlation is observed between structural position and Wm values indicated by Method 1 with Wm values decreasing slightly traced upwards towards the thrust plane. As discussed above, however, this apparent trend seems counter intuitive (one might expect the simple shear component to increase towards the overlying thrust plane) and may be an artifact of uncertainty in the data.

Shortening and Extension

By integrating the vorticity and strain data from the mylonitic Cambrian quartzites, stretches perpendicular to the gently dipping flow plane and parallel to the transport direction may be calculated using numerical relationships originally proposed by Wallis et al. (1993), and illustrated in Figure 5.14. No shortening perpendicular to the flow plane would occur if deformation was by strict simple shear. The original formulation by Wallis et al. (1993) for calculating stretch

For plane strain at constant volume:

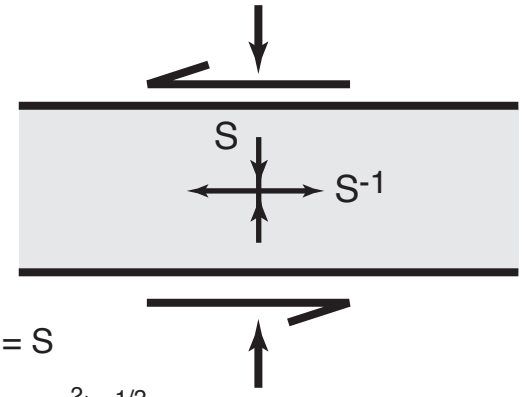

Thinning perpendicular to flow plane = S

$$S = \left\{ \frac{1}{2} \left(1 - W_k^2\right)^{1/2} \left[\left(R_{XZ} + R_{XZ}^{-1} + 2 \frac{(1 + W_k^2)}{(1 - W_k^2)} \right)^{1/2} + \left(R_{XZ} + R_{XZ}^{-1} - 2\right)^{1/2} \right] \right\}^{-1}$$

Stretch parallel to flow plane = S^{-1}

R_{XZ} = strain ratio in XZ section W_k = kinematic vorticity number

Figure 5.14 Schematic illustration of numeric relationships between Rxz strain ratios and vorticity numbers used to determine shortening perpendicular to the flow plane, based on Wallis et al. (1993). In cases of true plane strain deformation extension parallel to transport is simply the reciprocal of the shortening value (S-1). Since the strain analysis outlined in Chapter 4 indicates that quartzites from the APM stream section were deformed in the general flattening field (3D deformation), determining the extension is more complex, as outlined in Figure 5.15.

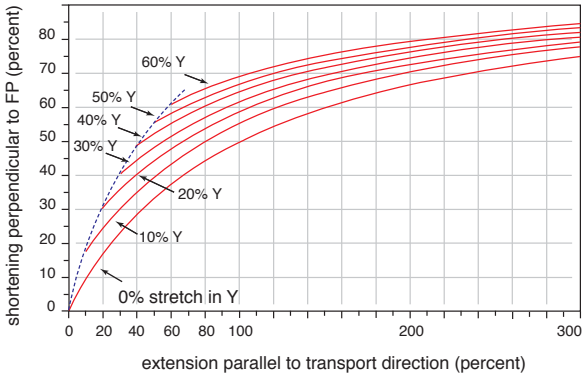

Figure 5.15 Curves of shortening perpendicular to flow plane versus extension in transport direction for plane strain (O% stretch in Y) and corresponding curves for general flattening with 10-60% stretch in Y; after Law et al. (2007) and Law (2010). Shortening values perpendicular to the flow plane are calculated using the numeric relationships between Wm and Rxz summarized in Fig. 5.14. Stretches parallel to Y indicated by 3D strain analysis of the APM stream section quartzites are compiled in Table 4.1.

parallel to the transport direction assumes plane strain constant volume deformation in which this stretch value is simply the reciprocal of shortening perpendicular to the flow plane (Fig. 5.14). However strain analyses of the Cambrian quartzites indicates that they have been deformed in the general flattening field. Therefore, stretching parallel to orogenic strike must be taken into account when determining extension parallel to the transport direction. A graphic method for solving this problem for flattening strains has been presented by Law et al. (2007) and Law (2010) and subsequently extended to constrictional strains by Xypolias et al. (2010). In Figure 5.15 it is shown that by

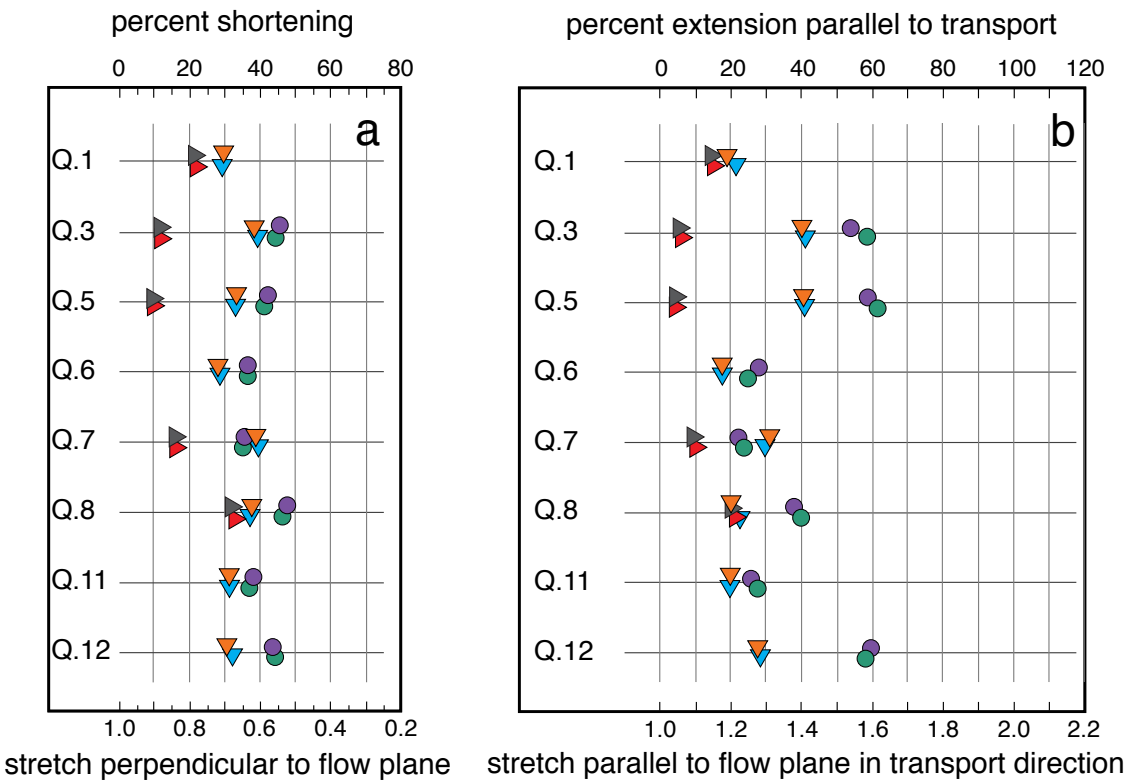

Figure 5.16 (a) Shortening values perpendicular to flow plane for APM stream section Cambrian quartzites. Results are coded for input data using different vorticity methods and strain calculations (Chew and Mulchrone & Meere strain programs). (b) Corresponding extensions in flow plane parallel to transport direction taking in to account extension in Y for different samples. Analyses indicate an approximate 20-45% shortening with resultant 20-50% extension parallel to transport direction.

plotting estimated shortening values perpendicular to the flow plane (indicated by integrated vorticity and strain analyses) against curves of equal stretch parallel to the Y principal strain axis (along strike stretch indicated by strain analysis; Table 4.1) percent extension parallel to the transport direction may be read off of the x-axis. It is important to note that these curves of constant stretch parallel to Y are extremely sensitive to minor variations in estimated shortening perpendicular to the flow plane. A small increase in estimated shortening value will result in a major increase in predicted transport parallel extension.

Estimates of shortening perpendicular to the flow plane (Fig. 5.16a) and stretching parallel to the transport direction (Fig. 5.16b) were made using data from each method of vorticity analysis, together with strain estimates based on both the Chew (2003) and Mulchrone & Meere (2001) programs. The majority of different combinations of vorticity and strain data used in these calculations indicate a shortening of 20-45% (Fig. 5.16a), assuming constant volume deformation. These shortening estimates, which take vorticity of flow in to account, may be compared with the 55-65% shortening perpendicular to foliation indicated solely from 3D strain analysis (Chapter 4). The highest estimates of shortening perpendicular to the flow plane are obtained using vorticity data from rigid grains (Method 1). This is because the lowest vorticity numbers (and hence the highest pure shear components) are indicated by this method. Calculated extensions parallel to the transport direction, taking stretching parallel to orogenic strike into account, range from 15-60% with a clustering of the data falling between 20-50% extension (Fig. 5.16b).

It should be noted that there is a greater scatter in estimated values of stretch parallel to tectonic transport than corresponding shortening perpendicular to the flow plane that is responsible for driving this stretching (cf. Figs. 5.16 a and b). This is simply because estimated transport-parallel stretch values are extremely sensitive to minor variations in both shortening perpendicular to the flow plane and stretch parallel to Y (Fig. 5.15). It should be kept in mind that measured stratigraphic thickness of the Cambrian quartzites indicate a thinning of 33-66% (Peach et al, 1888, Chapter 2) associated with penetrative deformation of the Aisinnan imbricates. These independently derived shortening estimates are closest to those based on Method 1 vorticity analysis, suggesting the importance of a significant pure shear component during progressive deformation. In contrast, Method 2 & 3 vorticity analyses more closely reflect the closing stages of penetrative flow which may have been dominated by simple shear.

Summary

1. Within the APM stream section Method 1 (rigid grain) analyses of the Cambrian quartzites indicate a slight upward apparent decrease in Wm values traced towards the overlying Moine thrust. Estimated Wm values ranged from 0.775 - 0.85, indicating the dominance of simple shear over pure shear deformation. Higher estimated vorticity values (Wm = 0.83 -0. 87) are indicated by Method 1 analyses in the mylonitic Moine psammites (but based on only two samples). Method 1 analyses produced the lowest estimated Wm values of the three analytical techniques employed for the Cambrian quartzites.
2. Oblique grain shape alignments used in combination with quartz c-axis fabric data (Method 2) also proved a suitable means for determination of vorticity values within the Cambrian quartzites. This method produced the highest estimated vorticity numbers (Wm = 0.85 - 0.99) and did not indicate any significant correlation between estimated Wm values and structural distance beneath the thrust plane.
3. 3D strain and quartz c-axis fabric data were integrated as a third method of vorticity analysis in the Cambrian quartzites. Estimated Wm values ranged from 0.78 - 0.94 and, similarly, did not show any convincing correlation with structural distance beneath the thrust.
4. Shortening perpendicular to the gently dipping flow plane in the mylonitic Cambrian quartzites, as well as the extension parallel to the transport direction, were calculated using integrated 3D strain and vorticity data. Shortening estimates range from 20-45% while associated transport-parallel extensions ranged from 20-50%. These calculations assume constant volume deformation, but take into account stretching parallel to orogenic strike (deformation in the general flattening field) that is indicated by 3D strain analysis.

References Cited:

BRITISH GEOLOGICAL SURVEY 2007. Assynt, Scotland Special Sheet, Bedrock, 1:50 000 Geology Series: Keyworth, Nottingham, British Geological Survey.

CHEW, D.M. 2003. An Excel spreadsheet for finite strain analysis using the R_f/phi technique. *Computers & Geosciences*, **29**, 795-799.

FOSSEN, H. & TIKOFF, B. 1997. Forward modeling of non-steady-state deformations and the "minimum strain path." *Journal of Structural Geology*, **19**, 987-996.

FOSSEN, H. & TIKOFF, B. 1998. Extended models of transpression and stranstension, and application to tectonic setting. *Journal of Structural Geology*, **135**, 15-33.

FRASSI, C., CAROSI, R., MONTOMOLI, C., & LAW, R.D. 2009. Kinematics and vorticity of flow associated with post-collisional oblique transpression in the Variscan Inner Zone of northern Sardinia (Italy). *Journal of Structural Geology*, **31**, 1458-1471.

GEOLOGICAL SURVEY OF GREAT BRITAIN (SCOTLAND), 1923. Geological Map of the Assynt District at 1:63,360. Geological Survey of Great Britain, Scotland.

GRASEMANN, B., FRITZ, H., VANNAY, J.-C., 1999. Quantitative kinematic flow analysis from the Main Central Thrust zone, (NW Himalaya): implications for a decelerating strain path and the extrusion of orogenic wedges. *Journal of Structural Geology,* **21**, 837-853.

IACOPINI, D., PASSCHIER, C.W., KOEHN, D., & CAROSI, R. 2007. Fabric attractors in general triclinic flow systems and their application to high strain shear zone; a dynamical system approach. *Journal of Structural Geology*, **29**, 298-317.

JIANG, D. 1998. Forward modeling of non-steady-state deformations and the 'minimum strain path': Discussion. *Journal of Structural* Geology, **20**, 975-977.

JOHNSON, S.E., LENFERINK, H.J., MARSH, J.H., PRICE, N.A., KOONS, P.O., & WEST, D.P. Jr. 2009. Kinematic vorticity analysis and evolving strength of mylonitic shear zones; new data and numerical results. *Geology*, **37**, 1075-1078.

LANGILLE, J.M., JESSUP, M.J., COTTLE, J.M., NEWELL, D., & SEWARD, A. 2010. Kinematic evolution of the Ama Drime detachment: Insights into orogen-parallel extension and exhumation of the Ama Drime Massif, Tibet-Nepal. *Journal of Structural Geology,* **32**, 900-919.

LAW, R.D., 2010. Moine thrust zone mylonites at the stack of Glencoul II: results of vorticity analyses and their tectonic significance. In: Law, R.D., Butler, R.W.H., Holdsworth, R., Krabbendam, M., Strachan, R. (Eds), Continental Tectonics and Mountain Building e The Legacy of Peach and Horne. Geological Society, London, Special Publications, **335**, 579 - 602.

LAW, R.D., CASEY, M., & KNIPE, R.J. 1986. Kinematic and tectonic significance of microstructures and crystallographic fabrics within quartz mylonites from the Assynt and Eriboll regions of the Moine thrust zone, NW Scotland. *Transactions of the Royal Society of Edinburgh: Earth Sciences*, **77**, 99-123.

LAW, R.D., SEARLE, M.P. & SIMPSON, R.L. 2004. Strain, deformation temperatures and vorticity of flow at the top of the Greater Himalayan Slab, Everest Massif, Tibet. *Journal of the Geological Society, London*, **161**, 305-320.

LAW, R.D., THIGPEN, J.R., COOK, B., 2007. Field excursion C - mylonites associated with the Stack of Glencoul: May 15th and 17th 2007. *In:* Strachan, R., Thigpen, J.R. (Eds.), Continental Tectonics and Mountain Building e the Peach and Horne Meeting. A Guide to Field Excursions, pp. 66e103. Joint meeting of the Geological Society of London (an Arthur Holmes meeting) and Geological Society of America to celebrate the centenary of the Peach and Horne 1907 Geological Survey of Scotland memoir on "The Geological Structure of the Northwest Highlands of Scotland", Ullapool, Scotland, 12-19 May 2007

MEANS, W.D. 1981. The concept of steady state foliation. *Tectonophysics*, **78**, 179-199.

MEANS, W.D., HOBBS, B.E., LISTER, G.S., & WILLIAMS, P.F. 1980. Vorticity and non-coaxiality in progressive deformations. *Journal of Structural Geology*, **2**, 371-378.

MULCHRONE, K.F. & MEERE, P.A. 2001. A Windows program for the analysis of tectonic strain using deformed elliptical markers. *Computers & Geosciences*, **27**, 1251-1255.

PASSCHIER, C.W. 1988. Analysis of deformation paths in shear zones. *Geologische Rundschau*, **77**, 309-318.

PEACH, B.N., HORNE, J., GUNN, W., CLOUGH, C.T., HINXMAN, L.W. & CADELL, H.M. 1888. Report on recent work of the Geological Survey in the N.W. Highlands of Scotland, based on field notes and maps of Messers. B.N. Peach, J. Horne, W. Gunn, C.T. Clough, L. Hinxman, and H.M. Cadell. *Quarterly Journal of the Geological Society, London*, **64**, 378-441.

STAHR, D.W., & LAW, R.D. Effect of finite strain on clast-based vorticity gauges. *Journal of Structural Geology*, in review.

WALLIS, S.R. 1992. Vorticity analysis in a metachert from the Sanbagawa Belt, SW Japan. *Journal of Structural Geology*, **14**, 271-280.

WALLIS, S.R. 1995. Vorticity analysis and recognition of ductile extension in the Sanbagawa belt, SW Japan. *Journal of Structural Geology*, **17**, 1077-1093.

WALLIS, S.R., PLATT, J.P. & KNOTT, S.D. 1993. Recognition of syn-convergence extension in accretionary wedges with examples from the Calabrian Arc and the Eastern Alps. *American Journal of Science*, **293**, 463-495.

XYPOLIAS, P. 2010. Vorticity analysis in shear zones: A review of methods and applications. *Journal of Structural Geology*, **32**, 2042-2071.

XYPOLIAS, P., SPANOS, D., CHATZARAS, V., KOKKALAS, S. & KOUKOUVELA. Vorticity of flow in ductile thrust zones: examples from the Attico-Cycladic Massif (Internal Hellenides, Greece). *In:* Law, R.D., Butler, R.W.H., Holdsworth, R., Krabbendam, M. & Strachan, R. (eds) *Continental Tectonics and Mountain Building - The Legacy of Peach and Horne*. Geological Society, London, Special Publications, **335**, 687-714.

Chapter 6: Quartz piezometry and strain rates

Abstract

In this Chapter analyses of dynamically recrystallized grain sizes from the Cambrian quartzites and the Moine psammites of the APM stream section are reported. These data are used to estimate flow stresses and strain rates associated with crystal plastic deformation. Dynamic recrystallization produced grain sizes ranging between 21-27 microns in the Cambrian quartzites, indicating differential flow stresses of approximately 48-61MPa. Incorporation of these stress estimates, together with an average estimated deformation temperature of 440 °C (Chapter 4), into a dislocation creep flow law indicates strain rates on the order of 10^{-12} sec^{-1} throughout the APM stream section quartzites. Larger grain sizes (50 microns) are recorded in the Moine psammites, indicating lower flow stresses (30-32 MPa). However, incorporation of higher deformation temperatures for the psammites located above the Moine thrust would indicate even higher strain rates (Chapter 7). A sensitivity analysis indicates, however, that strain rate estimates are critically dependent on experimentally derived flow parameters, and order of magnitude differences in strain rate are calculated using input parameters from different experimental data.

Introduction

Microstructural analysis plays a crucial role in understanding flow processes that have operated in plastically deformed rocks. Previous studies (e.g. Kirby & Raleigh 1971; White 1973, 1976, 1977; Mercier et al. 1977; Twiss 1977) have demonstrated that deformed and dynamically recrystallized minerals within such tectonites can provide useful information for estimating the paleostresses associated with their internal flow and deformation. The analytical techniques are based on the concept that in large strain magnitude steady-state dislocation creep (hotworking) stable microstructures develop at low to moderate strains (White, 1979). The primary stress-dependent microstructures are dislocation density, sub-grain size, and the size of the recrystallized grains. These microstructures, were originally argued to be solely dependent on differential stress, although later studies have also explored the potential roles of other extrinsic and intrinsic variables including deformation

temperature and chemical (hydrolytic) weakening (e.g. Stipp et al. 2006) and, for grain size-based piezometry, recrystallization mechanisms (see reviews by Passchier & Trouw 2005, p. 254-255; Stipp et al. 2010).

The study reported here employs the grain-size based piezometers proposed by Twiss (1977) and Stipp & Tullis (2003) to estimate flow stresses associated with mylonitization of the Cambrian quartzites and Moine psammites exposed in the APM stream section. Several other grain-size based piezometers have also been proposed by other authors, but here we have focused on using the currently regarded *"state of the art"* piezometer (Stipp & Tullis 2003) and comparing flow stress results obtained from this piezometer with flow stress results obtained using one of the first proposed grain size-based piezometers (Twiss 1977). Details of the analytic techniques are discussed, with attention focusing on the 2D and 3D aspects of grain size estimation from thin section analysis, and whether 2D or 3D grain size estimates should be used as input data for the different piezometers. Finally, flow stresses from the APM stream section quartzites, together with deformation temperature data (based on quartz c-axis fabric opening angles - Chapter 4), are incorporated in to a flow law for dislocation creep to estimate *'average'* strain rates associated with mylonitization. In Chapter 7, flow stress and strain rate estimates obtained using these piezometers will be compared with stress estimates obtained using grain size-, subgrain size- and dislocation density-based piezometers on mylonitic Cambrian quartzites that are located at a slightly higher structural position to the APM stream section (probably corresponding to the sheet of mylonites mapped by the Geological Survey, Fig. 2.4) between the Aisinnan imbricates and the Moine nappe, but outcrop further to the south at the Stack of Glencoul and in the Allt nan Sleach section of eastern and southern Assynt.

Linear intercept method for grain size analysis

To date, almost all analytical techniques for estimating grain size are based on using data collected on a 2D cut surface (e.g. thin section, polished slab) through an aggregate of grains. Within such 2D surfaces, two main analytical methods are used: a) the linear-intercept-length (LIM) method (e.g. Smith & Gutman 1953) and, b) methods based on estimating cross-sectional areas of grains (e.g. NIH software and

associated microstructural programs; e.g. Panozzo 1984). We have employed the LIM method for analysis of the APM stream section quartzites because: 1) no analytical facilities (hardware, software) beyond that of a standard petrographic microscope are required, 2) the LIM method is typically less time consuming than area-based methods and, 3) the LIM method is thought to provide a more meaningful estimate of grain size (Dayan 1981).

For spherical grains, grain size estimates based on 2D sections will underestimate the true grain size as statistically the majority of grains will not be sectioned through their centers and hence measured grain sizes will be less than the true grain diameter (see reviews by Pickering 1976; Dayan 1981, p. 309-323). This is colloquially referred to as the *'cut-effect'* in the materials science literature. Grain size analysis (both in 2D and 3D) is frequently further complicated by grains developing with polyhedral rather than spherical shapes, and by these grain shapes simultaneously developing a preferred alignment - e.g. relative to foliation and lineation. Additionally, when recrystallization occurs by grain boundary migration, secondary mineral phases, such as mica, may pin grain boundaries resulting in smaller average grain sizes in mica-rich domains and larger grain sizes in mica-poor domains (see reviews by Hobbs et al. 1976, p. 117-119; Passchier & Trouw 2005, p. 50).

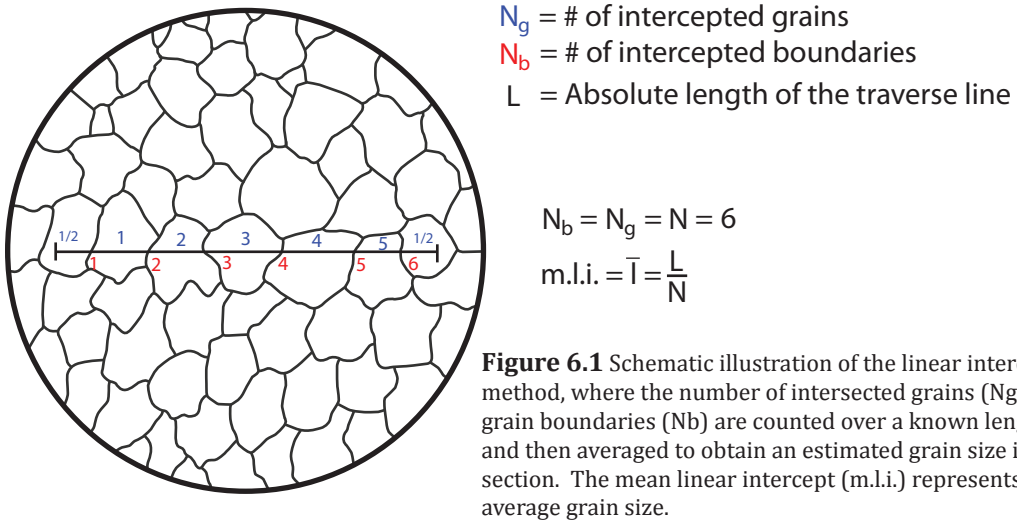

Figure 6.1 Schematic illustration of the linear intercept method, where the number of intersected grains (Ng) or grain boundaries (Nb) are counted over a known length, and then averaged to obtain an estimated grain size in thin section. The mean linear intercept (m.l.i.) represents the average grain size.

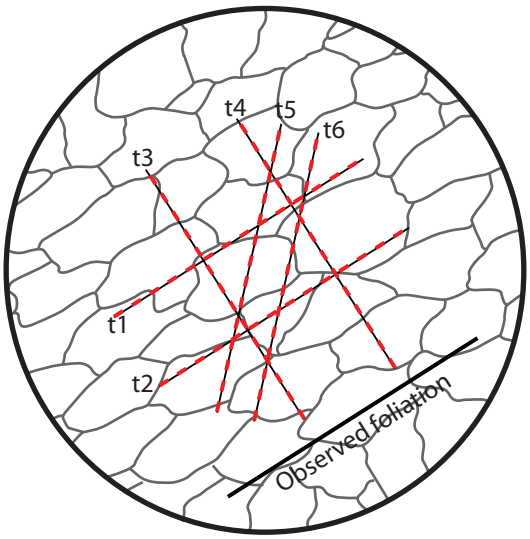

Figure 6.2 Application of the linear intercept method to a thin section where grains are non-equant and have a shape preferred orientation. Grain boundaries were counted over six traverses (t1, t2…) in domains of pure recrystallized quartz (lacking mica and relict detrital grains). For each thin section this procedure was repeated multiple times in different domains, in order to obtain a statistically valid representation of grain size. Each set of six traverses contained two traverses parallel to grain shape foliation, two traverses perpendicular to foliation, and two traverses at 45° to foliation.

Using the LIM method, grain size is determined by counting either the number of individual grains, N_g, or grain boundaries, N_b, crossed along the length of a linear traverse of known absolute length (Fig. 6.1). To at least partially allow for grain shape anisotropy, measurements are made along a series of traverses at different orientations to foliation and lineation (Fig. 6.2). In the analyses reported here, traverses were only measured on thin sections cut on the XZ plane (perpendicular to foliation and parallel to lineation). The mean-linear-intercept (MLI) is then determined by dividing the traverse length (L) by N (Fig. 6.1). It should be noted that this simple relationship will only hold true in cases where grains of a single mineral phase are present along a traverse line.

For the APM stream section, the LIM method proved applicable to all but two of the mylonitic Cambrian quartzites in the footwall to the Moine thrust, as well as one sample taken from Moine psammites in the hanging wall to the thrust. All of these samples are characterized by *'new'* dynamically recrystallized grains which, in the Cambrian quartzites, form a matrix of new grains surrounding relict plastically deformed detrital grains (Chapter 3). In each sample, domains of dynamically recrystallized quartz grains were measured using the ocular micrometer on an optical microscope. Care was taken to avoid areas of the thin section where second phase particles such as mica, or relict detrital grains, were present. The grains were measured using three pairs of parallel lines: parallel, perpendicular, and at 45° to the observed foliation in thin section (Fig. 6.2). Several of these locations were

Sample	Distance (m)	n	% Std Error	D_a (μm)	D_g (μm)	St. Dev. $s(d_a)$ (μm)	Rel. Error $s(d_a)/(d_a)$	Corrected grain size D_a (μm)	Corrected grain size D_g (μm)	Twiss D_a (MPa)	Twiss D_g (MPa)	Stipp D_a (MPa)	Stipp D_g (MPa)
M.2	51.1	433	3.36	50.49	49.49	10.24	.20	88.36	86.60	32.04	32.48	29.76	30.24
Q.1	7.5	562	2.95	27.53	27.09	5.26	.19	48.18	47.41	48.39	48.93	48.16	48.78
Q.2	20.0	680	2.68	27.00	26.73	4.01	.15	47.25	46.77	49.04	49.38	48.91	49.30
Q.3	27.1	607	2.84	25.16	24.81	4.24	.17	44.03	43.43	51.46	51.94	51.73	52.30
Q.4	31.6	1026	2.19	23.94	23.66	3.82	.16	41.89	41.40	53.23	53.65	53.81	54.32
Q.5	34.2	455	3.28	27.46	26.91	5.65	.21	48.05	47.09	48.49	49.15	48.26	49.04
Q.6	45.3	500	3.13	21.63	21.35	3.49	.16	37.85	37.37	57.03	57.53	58.33	58.92
Q.8	55.6	931	2.29	22.97	22.77	3.13	.14	40.20	39.84	54.73	55.07	55.60	56.00
Q.10	77.8	879	2.36	20.81	20.64	2.80	.13	36.42	36.12	58.54	58.87	60.13	60.53
Q.11	88.9	455	3.28	20.37	20.11	3.38	.17	35.65	35.20	59.40	59.91	61.16	61.79
Q.12	91.6	712	2.62	22.66	21.83	6.48	.29	39.65	38.20	55.25	56.67	56.21	57.90

Table 6.1 Results of recrystallized grain size analyses for the APM stream section and associated flow stress estimates. Arithmetic and geometric mean 2D grain size values for each sample, together with corrected values taking in to account the 'cut effect' and using the correction factor of 1.75 recommended by Pickering (1976), are indicated. Original 2D grain size data are used in the Stipp & Tullis (2003) piezometer; grain size values corrected for the cut-effect are used in applying the Twiss (1977) piezometer. Samples are arranged in order of structural position relative to the Moine thrust plane as defined by Geological Survey (1923).

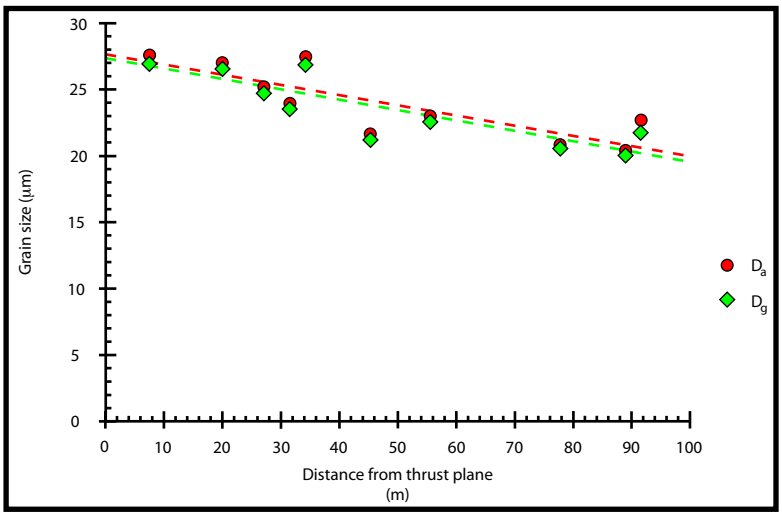

Figure 6.3 Relationship between size of dynamically recrystallized quartz grains and distance beneath the Moine thrust plane (as defined by Geological Survey1923) for the mylonitic Cambrian quartzites of the APM stream section. Data shown are arithmetic (Da) and geometric (Dg) means for uncorrected 2D grain sizes. Linear regression lines through arithmetic (red) and geometric (green) mean grain sizes for individual samples are shown and indicate a small decrease in grain size with increasing distance beneath the thrust.

measured within each sample to obtain a larger sample size and hence improve statistical reliability of the grain size estimates obtained. An average of 681 grains were measured in each thin section/sample for the APM stream section. Results of these grain size analyses are summarized in Table 6.1. The estimated grain size ranges from 20-27 microns for the Cambrian quartzites in the APM stream section, with only minor differences between grain sizes based on arithmetic and geometric mean values. Estimated grain sizes are plotted against distance beneath the Moine thrust plane (see Chapter 2 for discussion of structural position in the APM stream

section) in Figure 6.3. Linear regression analysis of the data indicates a progressive decrease in recrystallized grain size traced structurally downwards beneath the thrust plane towards the sheared contact between quartzites and underlying Lewisian gneiss. Recrystallized quartz grains in the overlying Moine psammites (sample M.1) have an estimated average grain size of 50 microns.

In measuring recrystallized grain sizes in individual thin sections, care was taken to avoid mica-rich areas where these second phase particles may have inhibited grain boundary migration. As noted above, recrystallized quartz grains are typically smaller in these mica-rich domains compared with adjacent domains that have no (or minimal) second phase particles. Dynamically recrystallized quartz veins that locally cross-cut the mylonitic foliation were also avoided in these analyses. In general, the recrystallized grain size within these veins is substantially larger than those within the surrounding host quartzite.

As also noted above, measurement of grain size in a 2D section will always lead to an underestimation of true (3D) grain size due to the *'cut effect'*. A range of different analytical procedures for correcting for the *'cut effect'* have been reported in the materials science and metallurgy literature. Some of these procedures also take in to account 3D non-equidimensional grain shapes and grain shape preferred orientations. Here we have adopted the procedure recommended by Pickering (1976) in which the average 2D-based grain size estimate is multiplied by a correction factor of 1.75 to obtain a more realistic 3D estimate of *'average grain size'*. Such grain size corrections are commonly made in materials science/metallurgy and yet seem to be only rarely applied in the geological sciences (e.g. Dayan 1981). These correction procedures have serious implications for using grain size data to estimate paleostress magnitudes.

Paleostress estimation

Over the last 35 years a number of piezometers for determining paleostress magnitudes in naturally deformed rocks, based on dynamically recrystallized grain size, have been proposed (see review by Passchier & Trouw 2005, p. 254-255). In some cases these piezometers are based on theoretically predicted relationships between dynamically recrystallized grain size and flow stress (e.g. Twiss 1977),

while in the majority of cases they are based on experimental rock deformation data in which grain size measured in thin sections of the deformed material is compared with the applied differential stress under which the microstructures have developed (e.g. Mercier et al. 1977, Christie et al. 1980, Christie & Ord 1980; and Stipp & Tullis 2003; Stipp et al. 2006). However, several of the experimentally calibrated piezometers (e.g. Mercier et al. 1977; Christie et al. 1980; Christie & Ord 1980) are now regarded as being unreliable (see discussion by Stipp & Tullis, 2003) because: a) the experiments had poor stress resolution, b) in some cases steady state deformation was not achieved and, c) no distinction was made between different mechanisms of dynamic recrystallization resulting in unrealistically high flow stresses being estimated when the experimental data is extrapolated to natural shear zone conditions. The potentially inter-connected influences of deformation temperature and recrystallization mechanism on dynamically recrystallized grain size, and the implications for piezometry, have recently been reviewed by Shimizu (2008) and Stipp et al. (2010).

In using measured recrystallized grain sizes for piezometry of deformed materials, care must be taken that appropriate measures of grain size are applied to the different piezometers. For example, in the experimentally calibrated piezometer of Stipp & Tullis (2003) the grain sizes employed were directly measured from thin section analysis of experimentally deformed material. No attempt was made to correct for the 3D cut-effect (M. Stipp pers. comm. 2010). Therefore original 2D grain size data (i.e. with no correction made for the *'cut effect'*) from thin section analysis should be used in applying the Stipp & Tullis (2003) piezometer to naturally deformed rocks. In contrast, the theory-based Twiss (1977) piezometer does not appear to be restricted to 2D shapes, and therefore it seems more appropriate to use thin-section based grain size data in which a correction has been made for the *'cut effect'* when applying the Twiss (1977) piezometer. This procedure has previously been followed by Dayan (1981) in applying the Twiss (1977) piezometer to mylonites from the Loch Eriboll region of the Moine thrust zone.

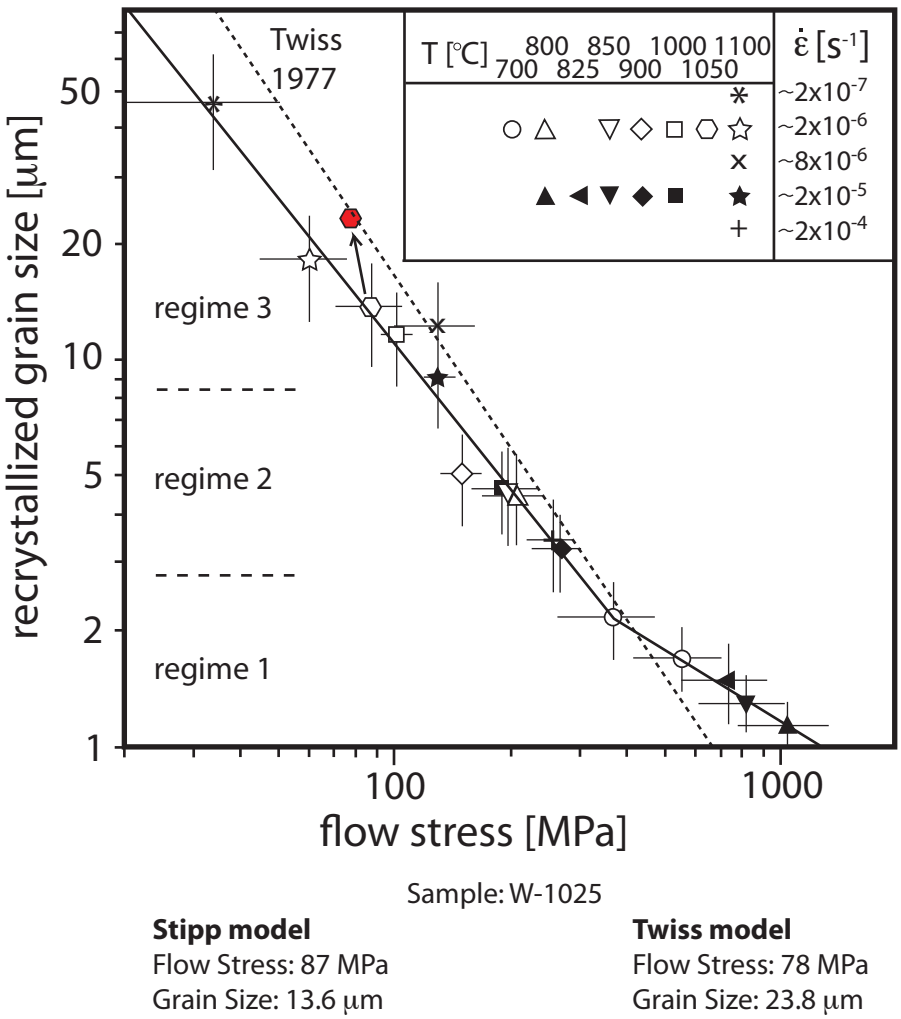

Figure 6.4 Relationships between flow stress and grain size of dynamically recrystallized quartz predicted by the Twiss (1977) and Stipp & Tullis (2003) piezometers; diagram is modified from Stipp & Tullis (2003, their figure 4). Experimentally calibrated piezometer of Stipp & Tullis uses 2D grain size data collected on individual thin sections that are not corrected for the 'cut-effect'. Application of the 1.75 correction factor for the cut-effect on measured grain size recommended by Pickering (1976) to experimentally deformed sample W-1025 of Stipp & Tullis (white hexagon) moves this data point to a new grain size position (red hexagon) on the line representing the Twiss piezometer. Note translation of this data point (indicated by arrow) does not occur at constant stress due to different variables employed in the two piezometers. See text for further details.

Stipp & Tullis (2003) have argued that in recrystallization regimes 2 (subgrain rotation) and 3 (grain boundary migration) the Twiss (1977) piezometer gives a greater flow stress magnitude at a given grain size than their experimentally calibrated piezometer (Fig. 6.4). Stated a different way, at a given flow stress the Stipp & Tullis piezometer is associated with a smaller grain size than the Twiss piezometer (Fig. 6.4). However, at least within regime 3, application of the correction factor of 1.75 for the 2D *'cut effect'* recommended by Pickering (1976) to

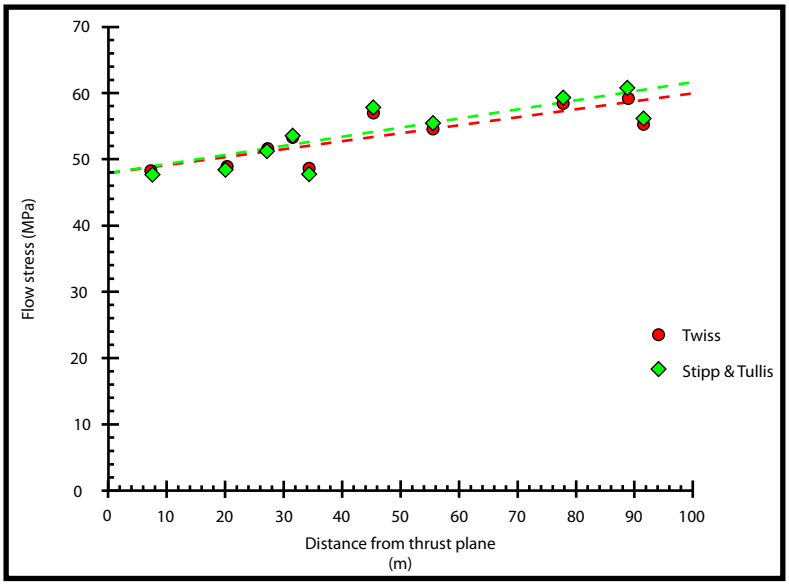

Figure 6.5 Relationship between flow stresses indicated by Twiss (1977) and Stipp & Tullis (2003) piezometers and distance beneath the Moine thrust plane (as defined by Geological Survey 1923) for the mylonitic Cambrian quartzites of the APM stream section. Uncorrected grain size data are used in the Stipp & Tullis piezometer, grain size data corrected for the cut-effect are used in the Twiss piezometer; arithmetic means are used in each piezometer. Linear regression lines for flow stresses indicated by the Stipp & Tullis (green) and Tullis (red) piezometers are indicated. Note small increase in estimated flow stress with increasing distance beneath thrust plane. See text for further details.

grain size data incorporated in to the Twiss (1977) piezometer brings flow stress estimates indicated by the two piezometers to almost identical values. For example, applying the 1.75 correction factor to the 2D average grain size for experimentally deformed sample W-1025 of Stipp & Tullis (2003) shifts this experimental data point upwards on to the theoretical Twiss piezometer (Fig. 6.4; data points joined by arrow). It should be noted that this is not a simple vertical translation on this grain size versus flow stress plot because different variables (other than grain size) are used in the two piezometers. It should also be noted that for the very small (1-2 micron) grain sizes associated with regime 1 recrystallization (grain boundary bulging) slightly larger grain sizes predicted by the Twiss piezometer are associated with a given flow stress than are predicted by the Stipp & Tullis piezometer (Fig. 6.4). In practice however, particularly with an optical microscope, it may be impossible to resolve the sub-micron difference in grain sizes.

Quartz deformation in the APM stream section samples is dominated by transitional sub-grain rotation to grain boundary migration recrystallization (regimes 2 and 3) with mean 2D (uncorrected) grain sizes of 20-27 microns (Table

6.1). Applying the Stipp & Tullis (2003) piezometer to these 2D grain size data (both arithmetic and geometric mean grain sizes) indicates flow stresses of 48-61 MPa. As expected, applying the Twiss (1977) piezometer to these samples, after the 1.75 correction factor of Pickering (1976) has been applied to the raw 2D grain size data, yields almost identical flow stress values of 48-59 MPa (compare data for individual samples in Table 6.1).

Flow stresses are plotted against structural distance beneath the Moine thrust (as defined by Geological Survey 1923) for the APM stream section Cambrian quartzites in Figure 6.5. Both the Twiss (1977) and Stipp & Tullis (2003) piezometers indicate a small increase in flow stress traced from 10 m (48 MPa) to 90-95 m (59-61 MPa) beneath the thrust. The observed progressive change in observed recrystallized grain size (Fig. 6.3) and estimated flow stresses (Fig. 6.5) with distance beneath the Moine thrust plane is surprising in that we had originally assumed that motion on the Moine thrust was responsible for *'driving'* mylonitization in the footwall quartzites. However, if this were so then intuitively one might expect to find an increase in flow stress traced structurally upwards towards the overlying thrust plane, not downwards away from the thrust. We therefore speculate that mylonitization of the quartzites may be tectonically associated with shearing on the underlying contact with the Lewisian gneiss (broadly synchronous with formation of the Aisinnan imbricates – see Chapter 7), rather than on the overlying Moine thrust. Alternatively, it could be argued that the larger grain size (and hence smaller inferred flow stress) at the top of the section of Cambrian quartzites is due to heat transfer from the overlying Moine nappe. However, although intuitively appealing, this does not seem to be supported by available thermal data based on quartz fabric opening angles (Table 4.2).

Strain rates

Rates of deformation associated with mylonitization of the APM stream section quartzites can be estimated by coupling calculated flow stresses and deformation temperatures for individual samples with the appropriate flow law for dislocation

creep:

$$\dot{e} = A\,\sigma^{n} \exp(-Q/RT)$$

where $\dot{e}$ is the strain rate, A and n are material constants, Q is the activation energy for dislocation creep, R is the gas constant and T is deformation temperature (in Kelvin). Koch et al. (1980) found that A = 4.36 ($kbar^{-n}\ sec^{-1}$), n = 2.44, and Q = 38.2 kcal/mole through performing coaxial axial shortening experiments on wet Simpson quartzite. A deformation temperature of 440°C, based on the average temperature indicated by the Kruhl (1998) thermometer using quartz c-axis fabric opening angles (Chapter 4), was used for the mylonitic Cambrian quartzites.

Sample	Twiss D_a $\dot{\varepsilon}$	Twiss D_g $\dot{\varepsilon}$	Stipp D_a $\dot{\varepsilon}$	Stipp D_a $\dot{\varepsilon}$
Q.1	$1.39x10^{-12}$	$1.43x10^{-12}$	$1.37x10^{-12}$	$1.41x10^{-12}$
Q.2	$1.43x10^{-12}$	$1.46x10^{-12}$	$1.42x10^{-12}$	$1.45x10^{-12}$
Q.3	$1.61x10^{-12}$	$1.65x10^{-12}$	$1.63x10^{-12}$	$1.68x10^{-12}$
Q.4	$1.75x10^{-12}$	$1.78x10^{-12}$	$1.80x10^{-12}$	$1.84x10^{-12}$
Q.5	$1.39x10^{-12}$	$1.44x10^{-12}$	$1.38x10^{-12}$	$1.43x10^{-12}$
Q.6	$2.07x10^{-12}$	$2.12x10^{-12}$	$2.19x10^{-12}$	$2.24x10^{-12}$
Q.8	$1.87x10^{-12}$	$1.90x10^{-12}$	$1.95x10^{-12}$	$1.98x10^{-12}$
Q.10	$2.21x10^{-12}$	$2.24x10^{-12}$	$2.36x10^{-12}$	$2.39x10^{-12}$
Q.11	$2.29x10^{12}$	$2.34x10^{12}$	$2.46x10^{12}$	$2.52x10^{12}$
Q.12	$1.92x10^{-12}$	$2.04x10^{-12}$	$2.00x10^{-12}$	$2.15x10^{-12}$

Table 6.2 Strain rate data for the APM stream section footwall Cambrian quartzites based on the Twiss (1977) and Stipp & Tullis (2003) piezometers. Data are listed with increasing distance from the Moine thrust plane (see Table 4.1 for distances).

The calculated strain rates for the APM stream section samples, based on the input parameters of Koch et al. (1980) are shown in Table 6.2, and range from $1.39x10^{-12}$ sec^{-1} close to the thrust plane (sample Q.1), to $2.29x10^{-12}$ sec^{-1} at the base of the measured section (Sample Q.12). Strain rate data, based on separate values from the Twiss (1977) and Stipp & Tullis (2003) piezometers, are plotted against structural position beneath the Moine thrust in Figure 6.6 and indicate a small increase in strain rate with increasing distance beneath the thrust plane (as defined by Geological Survey, 1923). This apparent increase in strain rate is simply a reflection of the increase in estimated flow stresses at greater distances beneath the thrust (Fig. 6.5). These strain rates - which are significantly greater than typically quoted *'average'* geologic strain rates of between 10^{-13} and 10^{-15} sec^{-1} (e.g. Pfiffner & Ramsay 1982) - should, at best, be considered as order of magnitude estimates (see discussion by Behrmann 1984).

Experimentally calibrated flow laws are derived from coaxial axially symmetric flattening experiments in which the strain component is measured

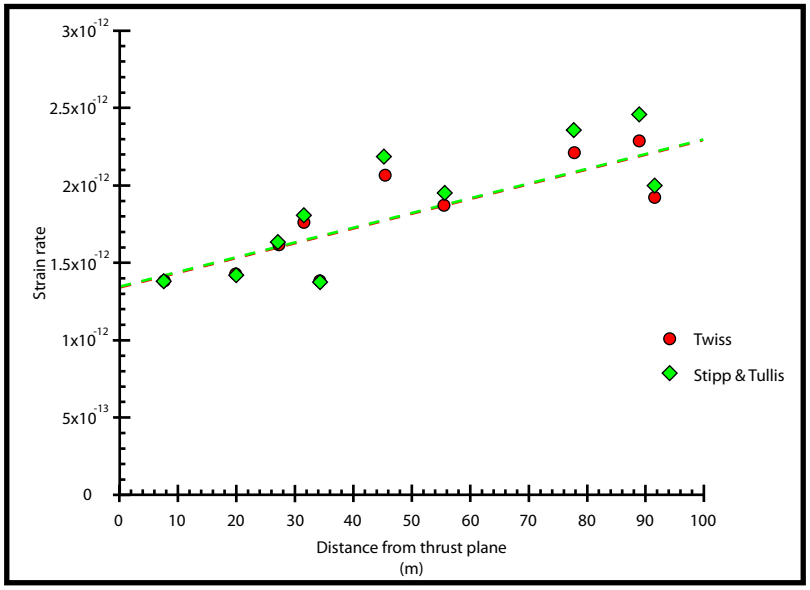

Figure 6.6 Relationship between strain rates and distance beneath the Moine thrust plane (as defined by Geological Survey 1923) for the mylonitic Cambrian quartzites of the APM stream section. Strain rate estimates based on flow stresses derived from the Twiss (1977) and Stipp & Tullis (2003) piezometers are indicated by red circles and green diamonds, respectively. Linear regression lines for strain rate data based on the two piezometers are indicated using the same color code. Note general trend of increasing estimated flow stress with increasing structural distance beneath the thrust.

parallel to the maximum principal shortening direction. Their application to naturally deformed rocks that have been subjected to radically different strain paths (e.g. plane strain, general flattening or constriction strains; and coaxial or non-coaxial steady state or non-steady-state flow paths, etc.) is far from straight-forward. In coaxial strain histories, strain rate will vary with direction relative to the evolving strain ellipsoid. The situation will be even more complex for non-coaxial strain histories (see discussions by Pfiffner & Ramsay 1982, Ramsay & Huber 1983, p. 218-223). Intuitively, it may be argued that strain rates calculated for naturally deformed rocks using flow stress and deformation temperature data, coupled to experimentally-calibrated flow laws, are probably most appropriate for estimating shortening rates at a high angle to the developing foliation.

As discussed in Chapter 2, comparison with the measured thickness of Basal Quartzite in the APM stream section with thicknesses measured in the foreland indicate a shortening/thinning of 33-60% associated with penetrative mylonitization. Similarly, Peach et al. (1888, p. 434) estimated that the Cambrian quartzites in the area *"have been reduced to a third of their original stratigraphic thickness"* - i.e. a 66% shortening. Strain analyses of the APM stream section

quartzites (Chapter 4) using deformed detrital grains indicate a shortening of 59-70% measured perpendicular to the gently dipping bedding-parallel foliation, assuming constant volume deformation. In summary, shortening estimates based on stratigraphic and strain analysis data range between 33 and 70%, corresponding to e_3 values of -0.33 and -0.70, respectively. At the median strain rate of 1.84×10^{-12} sec^{-1} calculated for the quartzites using the experimentally derived parameters by Koch et al. (1980), these strains would accumulate in between 5,000 and 12,000 years, which intuitively seems unreasonable. Strain rates would have to be two orders of magnitude slower (10^{-14} sec^{-1}) for these shortening strains to accumulate over time spans of 500,000 to 1,000,000 years.

A sensitivity analysis was conducted with the aim of explaining the geologically unreasonably short time interval indicated by the above analyses for accumulation of measured shortening strains in the mylonitic Cambrian quartzites. The initial assumption was that calculated strain rates would be particularly sensitive to deformation temperature estimates used in the calculations. To test this, strain rates were calculated over a range of set deformation temperatures (400, 450, and 500°C) and flow stresses (45-60MPa) that are representative of the temperatures and flow stresses obtained from the APM stream section quartzites (Chapters 4 and 6). An additional source of uncertainty in these strain rate calculations are the numerical values of experimentally derived parameters (A, n, and Q) used in the flow law. These vary significantly from one set of published experiments to another and have recently been reviewed by Mainprice & Jaoul (2009; their table 2). Numerical values of parameters (A, n, and Q) from experiments in which the starting material was broadly similar to the APM Cambrian quartzites (e.g. "*as is"* and "*water added"* Simpson, Black Hills and Heavitree quartzites) were included in this sensitivity analyses. Experiments where the starting materials used (e.g. vacuum dried quartzites, silica gel/acid) are not of obvious relevance to the quartzites studied here were excluded from this analysis. The specific publications and resulting strain rate calculations are summarized in Table 6.3.

	σ = 45 MPa	σ = 45 MPa	σ = 45 MPa	σ = 45 MPa
1				
400°C	2.221×10^{-15}	3.385×10^{-15}	4.956×10^{-15}	7.019×10^{-15}
450°C	3.495×10^{-14}	5.327×10^{-14}	7.800×10^{-14}	1.105×10^{-13}
500°C	3.851×10^{-13}	5.869×10^{-13}	8.593×10^{-13}	1.217×10^{-12}
2				
400°C	1.343×10^{-13}	1.785×10^{-13}	2.308×10^{-13}	2.920×10^{-13}
450°C	7.034×10^{-13}	9.350×10^{-13}	1.209×10^{-12}	1.530×10^{-12}
500°C	2.975×10^{-12}	3.953×10^{-12}	5.114×10^{-12}	6.468×10^{-12}
3.1				
400°C	5.058×10^{-12}	5.862×10^{-12}	6.699×10^{-12}	7.567×10^{-12}
450°C	3.073×10^{-11}	3.562×10^{-11}	4.070×10^{-11}	4.598×10^{-11}
500°C	1.479×10^{-10}	1.714×10^{-10}	1.958×10^{-10}	2.212×10^{-10}
3.2				
400°C	5.249×10^{-12}	6.346×10^{-12}	7.533×10^{-12}	8.810×10^{-12}
450°C	3.393×10^{-11}	4.102×10^{-11}	4.869×10^{-11}	5.694×10^{-11}
500°C	1.723×10^{-10}	2.083×10^{-10}	2.472×10^{-10}	2.891×10^{-10}
3.3				
400°C	1.052×10^{-13}	1.340×10^{-13}	1.669×10^{-13}	2.038×10^{-13}
450°C	8.705×10^{-13}	1.109×10^{-12}	1.381×10^{-12}	1.687×10^{-12}
500°C	5.481×10^{-12}	6.984×10^{-12}	8.695×10^{-12}	1.062×10^{-11}
4				
400°C	8.211×10^{-18}	1.150×10^{-17}	1.561×10^{-17}	2.062×10^{-17}
450°C	1.245×10^{-16}	1.744×10^{-16}	2.366×10^{-16}	3.126×10^{-16}
500°C	1.328×10^{-15}	1.861×10^{-15}	2.523×10^{-15}	3.335×10^{-15}

1: Gleason & Tullis, 1995 - Black Hills quartzite (as-is)
2: Koch et al., 1989 - Simpson quartzite (as-is)
3.1: Jaoul et al., 1984 - Heavitree quartzite (.28 wt% water)
3.2: Jaoul et al., 1984 - Heavitree quartzite (.39 wt% water)
3.3: Jaoul et al., 1984 - Heavitree quartzite (as-is)
4: Kronenberg & Tullis, 1984 - Heavitree quartzite (as-is)

Table 6.3 Strain rate calculations based on numerical values of experimentally derived parameters (A, n, and Q) summarized by Mainprice & Jaoul (2009, their table 2). Estimated strain rates generally range from about 10^{-17} sec^{-1} to 10^{-11} sec^{-1} depending on numerical values used but, for a given set of experimentally derived parameters, are less sensitive to assumed deformation temperature and/or flow stress.

The calculated strain rate values in this sensitivity analysis (Table 6.3) show no significant variation with regard to deformation temperature or applied flow stress. Instead, extreme variation in calculated strain rates is apparently directly related to the numerical values of the experimentally derived parameters used. The strain rates range in order of magnitude from $10^{-11}sec^{-1}$ to $10^{-17}sec^{-1}$. Using the

previously estimated shortening values (e_3 of -.33 and -.70) for the AMP quartzites, these experimentally derived parameters would indicated that the observed shortening strain in the quartzites could have accumulated in anywhere between 1,000 and 2,000,000,000 years. This broad, and geologically unreasonable, range of times suggests that either a), there is an inherent problem with extrapolating data from laboratory to natural strain rates or, b) the experimentally derived parameters are only of direct relevance to the starting quartzites used in the experiments and cannot be extrapolated to other materials.

Summary

1. Grain size of dynamically recrystallized quartz, measured optically by the linear intercept method on standard thin sections, ranged between 20-27 microns in the mylonitic Cambrian quartzites of the APM stream section. Grain size decreased slightly with increasing structural distance beneath the Moine thrust plane.
2. The average recrystallized grain size for each sample was used to determine flow stresses associated with mylonitization. Two piezometers were employed: the experimentally calibrated piezometer of Stipp & Tullis (2003) and the theory-based piezometer of Twiss (1977). Raw 2D grain size data were used in the Stipp & Tullis (2003) piezometer, while original 2D grain size data corrected for the 'cut-effect' were used in the Twiss (1977) piezometer. For individual samples, flow stresses estimate using the two piezometers were essentially identical (i.e. within c. 1 MPa) and progressively increased structurally downwards from 48 MPa in the footwall of the Moine thrust to 61 MPa at the base of the section.
3. Incorporation of the determined flow stress with an average deformation temperature of 440 °C determined from quartz c-axis fabric opening angles (Chapter 4) into a flow law for dislocation creep enabled strain rates to be estimated for individual quartz samples. Strain rates ranged from 1.39×10^{-12} to 2.29×10^{-12} sec^{-1} using the experimentally calibrated values of Koch et al. (1980) with strain rate increasing with structural depth beneath the thrust plane. These strain rates would predict that shortening and mylonitization of

the quartzites occurred in a geologically unreasonable time span of only 5,000 to 12,000 years. Sensitivity analysis indicates, however, that a wider range (order of magnitude) of strain rates can be calculated from input of flow stress and deformation temperature values, depending on which set of experimentally derived flow parameters are used.

References Cited:

BEHRMANN, J.H. 1984. Patterns of paleostress and strain beneath the Aguilon Nappe, Betic Cordilleras (Spain). *Zeitschrift der Deutschen Geologischen Gesellschaft,* **135**, 293-305.

CHRISTIE, J.M. & ORD, A. 1980. Flow stress from microstructures of mylonites; Example and current assessment. *Journal of Geophysical Research*, **85**, 6253-6262.

CHRISTIE, J.M., ORD, A., & KOCH, P.S. 1980. Relationship between recrystallized grain size and flow stress in experimentally deformed quartzite. *American Geophysical Union*, EOS Transactions, **61**, pp.377

DAYAN, H. 1981. *Deformation studies of the folded mylonites of the Moine Thrust, Eriboll District, Northwest Scotland* [Ph.D. thesis]: University of Leeds.

GEOLOGICAL SURVEY OF GREAT BRITAIN (SCOTLAND), 1923. Geological Map of the Assynt District at 1:63,360. Geological Survey of Great Britain, Scotland.

GLEASON, G.C. & TULLIS, J. 1995. A flow law for dislocation creep of quartz aggregates determined with the molten salt cell. *Tectonophysics*, **247**, 1-23.

HOBBS, B.E., MEANS, W.D., & WILLIAMS, P.F. 1976. Outline of Structural Geology. John Wiley & Sons, Inc., New York, NY. 571 pp.

JAOUL, O., TULLIS, J., KRONENBERG, A.K., 1984. The effect of varying water contents on the creep behavior of Heavitree quartzite. *Journal of Geophysical Research*, **89**, 4298–4312.

KIRBY, S.H. & RALEIGH, C.B. 1973. Mechanisms of high-temperature, solid-state flow in minerals and ceramics and their bearing on the creep behavior of the mantle. *Tectonophysics,* **19**, 165-194.

KOCH, P.S., CHRISTIE, J.M. & GEORGE, R.P. 1980. Flow laws of "wet" quartzite in the alpha-quartz field. *American Geophysical Union, EOS Transactions,* **61**, p. 376.

KOCH, P.S., CHRISTIE, J.M., ORD, A., GEORGE Jr., R.P., 1989. Effect of water on the rheology of experimentally deformed quartzite. J. Geophys. Res. 94, 13975–13996.

KRONENBERG, A.K., & TULLIS, J., 1984. Flow strengths of quartz aggregates: Grain size and pressure effects due to hydrolytic weakening. *Journal of Geophysical Research*, **89**, 4298–4312.

KRUHL, J.H., 1998, Reply: Prism- and basal-plane parallel subgrain boundaries in quartz: a microstructural geothermobarometer. *Journal of Metamorphic Geology*, **16**, 142-146.

MERCIER, J.C., ANDERSON, D.A., & CARTER, N.L. 1977. Stress in the lithosphere; inferences from steady state flow of rocks. *Pure and Applied Geophysics,* **115**, 199-226.

PANOZZO, R.H. 1984. Two-dimensional strain from the orientation of lines in a plane. *Journal of Structural Geology*, **6**, 215-221.

PASSCHIER, C.W., TROUW, R.A.J., 2005. Micro-tectonics, Second Edition Springer, 366 pp.

PEACH, B.N., HORNE, J., GUNN, W., CLOUGH, C.T., HINXMAN, L.W. & CADELL, H.M. 1888. Report on recent work of the Geological Survey in the N.W. Highlands of Scotland, based on field notes and maps of Messers. B.N. Peach, J. Horne, W. Gunn, C.T. Clough, L. Hinxman, and H.M. Cadell. *Quarterly Journal of the Geological Society, London*, **64**, 378-441.

PFIFFNER, O.A. & RAMSAY, J.G. 1982. Constraints on geological strain rates; arguments from finite strain states of naturally deformed rocks. *Journal of Geophysical Research*, **87**, 311-321.

PICKERING, F.B. 1976. The basis of quantitative metallography. *Institute of Metallurgical Technicians*, Monograph no. 1, p. 1-55.

RAMSAY, J. G., HUBER, M. I., 1983. The techniques of Modern Structural Geology; v.1, Academic Press: London, 462 p.

SHIMIZU, I. 2008. Theories and applicability of grain size piezometers: The role of dynamic recrystallization mechanisms. *Journal of Structural Geology*, **30**, 899-917.

SMITH, C.S. & GUTTMAN, L. 1953. Measurement of internal boundaries in three dimensional structures by random sectioning. *Trans. AIME*, **197**, 81–92.

STIPP, M. & TULLIS, J. 2003. The recrystallized grain size piezometer for quartz. *Geophysical Research Letters,* **30**, 5.

STIPP, M., TULLIS, J., & BEHRENS, H. 2006. Effect of water on the dislocation creep microstructure and flow stress of quartz and implications for the recrystallized grain size piezometer. *Journal of Geophysical Research*, **111**, 19 pp.

STIPP, M., TULLIS, J. SCHERWATH, M. & BEHRMANN, J. 2010. A new perspective on paleopiezometry; dynamically recrystallized grain size distribtions indicate mechanism changes. *Geology*, **38**, 759-762.

TWISS, R.J. 1977. Theory and applicability of a recrystallized grain size paleopiezometer. *Pure and Applied Geophysics*, **115**, 227-244.

WHITE, S.H. 1973. Syntectonic recrystallization and texture development in quartz. *Nature*, **244**, 276-278.

WHITE, S.H. 1976. The effects of strain on the microstructures, fabrics, and deformation mechanisms in quartzites. *Philosophical Transactions Royal Society London*, **A 283**, 69-86.

WHITE, S.H. 1977. Geological significance of recovery and recrystallization and recrystallization processes in quartz. *Tectonophysics*, **39**, 143-170.

WHITE, S. H. 1979. Difficulties associated with paleo-stress estimates, *Bulletin de Mineralogy*, 102, 210– 215.

Chapter 7: Comparison with the Stack of Glencoul and analyses along strike

Abstract

The previously reported analyses of 3D strain, vorticity, and quartz piezometry specifically laid out the specific deformation mechanisms present at the APM stream section. While this alone is significant, greater importance lies in understanding how the deformation styles present at the APM stream section are related to deformation along strike of the Moine thrust. To suit this purpose, the data present here is compared with previously reported data from the Stack of Glencoul (approximately 6.5km along strike from the APM stream section) and other samples along the Moine thrust between these two locations.

Introduction

The previous Chapters describe results from applying three microstructural and petrofabric based analytical techniques to mylonites exposed in the APM stream section of northern Assynt. This stream section provided a semi-continuous exposure of mylonitic Cambrian quartzites in the footwall to the Moine thrust, together with more limited exposure of Moine rocks in the hanging wall. Previously reported microstructural- and petrofabrics - based analyses of mylonites exposed at similar structural positions along strike from the APM stream section (Fig. 7.1) include; a) studies focusing on the internationally well known exposures at the Stack of Glencoul (e.g. Callaway 1884; Christie 1963; Weathers et al. 1979; Law et al. 1986, 2010; Law 1987, 1998, 2010; Halfpenny et al. 2006; Lloyd et al. 2010), b) studies describing in lesser detail footwall and hanging wall mylonites between Loch Strath nan Aisinnin (adjacent to the APM stream section) and the Stack of Glencoul (e.g. Strine & Mitra 2004, Strine & Wojtal 2004; Mookerjee & Mitra 2009; Thigpen 2009; Thigpen et al. 2010b) and, c) similar studies of mylonites between the Stack of Glencoul and the Allt nan Sleach stream section of southern Assynt (e.g. Christie 1963; Ord & Christie 1984; Law et al. 1986; Law 1998, 2010; Thigpen et al. 2010).

It should be emphasized that although the Cambrian quartzites exposed in the APM stream section can be referred to as being *'mylonitic'*, in that they have

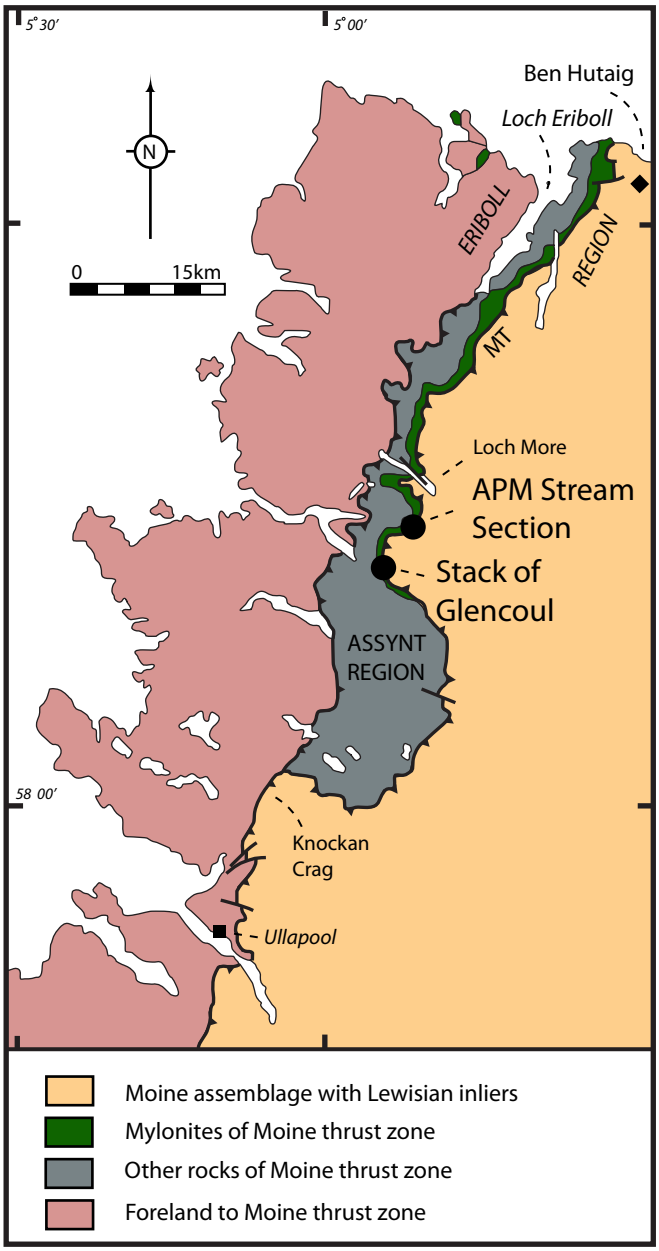

Figure 7.1 Location of the APM stream section (adjacent to Loch Strath nan Aisinnin) and the Stack of Glencoul in the northern part of the Assynt region. The Stack of Glencoul is located approximately 6.5km to the SW along strike from the APM stream section.

acquired significant finite strains through crystal plastic deformation and dynamic recrystallization, they are located in the immediate footwall to the discontinuous sheet(s) of mylonite (of variable protolith) mapped by the Geological Survey (Peach et al. 1888, 1907; Geological Survey 1923, BGS 2007) at the base of the Moine nappe. These mapped sheets of mylonite include the exposures referred to above at the Stack of Glencoul, and between the Stack of Glencoul and the Allt nan Sleach stream section of southern Assynt.

On the published Survey maps, the Cambrian quartzites adjacent to the APM stream section are not explicitly mapped as mylonites although their high strain deformation features are described in the accompanying Survey reports (e.g. Peach et al. 1888, p. 433; Peach et al. 1907, p. 499, Read 1931, p. 23). The Cambrian quartzites of the APM stream section structurally belong to the *'Aisinnin imbricates'* as mapped by the Geological Survey within, but near the top of, the Glencoul thrust sheet (Peach et al. 1907, p. 498). Butler (1984, p. 172) has argued that the high strain deformation fabrics that are sub-parallel to bedding in the Aisinnin imbricates,

developed before imbrication because they are locally folded around ramps associated with imbrication. Butler (1984, p. 174-5) has speculated that these imbricate faults may branch on to the Moine thrust in the transport direction (see particularly field sketch in Butler 1988, p. 186), and that the high strain penetrative deformation fabrics are associated with an early episode of gravity spreading during emplacement of the overlying Moine nappe. The imbricates, in turn, are themselves folded about the underlying Bhurich Dome exposed to the north of Loch Aisinnin, indicating a foreland-propagating deformation sequence.

Timing of penetrative deformation in the Aisinnin imbricates (including the APM stream section Cambrian quartzites) relative to deformation in the overlying mapped sheet(s) of mylonite that separate these quartzites from the Moine nappe remains uncertain. In both units, penetrative deformation associated with top to the WNW shearing under mid-upper greenschist facies conditions is indicated by microstructures and crystal fabrics, suggesting flow at similar structural levels and times. Assuming a foreland propagating sequence, penetrative deformation in the Aisinnin imbricates may have developed, relative to the overlying mylonite sheet, slightly later and in a more foreland position.

This caveat needs to be kept in mind when comparing results from the APM stream section with data from other mylonites, such as at the Stack of Glencoul, located approximately 4km (6.5km along strike) to the southwest of the APM stream section (Fig. 7.1). In the following discussion, samples from the Stack of Glencoul are prefixed with the label 'SG' to distinguish them from APM stream section samples. Unless otherwise indicated, data from the Stack of Glencoul samples are taken from Law et al. (2010) and Law (2010).

Strain and vorticity comparison

2D and 3D strain analyses performed on the Cambrian quartzites from the APM stream section indicate a general flattening (Lode's unit υ ranging from 0.17-0.50) associated with penetrative deformation (Fig. 7.2). Measured in sections cut perpendicular to foliation and parallel to lineation, R_{XZ} strain ratios range from 4.5-7.6, based on the Chew (2003) method. Es values, which are a measure of 3D strain

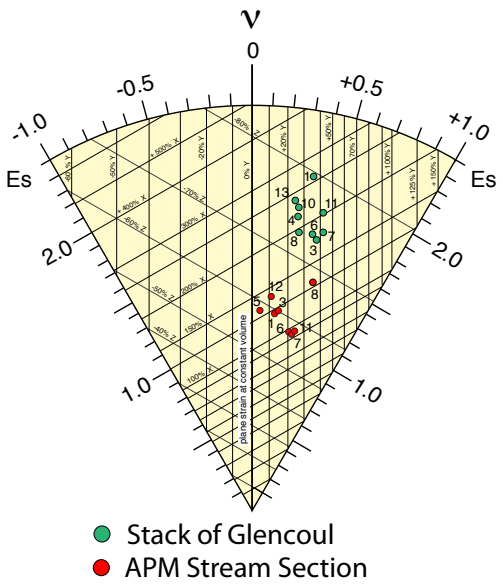

Figure 7.2 Comparison of 3D strain data from Cambrian quartzites exposed in the APM stream section (near Loch Strath nan Aisinnin) and in the immediate footwall to the Moine thrust at the Stack of Glencoul (data from Law et al. 2010). Note: mylonitic Cambrian quartzites at the Stack belong to a structurally higher thrust sheet than the APM quartzites. Both suites of quartzites plot within the general flattening field as expressed by Lode's parameter υ but strain magnitudes (expressed by Es) are higher in the Stack quartzites. Assuming constant volume deformation, transport parallel stretches (extensions) of 90-140% and stretches along strike of 10-40% are estimated in the APM quartzites, compared to 170-260% and 26-49%in the Stack quartzites. These foliation-parallel stretches are accompanied by shortening perpendicular to the gently dipping foliation of 55-65% and 72-80% for the APM and Stack quartzites, respectively.
Sample numbers for the two localities are indicated.

magnitude, for these quartzites range between 1.09 and 1.49 (Fig. 7.2; Table 4.1). Using the same analytical techniques, mylonitic Cambrian quartzites at the Stack of Glencoul in general plot slightly further from the plane strain line (Lode's unit υ ranging from 0.26-0.46) than the APM quartzites, indicating a greater component of along strike stretching parallel to Y (Fig. 7.2). R_{XZ} strain ratios for the Stack of Glencoul quartzites range from 9.2-18.8, while Es values range from 1.76-2.12 indicating significantly higher strain magnitudes than in the quartzites from the APM stream section (Fig. 7.2). For the APM quartzites calculated stretches parallel to X (lineation) and Y range between 90-130% and 11-14%, respectively, while shortening parallel to Z (i.e. perpendicular to foliation) ranges from 58-63% (Table 4.1); all assuming constant volume deformation. In contrast, for the Stack of Glencoul quartzites calculated stretches parallel to X and Y range between 180-260% and 29-49%, respectively, while shortening parallel to Z ranges from 73-80% (Law et al. 2010, their table 1). Compared with the APM stream section, this indicates a minimum increase of 60% and 15% in stretches parallel to X and Y, respectively, at the Stack of Glencoul, as well as a minimum increase of 10% in shortening parallel to Z. To explain the observed 3D strains that plot within the apparent flattening field as a true plain strain would require a volume loss of 20-50% for the APM stream section

quartzites, and a volume loss of 50-75% for the Stack of Glencoul quartzites (Fig. 7.3).

Flow vorticities associated with mylonite formation in both the APM stream section and at the Stack of Glencoul have been estimated using Methods 1 (rigid grain data), 2 (combined c-axis fabric and oblique recrystallized grain shape data) and 3 (combined c-axis fabric and R_{XZ} strain data). Method 1 analyses indicate higher flow vorticities in the APM stream section (Wm c. 0.75-0.85), compared with the Stack of Glencoul (Wm c. 0.68-0.78), for both mylonitic Cambrian quartzites and Moine rocks (Figs. 7.4a and b). The highest vorticity estimates are recorded in the mylonitic Moine rocks from the APM section (Fig. 7.4a; samples M1 and M2). Method 1 results indicate a c. 45-35% pure shear component for the APM stream section Cambrian quartzites samples and a c. 55-45% pure shear component for the Stack of Glencoul Cambrian quartzite samples. Method 1 indicates a slight decrease in Wm values traced upwards through the mylonitic Cambrian quartzites of the APM section (Fig. 7.4a; samples Q.6 to Q.2) while a slight increase in Wm is detected in the quartzites traced upwards towards the Moine thrust at the Stack of Glencoul (Fig. 7.4b). However, as discussed above, it must be kept in mind that the APM mylonites may represent a structurally lower, and slightly younger, sheet of mylonites than those exposed at the Stack of Glencoul.

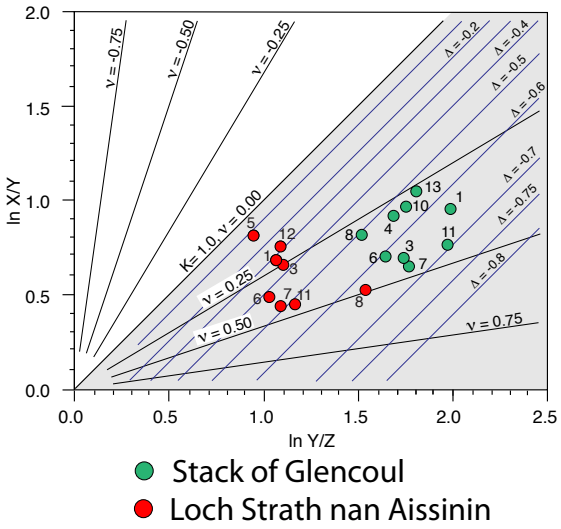

Figure 7.3 Comparison on a Log Flinn plot of 3D strain data from Cambrian quartzites exposed in the APM stream section and in the immediate footwall to the Moine thrust at the Stack of Glencoul (data from Law et al. 2010). All data plot within the general flattening field expressed by the Lode's parameter υ and Flinn parameter K. Contours for plane strain at different volume losses (Δ) are shown. Volume losses of 20-60% and 50-70% are required for the APM and Stack quartzites to develop under true plane strain conditions with no finite elongation parallel to Y; i.e. along orogenic strike.

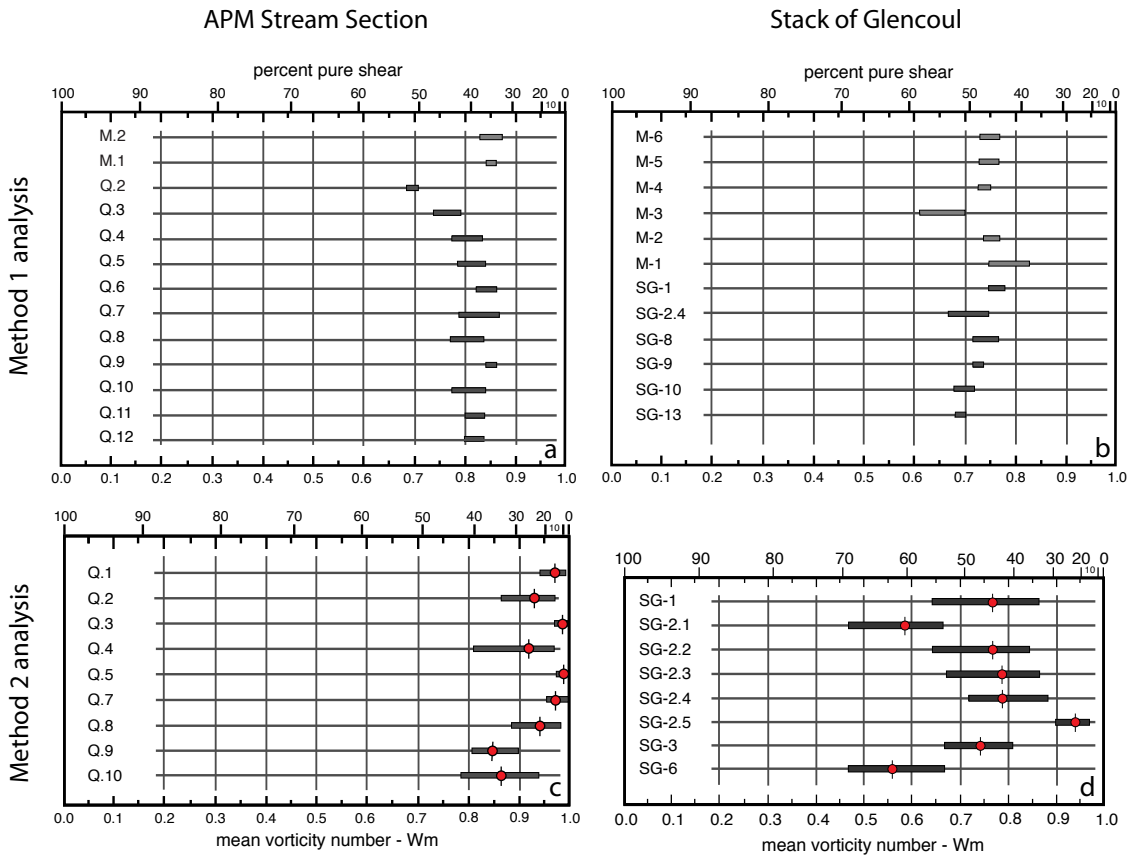

Figure 7.4 Comparison of vorticity estimates obtained by Method 1 (a & b) and Method 2 (c & d) analyses in the APM section (a & c) and at the Stack of Glencoul (b & d). Length of bars indicate degree of uncertainty in analyses. In Method 1 degree of uncertainty is controlled by possible range of rigid grain critical aspect ratios; in Method 2 degree of uncertainty is primarily controlled by likely error in assigning β value from quartz c-axis fabric data - Wm estimates indicated by best fit b values indicated by red circles; see discussion in Chapter 4. Samples arranged in order of descending structural position. Samples from Moine nappe (M series) indicated by light gray bars; samples of Cambrian quartzite from the Aisinnin imbricates (Q series) and Stack of Glencoul mylonites (SG series) indicated by dark gray bars.

Flow vorticities estimated using Method 2 (Figs. 7.4c and d) generally have a greater degree of uncertainty than those obtained using Method 1 (compare lengths of bars in Figs. 7.4c and d with Figs. 7.4a and b). For a given sample from either the APM or Stack of Glencoul sections, Wm values from Method 2 analyses are higher than those from Method 1 analyses. This is a common observation in vorticity analyses and could indicate that Method 2 analyses are only providing information on the last increments of deformation that are dominated by sub-simple shear, while Method 1 is giving some form of time-averaged Wm estimate. Alternatively, the difference in Wm estimates could be more directly related to problems with the analytical techniques themselves. For example, high Wm values (>0.85) can only be obtained with Method 1 when rigid grains of unusually large critical aspect ratio

(>4:1) are present (see discussions by Law et al. 2004; Stahr & Law in review). Nonetheless, in agreement with results from Method 1, Method 2 analyses of the APM stream section mylonites consistently yield higher Wm estimates than those obtained from the Stack of Glencoul mylonites (cf. Figs. 7.4c and d).

Using c-axis fabrics measured on deformed detrital grains, Method 3 Wm estimates for mylonitic Cambrian quartzites from the APM stream section range from 0.8-0.9 while Wm estimates for the Stack of Glencoul quartzites range from 0.0 to 0.73 (Figs. 7.5a and b). Thus using these data, higher flow vorticities are indicated for the APM quartzites. Particularly for the higher strain quartzites at the Stack, these Wm estimates are extremely sensitive to uncertainties in β values (denoted by error bars) measured on the quartz fabrics. Flow vorticities for the Stack mylonites have also been calculated using c-axis fabrics measured on recrystallized quartz grains (Fig. 7.5c); Wm estimates range between 0.25 and 0.98,

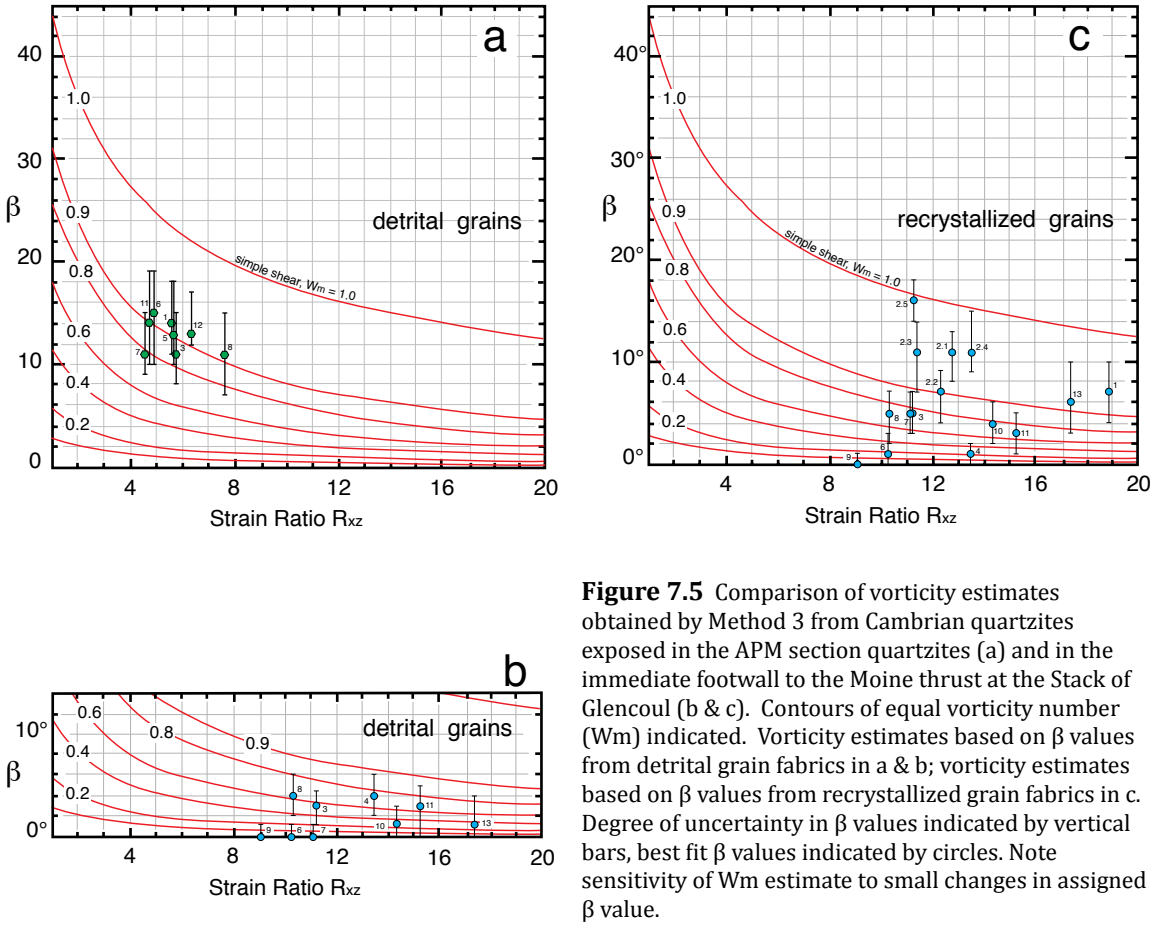

Figure 7.5 Comparison of vorticity estimates obtained by Method 3 from Cambrian quartzites exposed in the APM section quartzites (a) and in the immediate footwall to the Moine thrust at the Stack of Glencoul (b & c). Contours of equal vorticity number (Wm) indicated. Vorticity estimates based on β values from detrital grain fabrics in a & b; vorticity estimates based on β values from recrystallized grain fabrics in c. Degree of uncertainty in β values indicated by vertical bars, best fit β values indicated by circles. Note sensitivity of Wm estimate to small changes in assigned β value.

with highest flow vorticities (sample SG.1 and SG.2.1-5; Wm range of 0.89-0.99) at less than 30 cm beneath the Moine thrust plane. Measurement of recrystallized grain fabrics for the APM quartzites is currently underway, and Method 3 estimates of flow vorticities can then be directly compared with data based on recrystallized grain fabrics from the Stack mylonites.

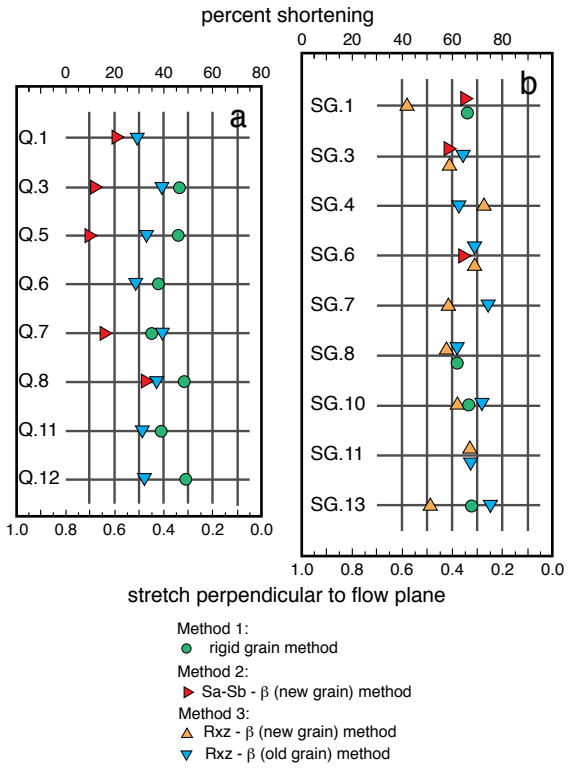

Figure 7.6 Comparison of shortening values perpendicular to flow plane for Cambrian quartzites from the APM stream section (a), and in the immediate footwall to the Moine thrust at the Stack of Glencoul (b). Samples are arranged in order of structural position. Shortening estimates take in to account flow vorticity and Rxz strain ratio for each sample; but assume zero volume loss. Results are coded for input data using different methods of vorticity analysis. A median shortening of 20-45% is estimated for the APM stream section, compared with a shortening of 50-75% at the Stack of Glencoul.

Strain and vorticity data from the APM and Stack of Glencoul sections may be combined to estimate shortening perpendicular to the imposed flow plane, and resultant stretching within the flow plane parallel to the transport direction, using numerical relationships proposed by Wallis et al. (1993). For strict simple shear there will be no shortening perpendicular to the flow plane, regardless of finite strain values; see discussion in Chapter 5. Shortening values for the Cambrian quartzites of the APM and Stack of Glencoul sections are summarized graphically in Fig. 7.6 and coded for the different methods of vorticity analysis used in the calculations. Shortening estimates for the APM quartzites range from c. 20-45% shortening, compared to c. 50-75% shortening for the Stack quartzites (cf. Figs. 7.6a & b). For a given R_{xz} strain value, the greater the component of pure shear the greater the estimated shortening. The influence of the three methods of vorticity analysis on shortening estimates is particularly clear in the results from the APM quartzites (Fig. 7.6a) where, for any given sample, the greatest shortening values are always associated with Method 1

vorticity analysis data, while minimum shortening values are always associated with Method 3 data. These inter-relationships are far less clear in the Stack of Glencoul shortening estimates (Fig. 7.6b) due to greater overlapping between flow vorticities estimated by the three analytical methods.

Estimates of stretching parallel to the transport direction within the flow plane that is driven by this sub-vertical shortening are summarized in Fig. 7.7. These estimates take in to account calculated stretches parallel to the intermediate principal strain axis (Y), but assume a constant volume deformation. The estimates for transport parallel stretching are far more scattered than estimates for shortening perpendicular to the flow plane, and this is particularly true for the Stack of Glencoul data (cf. Figs 7.7a & b). This greater scattering of the estimated stretches parallel to transport is because small changes in the amount of shortening lead to significantly greater changes in the resultant amount of transport parallel

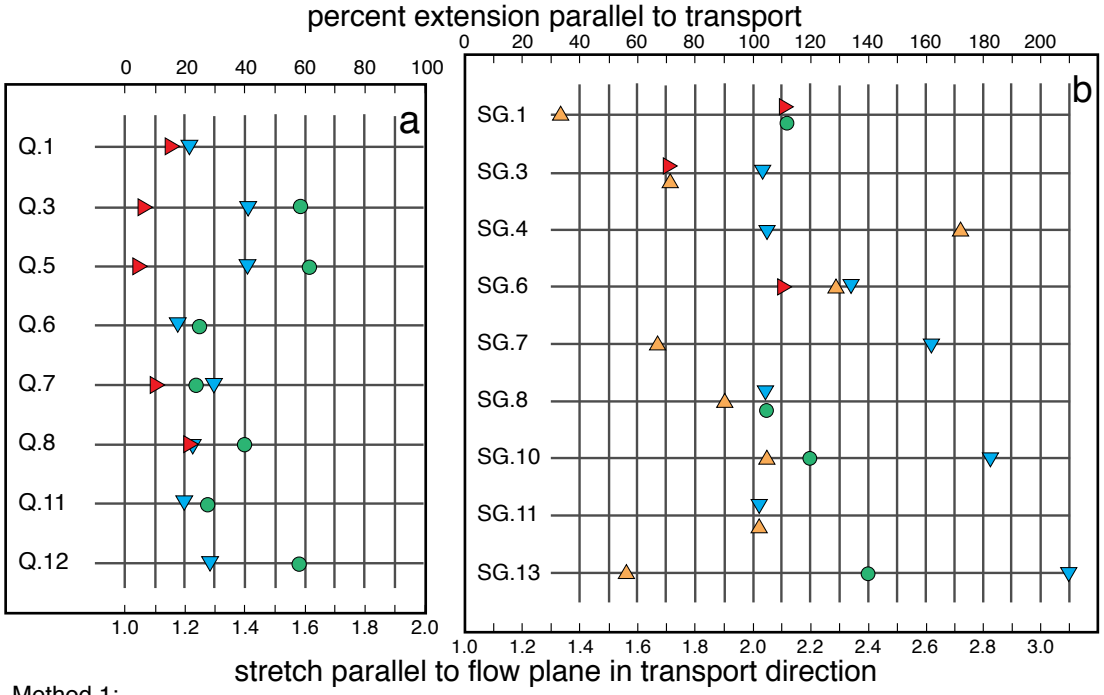

Figure 7.7 Comparison of transport parallel extension values estimated for Cambrian quartzites from the APM stream section (a), and in the immediate footwall to the Moine thrust at the Stack of Glencoul (b). Estimates take in to account shortening perpendicular to flow plane (Fig. 7.6) and stretching parallel to Y; but assume zero volume loss. The results are coded by vorticity method. A median transport-parallel extension of 20-50% is estimated for the APM stream section, compared with an extension of 100-130% at the Stack of Glencoul.

stretching (Fig. 7.8). Also to be taken in to account is variability in the amount of stretching parallel to Y as stretching parallel to Y will reduce the total amount of transport parallel stretching. Stretches parallel to Y for the APM quartzites range from 11-60% (Table 4.1), although the majority of samples fall in the more restricted range of 11-25%. In contrast, stretches parallel to Y for the Stack quartzites range from 29-49%. Due to the combination of greater shortening magnitudes and greater variability in stretching parallel to Y in the Stack quartzites, compared to the APM quartzites, this leads directly to a greater variability in transport parallel stretch estimates for the Stack quartzites (Fig. 7.8).

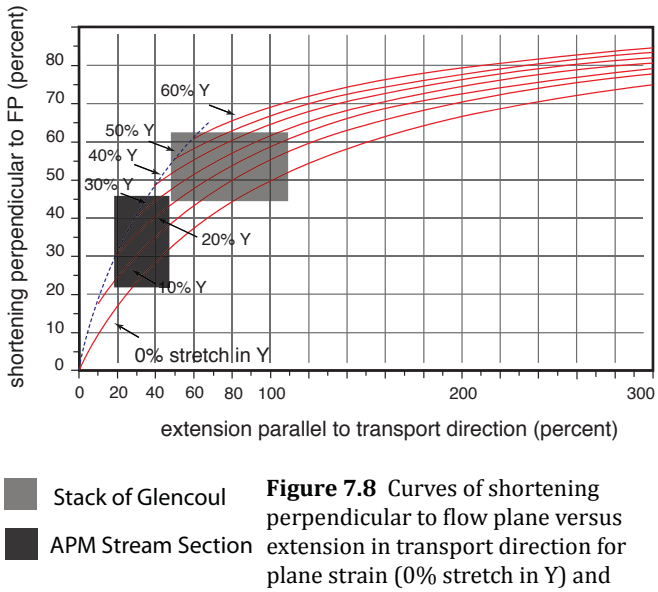

Figure 7.8 Curves of shortening perpendicular to flow plane versus extension in transport direction for plane strain (0% stretch in Y) and corresponding curves for general flattening with 10-60% stretch in Y (after Law 2010). At high shortening strain magnitudes, a small increase in shortening produces a large increase in estimated transport parallel extension, explaining why transport-parallel stretch estimates are more scattered than shortening estimates (cf. Figs 7.6 and 7.7). The boxes indicate the general areas on the figure where the data for the APM stream section and Stack of Glencoul plot, explaining the larger range in transport parallel extension seen at the Stack of Glencoul.

Although the data are scattered, transport parallel stretches for the APM quartzites cluster in the 20-50% range, while stretch estimates for the Stack of Glencoul quartzites cluster in the 100-130% range (Fig. 7.7). These data indicate that sub-vertical shortening, and resultant transport parallel stretching/extension, associated with penetrative deformation is of significantly lower magnitude in the APM quartzites (Aisinnin imbricates) than in the mylonites associated with the Moine thrust at the Stack of Glencoul. This in turn may indicate that mylonites in the immediate hangingwall and footwall to the Moine thrust may have developed under a greater lithostatic load than the quartzites of the Aisinnin imbricates which, assuming a foreland propagating sequence, may have developed slightly later and further towards the foreland.

Quartz piezometry

Estimates of flow stresses for the Stack of Glencoul mylonites based on dynamically recrystallized grain size (as well as dislocation density and subgrain size measured by transmission electron microscopy) have previously been published by Weathers et al. (1979) and Ord & Christie (1984). In estimating flow stresses from recrystallized grain size, the piezometers of Twiss (1977) and Mercier et al. (1977) were used in both studies. However, no information was given in either of these publications on if a correction was made for the cut-effect (see Chapter 6 for details) in using grain sizes measured in petrographic thin section to estimate flow stress. Therefore, in order to compare flow stresses in the APM and Stack of Glencoul quartzites, recrystallized grain sizes were measured in the suite of mylonites described by Law et al. (1986, 2010) from the Stack of Glencoul using the same analytical procedures followed for the APM quartzites (Chapter 6).

At the Stack of Glencoul the position of the Moine thrust plane is taken to be at the well-exposed foliation-parallel contact between mylonitic Moine pelites/psammites and underlying, similarly intensely deformed, Cambrian quartzites (see discussion in Law et al. 1986, 2010; and photographs in Law 1998). Positioning of the Moine thrust plane *sensu-stricto* is less certain above the Cambrian quartzites of the Aisinnin imbricates exposed in the APM stream section (see Chapter 2, Figure 2.4). During the original late 19th century mapping by the Geological Survey the base of the overlying sheet of mylonite (of probable Moine protolith) was taken to represent the Moine thrust plane. In contrast on the revised Assynt Special Sheet (BGS 2007) Cambrian quartzites are regarded as forming the protolith for these mylonites, necessitating moving the Moine thrust plane *sensu-stricto* to the upper surface of the mylonite sheet. For our present purposes we have used the lower surface of the mylonite sheet as marking the Moine thrust plane because, due to lack of exposure, we have been unable to confirm that these mylonites are derived from Cambrian quartzite. However, the critical point remains that mylonitic Cambrian quartzites exposed in the APM section, which structurally belong to the Aisinnin imbricates, represent a structurally lower, probably slightly younger suite of mylonites that developed further towards the foreland than the

Sample	Distance (m)	n	% Std Error	D_a (μm)	D_g (μm)	St. Dev. $s(d_a)$ (μm)	Rel. Error $s(d_a)/(d_a)$	Corrected grain size D_a (μm)	Corrected grain size D_g (μm)	Twiss D_a (MPa)	Twiss D_g (MPa)	Stipp D_a (MPa)	Stipp D_g (MPa)
SG-M.4	(+) 7.5	1233	1.99	19.92	19.69	3.12	.16	34.86	34.46	60.30	60.79	62.25	62.84
SG-1	(-) 0.001	840	2.42	22.01	21.72	3.67	.17	38.52	38.00	56.35	56.87	57.52	58.14
SG-2.1	(-) 0.05	1039	2.17	21.03	20.62	4.17	.20	36.81	36.09	58.12	58.90	59.63	60.57
SG-4	(-) 0.07	879	2.36	21.18	20.81	4.18	.20	37.06	36.42	57.85	58.53	59.31	60.13
SG-6	(-) 1.9	606	2.84	20.39	20.09	3.73	.18	35.69	35.15	59.35	59.97	61.11	61.85
SG-9	(-) 3.5	786	2.50	19.49	19.29	2.87	.15	34.11	33.75	61.21	61.65	63.35	63.88
SG-11	(-) 4.6	745	2.56	20.52	20.09	4.25	.21	35.90	35.16	59.11	59.96	60.82	61.84

Table 7.1 Table 7.1 Recrystallized grain size and resultant piezometry data for Moine psammite (SG-M.4) and mylonite Cambrian quartzites at the Stack of Glencoul. Distance of individual samples above (+)/below (-) the Moine thrust plane are indicated.

mylonites derived from Cambrian quartzite that are exposed at the Stack of Glencoul.

Recrystallized grain sizes and associated paleostress estimates, based on the Twiss (1977) and Stipp & Tullis (2003) piezometers, for the Stack mylonites are summarized in Table 7.1. Grain size for the Stack mylonites ranged from 19-22 μm, compared to 20-27 μm for the APM stream section. Average grain size for the Stack mylonites is estimated at 20μm, compared with 24μm for the APM stream section quartzites. Somewhat surprisingly, grain size in the mylonitic quartzites in the footwall to the Moine thrust plane (*sensu-stricto*) at the Stack was found to statistically decrease (and therefore estimated flow stresses should increase) with increasing structural distance beneath the thrust plane (Fig. 7.9), at least over the 4.5 m of footwall mylonites represented by samples SG.1 to SG.11 (Law et al. 1986, 2010). Grain size also decreases with increasing structural depth in the APM stream section quartzites (Fig. 7.9).

Application of the Twiss (1977) and Stipp & Tullis (2003) piezometers to the Stack mylonites indicates flow stresses of 56-63MPa. In applying these piezometers raw (uncorrected) 2D grain size data, and data corrected for the *'cut effect'* using the 1.75 correction factor recommended by Pickering (1976), were used in the Stipp & Tullis (2003) and Twiss (1977) piezometers, respectively. Both Weathers et al. (1979) and Ord & Christie (1984) have previously reported recrystallized grain sizes of 10-20 μm in mylonitic Cambrian quartzites collected at less than 10 m beneath the Moine thrust plane at the Stack of Glencoul. Weathers et al. (1979) calculated an average differental flow stress of 56 Mpa for the Stack mylonites. Christie & Ord (1984, their table 3) for their sample #3 from the Stack mylonites

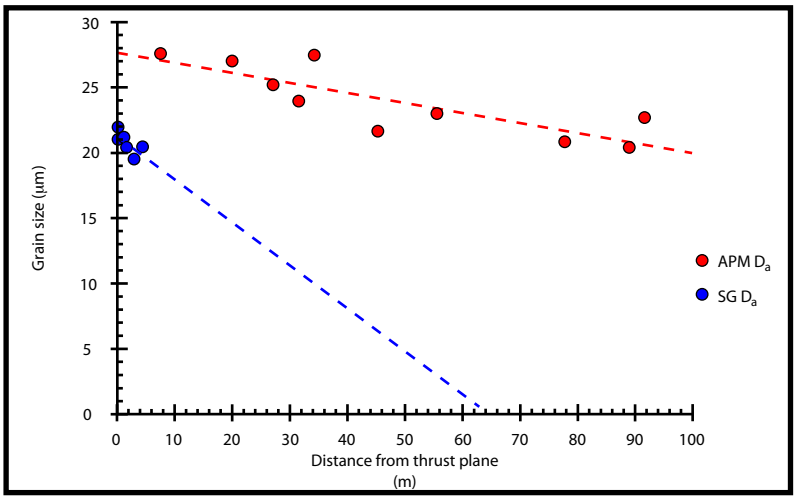

Figure 7.9 Variation in recrystallized grain size in Cambrian quartzites from the APM stream section and from the Stack of Glencoul. Grain size for the Stack quartzites (blue circles) are plotted against distance beneath the Moine thrust. Grain size for APM samples (red circles) are plotted against distance beneath the base of the overlying 40 m thick mylonite sheet (Fig. 2.4). This surface would mark the Moine thrust plane if the unexposed mylonites were derived from Moine rocks as depicted on the original Geological Survey maps (e.g. Geological Survey 1923), but an un-named thrust (possibly equivalent to the Lochan Riabach thrust at Loch Eriboll, see discussion in Thigpen et al. 2010) if the mylonites were derived from Cambrian quartzite as depicted on the revised Assynt Special Sheet (BGS 2007). In the second case, the upper surface of the mylonite sheet would mark the position of the Moine thrust. Arithmetic mean grain sizes (not corrected for cut-effect) are shown. Grain size for the Stack quartzites ranges from 19-22µm compared to 20-27µm for the APM quartzites.

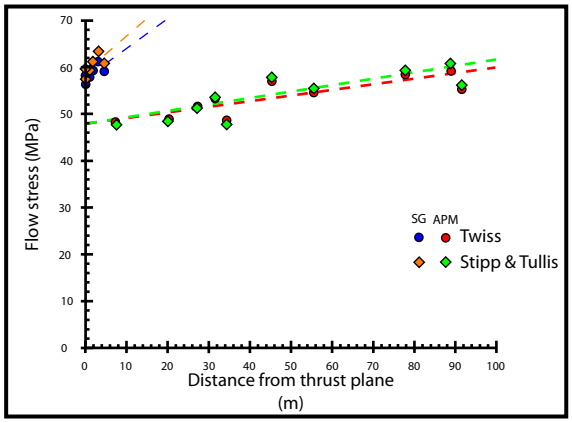

Figure 7.10 Variation in estimated flow stresses with distance beneath overlying thrust plane(s) in Cambrian quartzites from the APM stream section (red circles and green diamonds) and from the Stack of Glencoul (blue circles and orange diamonds). See Fig. 7.9 for explanation of structural reference frames used on horizontal axis for APM and Stack samples. Flow stress estimates based on quartz recrystallized grain size; raw 2D grain size data were used in the Stipp & Tullis (2003) piezometer; 2D data corrected for the cut-effect were used in the Twiss (1977) piezometer, see Chapter 6 for details. Linear regression lines of flow stress (based on Stipp & Tullis and Twiss piezometers) versus structural distance are shown. Note higher flow stresses in mylonitic Cambrian quartzites at Stack of Glencoul that are located in immediate footwall to Moine thrust.

estimated flow stresses of 52 and 90 Mpa using the piezometers of Mercier et al. (1977) and Twiss (1977) respectively, for a recrystallized grain size of 16.5 microns. In comparing these results with our data, it seems likely that a correction was not made for the *'cut effect'* in at least the grain size data used by Ord & Christie (1984).

Our calculated flow stresses for Stack mylonites are plotted against structural distance beneath the Moine thrust plane in Fig. 7.10 and confirm a small apparent increase in flow stress traced

structurally downwards from the thrust plane. However, it must be emphasized that at present we only have statistically robust grain size, and hence flow stress, data for a distance of 4.5 m beneath the thrust. Flow stress also increases with increasing structural depth in the APM stream section quartzites (Fig. 7.9) reaching a maximum value (63 MPa) close to the sheared contact between the Basal Quartzite and underlying Lewisian gneiss.

Strain rate comparison

Strain rate calculations are dependent on both estimated flow stress magnitude and deformation temperature, as well as other experimentally calibrated intrinsic and extrinsic variables that factor in to the relevant flow law (see discussion in Chapter 6). As discussed above, estimated flow stresses for the Stack of Glencoul mylonites are slightly higher than for the APM stream section quartzites. However, deformation temperatures calculated from the opening angles of quartz c-axis fabrics measured on plastically deformed detrital grains in the Stack mylonites (Law et al. 2010, their Fig. 16e, p. 569) are slightly lower than in the APM section quartzites (for details see Chapter 4). For the Stack samples in which flow stresses could be calculated, quartz c-axis fabric opening angles (measured on detrital grains) indicate an average deformation temperature of 416°C, compared with an average deformation temperature of 440°C for the APM section quartzites. Strain rates calculated for the APM quartzites ranged from 1.39×10^{-12} sec^{-1} to 2.29×10^{-12} sec^{-1} (Table 6.2) using the experimentally derived flow parameters of Koch et al. (1980), while strain rates estimated for the Stack

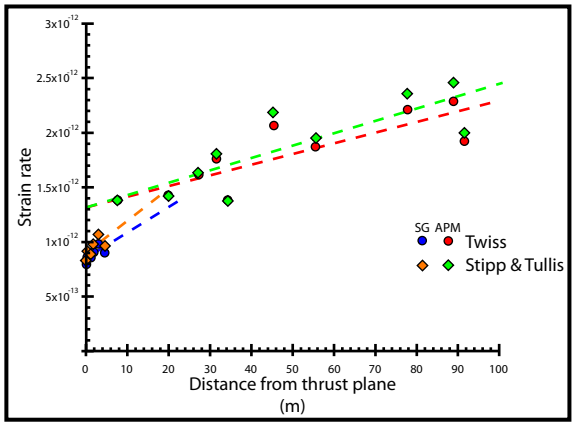

Figure 7.11 Variation in estimated strain rate with distance beneath overlying thrust plane(s) in Cambrian quartzites from the APM stream section (red circles and green diamonds) and from the Stack of Glencoul (blue circles and orange diamonds). See Fig. 7.9 for explanation of structural reference frames used on horizontal axis for APM and Stack samples. Faster strain rates occur on the vertical axis with increasing distance from origin of graph. Strain rate estimates for individual samples are coded for piezometer used. Note: constant deformation temperatures of 440 and 416 °C were used in estimating strain rates for the APM and Stack samples, respectively. Flow parameters of Koch et al. (1980) were used for both localities.

mylonites using the same flow parameters range from $8.07x10^{-13}$ – $1.07x10^{-12}$ (Fig. 7.11). These slower estimated strain rates for the Stack mylonites illustrate the influence of very small changes in deformation temperature. However, as discussed in Chapter 6, estimated strain rates are even more sensitive to variation in the different experimentally calibrated flow parameters available.

Along strike variability in flow parameters near base of Moine nappe

The above comparison of flow parameters between the APM stream section and the Stack of Glencoul have highlighted important differences between the two transects, in terms of finite strain, flow vorticity and flow stresses. However, it must be kept in mind that these two traverses do not occupy exactly equivalent along strike structural positions because the mylonitic Cambrian quartzites exposed in the APM section, which structurally belong to the Aisinnin imbricates, represent a structurally lower, probably slightly younger suite of mylonites. In order to more meaningfully compare along strike variation in flow properties, at a closely similar structural level, a suite of penetratively deformed Moine psammites collected by Thigpen (2009) near the base of the Moine nappe (i.e. in the hanging wall to the Moine thrust) between Beinn Lice - 3 km to the NE of the APM stream section - and

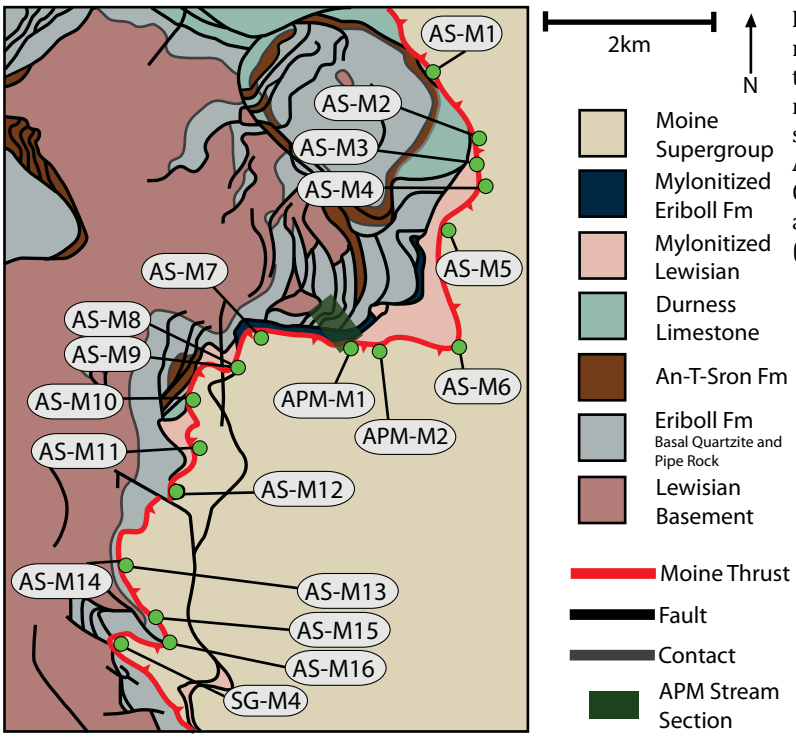

Figure 7.12 Simplified geologic map showing the locations of the Along-Strike (AS) samples relative to the APM stream section shown in green (samples APM-M1&M2) and the Stack of Glencoul (sample SG-M4); adapted from Thigpen et al. (2010).

the Stack of the Glencoul to the south (Fig. 7.12) have been examined.

No strain markers are present in these pervasively deformed psammites, although they do contain feldspar clasts appropriate for Method 1 vorticity analyses and dynamically recrystallized quartz grains appropriate for piezometry. Method 1 vorticities analyses have previously been run on several of these samples by Thigpen et al. (2010b). Vorticity, recrystallized grain size, flow stress, and strain rate estimates for these samples are summarized in Table 7.2. Based on the opening angles of quartz c-axis fabrics measured on recrystallized grains in these samples, Thigpen et al. (2010) have estimated deformation temperatures of 520-585°C. For the purpose of calculating strain rates, a median temperature of 550°C and the experimentally derived parameters of Koch et al. (1980) were used.

Sample	Distance (km)	Wm	Twiss D_a (MPa)	Twiss D_g (MPa)	Stipp D_a (MPa)	Stipp D_g (MPa)	Twiss D_a $\dot{\varepsilon}$	Twiss D_g $\dot{\varepsilon}$	Stipp D_a $\dot{\varepsilon}$	Stipp D_a $\dot{\varepsilon}$
AS-M1	11.375	.60-.63	42.21	42.87	41.06	41.80	$8.28x10^{-12}$	$8.60x10^{-12}$	$7.74x10^{-12}$	$8.08x10^{-12}$
AS-M2	10.463	.64-.80	40.95	41.73	39.63	40.51	$7.69x10^{-12}$	$8.06x10^{-12}$	$7.10x10^{-12}$	$7.49x10^{-12}$
AS-M3	10.175	.60-.71	40.91	42.98	39.58	41.95	$7.67x10^{-12}$	$8.66x10^{-12}$	$7.08x10^{-12}$	$8.14x10^{-12}$
AS-M4	9.875	.69-.74	--	--	--	--	--	--	--	--
AS-M5	9.238	.74-.78	38.10	38.85	36.43	37.27	$6.45x10^{-12}$	$6.77x10^{-12}$	$5.78x10^{-12}$	$6.11x10^{-12}$
AS-M6	7.713	.77-.81	36.73	37.10	34.91	35.31	$5.90x10^{-12}$	$6.05x10^{-12}$	$5.21x10^{-12}$	$5.36x10^{-12}$
APM-M2	6.688	.83-.87	32.04	32.48	29.76	30.24	$4.23x10^{-12}$	$4.37x10^{-12}$	$3.53x10^{-12}$	$3.67x10^{-12}$
APM-M1	6.342	.85-.87	--	--	--	--	--	--	--	--
AS-M7	5.663	.78-.83	--	--	--	--	--	--	--	--
AS-M8	5.188	--	57.84	58.24	59.29	59.82	$1.79x10^{-11}$	$1.81x10^{-11}$	$1.90x10^{-11}$	$1.94x10^{-11}$
AS-M9	5.188	--	52.10	52.68	52.49	53.17	$1.38x10^{-11}$	$1.42x10^{-11}$	$1.41x10^{-11}$	$1.45x10^{-11}$
AS-M10	4.25	--	46.03	46.68	45.42	46.18	$1.02x10^{-11}$	$1.06x10^{-11}$	$9.91x10^{-12}$	$1.03x10^{-11}$
AS-M11	3.888	--	42.56	42.95	41.45	41.89	$8.45x10^{-12}$	$8.64x10^{-12}$	$7.92x10^{-12}$	$8.13x10^{-12}$
AS-M12	3.125	.53-.68	45.48	46.19	44.79	45.61	$9.94x10^{-12}$	$1.03x10^{-11}$	$9.57x10^{-12}$	$1.00x10^{-11}$
AS-M13	1.975	.56-.65	47.03	47.88	46.58	47.56	$1.08x10^{-11}$	$1.44x10^{-11}$	$1.05x10^{-11}$	$1.11x10^{-11}$
AS-M14	1.975	--	43.18	44.43	42.15	43.58	$8.75x10^{-12}$	$9.39x10^{-12}$	$8.26x10^{-12}$	$8.96x10^{-12}$
AS-M15	1.175	.54-.60	52.30	52.99	52.72	53.54	$1.40x10^{-11}$	$1.44x10^{-11}$	$1.42x10^{-11}$	$1.48x10^{-11}$
AS-M16	.75	.60-.67	51.82	52.46	52.16	52.91	$1.34x10^{-11}$	$1.41x10^{-11}$	$1.38x10^{-11}$	$1.44x10^{-11}$
SG-M4	0.0	.73-.77	60.30	60.77	43.04	43.39	$1.98x10^{-11}$	$2.02x10^{-11}$	$8.69x10^{-12}$	$8.86x10^{-12}$

Table 7.2 Vorticity, flow stress and strain rate data for samples of quartz-rich Moine psammite collected close to the base of the Moine nappe. See Fig. 7.12 for location map. Samples are arranged in order of increasing along strike distance to the north and east of the Stack of Glencoul (sample SG-M.4). Samples MT-02-05 (M.1) and MT-07-72 (M.2) are from above the APM stream section. See text for details of deformation temperatures and flow parameters used.

Results of the Method 1 rigid grain vorticity analysis are shown in Figure 7.13, with the samples arranged from north – south and scaled for distance along strike. The highest estimated vorticities are recorded in samples APM-M1 and APM-M2 collected directly above the APM stream section. Flow vorticities steadily decrease traced along strike to the east and north of the APM stream section

(samples AS-M6 to M1). Vorticity values also steadily decrease traced to the west and south of the APM section (samples AS-M7 to M15) and then increase within 0.5 km of the Stack of Glencoul.

Along strike variations in estimated flow stress and strain rates are shown in Figures 7.14 and 7.15, respectively. For the along strike traverse, a minimum flow stress magnitude is recorded in sample APM-M2 collected directly above the APM stream section (Fig. 7.14). Flow stresses steadily increase traced along strike to the east and north of the APM stream section (samples AS-M6 to M1). With the exception of one or two individual samples (AS-M8 & 9) flow stresses also steadily increase traced along strike to the west and south of the APM stream section towards the Stack of Glencoul. An identical trend is observed in along strike variation in estimated strain rate (Fig. 7.15), but this is simply a consequence of assuming a constant deformation temperature while allowing flow stress to vary. A meaningful correlation between along strike variation in flow stress and strain rate would require deformation temperatures to be calculated for each sample. Estimated strain rates (on the order of 10^{-11} sec^{-1}) are, geologically, unrealistically fast and indicate that either too high a deformation temperature has been assumed in these calculations, or that a suitable suite of experimentally derived flow parameters has not been used (see Table 6.3).

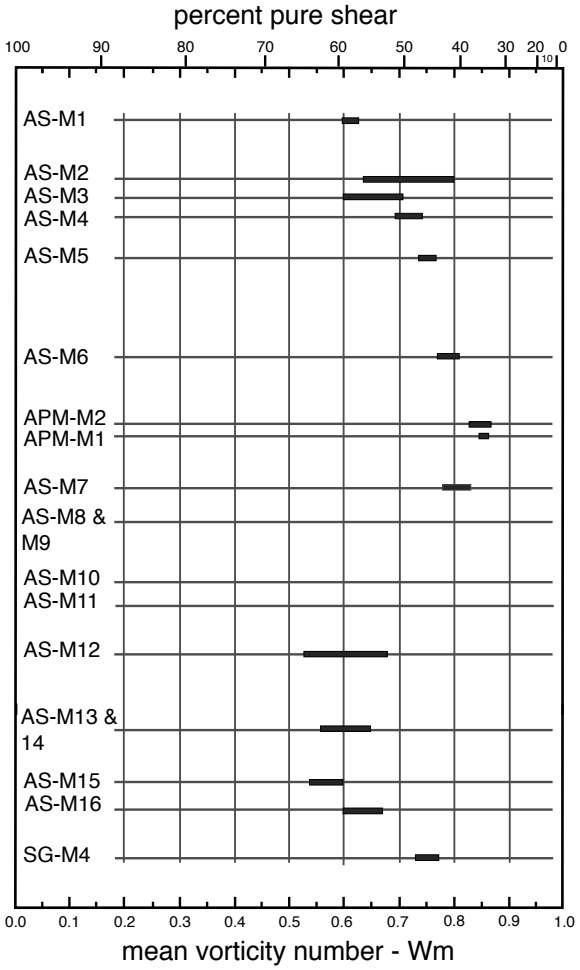

Figure 7.13 Results of Method 1 vorticity analyses for Moine psammites near the base of the Moine nappe containing rigid feldspar and epidote clasts. Samples are arranged from north (top) to south (bottom) and positioning of samples on vertical axis of diagram is scaled to reflect along strike distance to the north of the Stack of Glencoul (sample SG-M.4). Samples M8 to M11 did not contain suitable rigid grain clasts for Method 1 vorticity analysis.

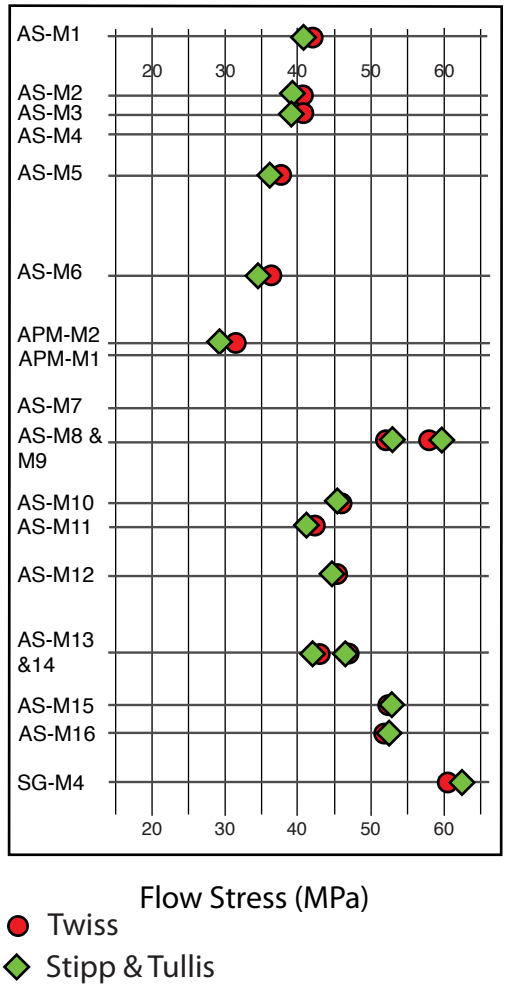

Figure 7.14 Estimated flow stresses for Moine psammites near the base of the Moine nappe. Samples are arranged from north (top) to south (bottom) and positioning of samples on vertical axis of diagram is scaled to reflect along strike distance to the north of the Stack of Glencoul (sample SG-M.4).

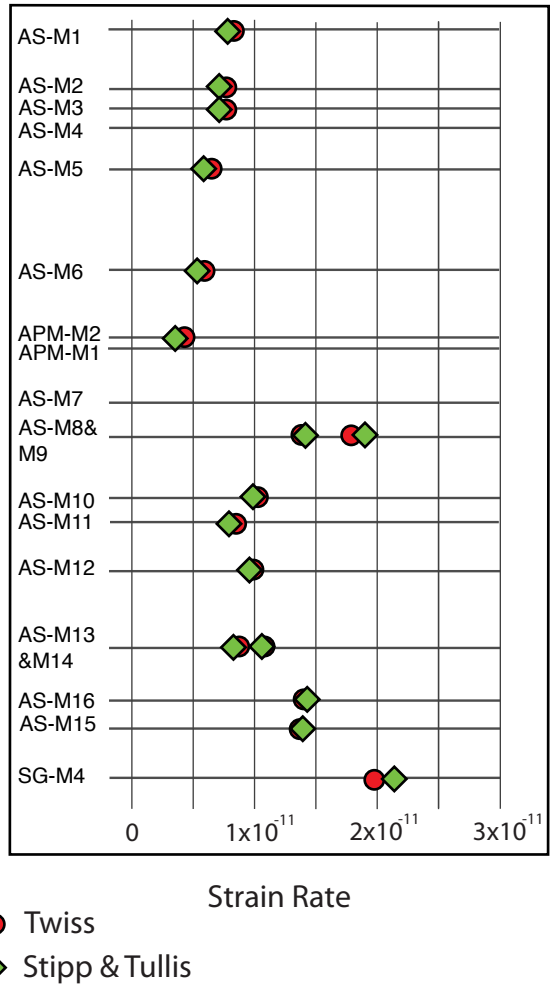

Figure 7.15 Estimated strain rates for Moine psammites near the base of the Moine nappe assuming a deformation temperature of 550 C and using the flow parameters of Koch et al. (1980). Faster and slower strain rates plot to the right and left hand sides, respectively on the horizontal axis. Samples are arranged from north (top) to south (bottom) and positioning of samples on vertical axis of diagram is scaled to reflect along strike distance to the north of the Stack of Glencoul (sample SG-M.4). Direct correlation with along strike variation in flow stress (Fig. 7.14) is simply the result of using a constant deformation temperature in strain rate calculations for all samples.

At least traced towards the east and north of the APM stream section there does seem to be a meaningful inverse correlation between along strike variation in flow stress and vorticity (Wm), with flow stress increasing as vorticity decreases (cf. Figs . 7.13 and 7.14). In contrast, to the south of the APM section (samples AS-M12 to SG-M.4) there seems to be a direct correlation between flow stress and vorticity,

with both flow parameters increasing in magnitude traced southwards to the Stack of Glencoul. Plotting of vorticty (Wm) against flow stress (Fig. 7.16) suggests a previously unobserved apparent correlation between Wm and flow stress, with minimum Wm values (c. 0.55-0.60) at flow stresses of c. 45-50 MPa, and higher Wm values at <45 MPa and >50 MPa. Samples with flow stresses > 50 MPa are all from locations within 1-2 km of the Stack of Glencoul at the southern end of the along-strike traverse. The significance of this correlation, if real, is unknown.

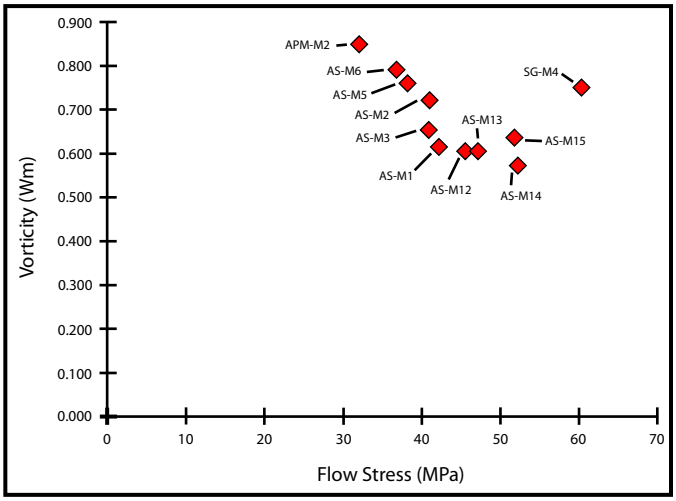

Figure 7.16 Plot of vorticity number (Wm) versus flow stress for quartz-rich Moine psammites collected near the base of the Moine nappe. Locations for individual samples are indicated in Fig. 7.12. Samples collected to the north of the APM stream section display a negative approximately linear correlation between Wm and flow stress (left hand side of data plot). Samples collected south of the APM section closer to the Stack of Glencoul (sample SG-M.4) display a scattered but positive correlation between WM and flow stress (right hand side of data plot.

Tectonic implications

APM Stream Section

Traced structurally down section in the Cambrian quartzites (Q1-12) towards the sheared contact with underlying Lewisian gneiss: 1) Wm values indicated by Method 1 analyses steadily increase (Fig. 5.5); 2) dynamically recrystallized grain sizes progressively decrease (Fig. 6.3); 3) associated flow stress estimates progressively increase (Fig. 6.5); and 4) estimated strain rates, although scattered, broadly increase (Fig. 6.6). These trends suggest that penetrative deformation in the APM section is more directly related to shearing along the base of the section than shearing along the top of the section where the quartzites are overlain by a 40m thick sheet of mylonite derived either from the Moine (Geological Survey 1923) or Cambrian quartzite (BGS 2007). This in turn would suggest that penetrative deformation fabrics in the APM quartzites, which structurally belong to the Aisinnin

imbricates located at the top of the Glencoul thrust sheet, largely accumulated as shearing stepped downwards and forwards (foreland propagating) from the Moine nappe and its basal sheet(s) of mylonite into the top of the underlying Glencoul thrust sheet.

Butler (1984, p. 172) has argued that these intense bedding-parallel fabrics, that are spatially associated with the Aisinnin imbricates, pre-date motion on the imbricate faults as the fabrics are folded around ramps on the imbricate thrusts. Nonetheless, the Aisinnin imbricates appear to roof in to the overlying Moine thrust (Butler 1988, p. 186-187) and its associated sheet(s) of mylonite, suggesting that penetrative deformation and imbrication at the top of the Glencoul thrust sheet (APM stream section quartzites) was at least broadly contemporaneous with shearing and mylonitization along the base of the overlying Moine nappe (Butler 1984, p. 178). This does not, of course, preclude the possibility that shearing and mylonitization along the base of the Moine nappe may have *begun* at an earlier stage of thrust belt evolution; i.e. before the Cambrian quartzites and Lewisian gneiss exposed in the APM stream section (Aisinnin imbricates / Glencoul thrust sheet) were accreted on to the base of the Moine nappe during foreland propagating thrusting. Butler (1984) has argued that all these penetrative fabrics underlying the Moine nappe are associated with gravity spreading and thrust transport-parallel stretching (extension/spreading) as the nappe climbed towards the WNW on to the Cambrian shelf sedimentary rocks. The relationship between the formation of the Aisinnan imbricates and the two fault systems that were active during accumulation of the penetrative deformation seen in the APM stream section quartzites is shown schematically in Figure 7.17.

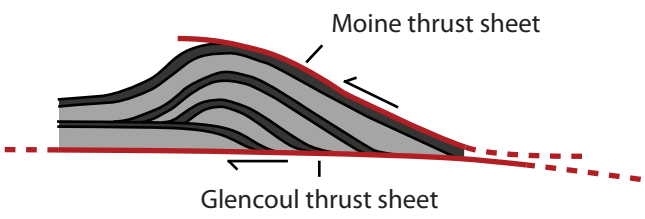

Figure 7.17 Schematic drawing illustrating simultaneous movement along the two fault systems; the Glencoul thrust at the base of and the Moine thrust at the top of the section.

Thrusting of relatively hot Moine nappe rocks (and associated sheets of basal mylonite) on to cooler sedimentary rocks (that will subsequently be incorporated in to the Asinnin imbricates of the

Glencoul thrust sheet) is supported by the observation that recrystallized grain size increases up section in the APM quartzites towards the overlying Moine nappe (Fig. 6.3). The recrystallized grain size data indicate that flow stresses should increase in magnitude structurally downwards towards the underlying sheared contact with the Lewisian gneiss (Fig. 6.4). In Chapter 6, it was proposed that shearing focused along the base of the quartzite section may have been responsible for the structural distribution of flow stresses inferred from recrystallized grain sizes. However, if the quartzites at the top of the section were at a higher temperature than those at the base of the section, then they would deform plastically at lower flow stresses. Unfortunately no convincing correlation between structural position and deformation temperatures that might be inferred from quartz c-axis fabric opening angles (Table 4.2) measured in plastically deformed detrital grains has been found to support this interpretation.

Broadly contemporaneous motion on the fault systems at the top and at the base of the APM quartzite section is compatible with the observation that not all flow attributes can be directly correlated with structural position. For example, although recrystallized grain size (Fig. 6.3), flow stresses (Fig. 6.5) and strain rates (Fig. 6.6) seem to correlate with structural position (see above), no convincing correlation has been found between structural position and: 1) finite strain magnitude or 3D strain type (general flattening, plane strain, Table 4.1), 2) sub-vertical shortening perpendicular to the flow plane (Fig. 5.16) or quartz c-axis fabric opening angle (Table 4.2). Additionally, although Method 1 vorticity analyses indicated a progressive increase in Wm traced down section towards the sheared contact between the quartzites and the underlying Lewisian gneiss (Fig. 5.5), Method 2 analyses yield the highest Wm values in the middle and upper parts of the quartzite section (Fig. 5.10). In contrast, Method 3 analyses indicate only minor variations in Wm value with structural position (Fig. 5.13). As Methods 2 and 3 are partially based on crystal fabric data, Wm values calculated from these methods (and particularly Method 2) are likely to be sensitive to the closing increments of penetrative crystal plastic deformation and dynamic recrystallization. Here we note that the highest Wm values for Method 2 (sub-simple shear) are recorded (cf. Figs

2.4 and 5.10) very close to where an imbricate thrust has been mapped through the APM stream section placing Basal Quartzite on top of Pipe Rock (BGS 2007).

Our strain analyses indicate that the APM quartzites have been deformed within the general flattening field (Figs. 4.3 and 7.2), although under closer to plane strain conditions than the mylonitic Cambrian quartzites at the Stack of Glencoul (Figs. 7.2 and 7.3). General flattening strains in Cambrian quartzites from the Aisinnin imbricates (adjacent to the APM stream section) have previously been reported by Strine & Wojtal (2004) who argued that such non-plane strain should not be expected in thrust zones. To explain these apparently anomalous flattening strains, Strine & Wojtal (2004, p. 1768-1769) proposed a model in which imbrication in the footwall to a thrust leads to local steepening of the thrust surface and non-plane strain deformation as the over-ridding thrust sheet is forced to flow around and over this obstacle (see also Strine & Mitra 2004; Mookerjee & Mitra 2008, 2009). Strine & Wojtal (2004) cautioned that application of this model to the Cambrian quartzites they had studied around Loch Strath nan Aisinnin requires that movement on the Moine thrust continued during development of the footwall imbricate stack.

Although conceptually appealing, there are problems associated with applying this model to the northern Assynt part of the Moine thrust zone. 1) The Cambrian quartzites (including the APM stream section) surrounding Loch Strath nan Aisinnin structurally belong to the Aisinnin imbricates, not the overlying sheet(s) of mylonites located at the base of the Moine nappe. They are therefore not the lateral equivalents of the mylonitic Cambrian quartzites exposed at the Stack of Glencoul. 2) Although motion on the Aisinnin imbricates and the overlying Moine thrust may be broadly contemporaneous (see above discussion) penetrative deformation fabrics in the Cambrian quartzites of the Aisinnin imbricates appear to be older than the imbricate faults because they are folded around ramps in the imbricate system (Butler 1984).

Along Strike Analysis

Strine & Mitra (2004) have argued that Cambrian quartzites in the Aisinnin area have different strain characteristics (lower strain magnitudes, greater flattening strains) compared with their lateral equivalents along strike to the south and west, i.e. traced towards the Stack of Glencoul. They correlate this apparent domainal variation in strain with an apparent salient-recess map pattern marked by the overlying Moine thrust plane, although this map pattern could also be largely due to intersection between topography and the gently dipping Moine thrust. However, a structural origin for the salient-recess map pattern is supported by structure contours on the Moine thrust (Elliot & Johnson 1980, p. 71; R.D. Law, unpublished data) where the recess (Aisinnin area) and salient (Stack of Glencoul area to the southwest) coincide with a late stage ESE-plunging fold crest and trough, respectively. Strine & Mitra (2004) argued that different kinematic histories associated with formation of the salient and recess may be responsible for the contrast in strains. However, the recess map pattern of the Moine thrust traced around the Aisinnin area (Fig. 2.1) is at least spatially associated with the underlying Bhurich Dome, and this is demonstrably younger than the Aisinnin imbricates, and probably developed by relatively late-stage imbrication in the footwall to the Glencoul thrust (Butler 1984, p. 176). Thus the salient-recess map pattern, even if not a dominantly topographically controlled feature, must be related to relatively late stage imbrication, rather than an early stage of imbrication that might, as proposed by Strine & Mitra (2004), have influenced contemporaneous ductile flow in over-ridding thrust sheets.

We do agree, however, that there are important along-strike differences in the structural evolution of the Aisinnin and Stack of Glencoul areas. A relatively thin (c. 40m) sheet of mylonite (locally of either Moine or Cambrian quartzite protolith) is located directly beneath the Moine nappe in both areas. In the APM stream section of the Aisinnin area this mylonite sheet is underlain by c. 95 m of highly strained Cambrian quartzites characterized by subgrain rotation recrystallization indicating deformation temperatures of c. 400-500 °C (Stipp et al. 2002). In contrast, at the Stack of Glencoul the lateral equivalent of this mylonite sheet is

underlain by very low strain Cambrian quartzites (Law et al. 1986, their figs. 4a & b) characterized by limited grain boundary bulging recrystallization indicating deformation temperatures of c. 290-400 °C; see also discussion by Thigpen et al. (2010).

The Aisinnin quartzites were presumably penetratively deformed and vertically shortened at a greater structural depth and in a more hinterland position than the low strain quartzites now exposed beneath the Stack of Glencoul. This is compatible with the restored state section of Butler (1984, his fig. 11c) where the Aisinnin Cambrian quartzites are located at the trailing (hinterland) end of his Aisinnin thrust sheet, while the low strain quartzites exposed beneath the Stack of Glencoul mylonites could be located some 5-10 km further to the foreland in what would later become the Glencoul thrust sheet. This deeper and hotter Aisinnin thrust sheet presumably extends laterally to the south for some distance beneath the Moine nappe. However, it does not re-appear beneath the Moine thrust in eastern Assynt (to the southeast of the Stack of Glencoul) suggesting that it may be terminated against some form of lateral ramp in the subsurface.

References Cited:

BRITISH GEOLOGICAL SURVEY 2007. Assynt, Scotland Special Sheet, Bedrock, 1:50 000 Geology Series: Keyworth, Nottingham, British Geological Survey.

BUTLER, R.W.H. 1984. Structure evolution of the Moine thrust belt between Loch More and Glendhu, Sutherland. *Scottish Journal of Geology*, **20**, 161-179.

BUTLER, R.W.H. 1988. Excursion 9: The thrust belt in northern Assynt. In: Allison, I., May, F., & Strachan, R.A. (*eds*) *An Excursion Guide to the Moine Geology of the Scottish Highlands*. Scottish Academic Press on belhalf of Edinburgh Geological Society and the Geological Society of Glasgow, Edinburgh, pp. 176-188.

CALLAWAY, C. 1884. Notes on progressive metamorphism. *Geological Magazine*, **1**, 218-224.

CHEW, D.M. 2003. An Excel spreadsheet for finite strain analysis using the R_f/phi technique. *Computers & Geosciences*, **29**, 795-799.

CHRISTIE, J.M. 1963. The Moine thrust zone in the Assynt region, northwest Scotland. *University of California Publications in Geological Sciences,* **40**, 345-440.

ELLIOTT, D. & JOHNSON, M.R.W. 1980. The structural evolution of the northern part of the Moine thrust zone: *Transactions of the Royal Society of Edinburgh: Earth Sciences,* **71**, 69-96.

GEOLOGICAL SURVEY OF GREAT BRITAIN (SCOTLAND), 1923. Geological Map of the Assynt District at 1:63,360. Geological Survey of Great Britain, Scotland.

HALFPENNY, A., PRIOR, D.J., & WHEELER, J. 2006. Analysis of dynamic recrystallization and nucleation in a quartzite mylonite. *Tectonophysics*, **427**, 3-14.

KOCH, P.S., CHRISTIE, J.M. & GEORGE, R.P. 1980. Flow laws of "wet" quartzite in the alpha-quartz field. *American Geophysical Union, EOS Transactions,* **61**, p. 376.

LAW, R.D. 1987. Heterogenous deformation and quartz crystallographic fabric transitions: natural examples from the Moine thrust zone at the Stack of Glencoul, northern Assynt. *Journal of Structural Geology,* **9**, 819-833.

LAW, R.D. 1998. Quartz mylonites from the Moine thrust zone at the Stack of Glencoul, Northwest Scotland. *In*: Snoke, A.W., Tullis, J. & Todd, V.R (eds) *Fault - Related Rocks: A Photographic Atlas.* Princeton University Press, Princeton, New Jersey, p. 490-493.

LAW, R.D., 2010. Moine thrust zone mylonites at the stack of Glencoul II: results of vorticity analyses and their tectonic significance. In: Law, R.D., Butler, R.W.H., Holdsworth, R., Krabbendam, M., Strachan, R. (Eds), Continental Tectonics and Mountain Building - The Legacy of Peach and Horne. Geological Society, London, Special Publications, **335**, 579 - 602.

LAW, R.D., CASEY, M., & KNIPE, R.J. 1986. Kinematic and tectonic significance of microstructures and crystallographic fabrics within quartz mylonites from the Assynt and Eriboll regions of the Moine thrust zone, NW Scotland. *Transactions of the Royal Society of Edinburgh: Earth Sciences*, **77**, 99-123.Lister 1977

LAW, R.D., SEARLE, M.P. & SIMPSON, R.L. 2004. Strain, deformation temperatures and vorticity of flow at the top of the Greater Himalayan Slab, Everest Massif, Tibet. *Journal of the Geological Society, London*, **161**, 305-320.

LAW, R.D., MAINPRICE, D.H., CASEY, M., LLOYD, G.E., KNIPE, R.J., COOK, B., & THIGPEN, J.R., 2010. Moine thrust zone mylonites at the stack of Glencoul I - microstructures, strain and influence of recrystallization on quartz crystal fabric development. *In:* Law, R.D., Butler, R.W.H., Holdsworth, R., Krabbendam, M., Strachan, R. (eds), *Continental Tectonics and Mountain Building – The Legacy of Peach and Horne*. Geological Society, London, Special Publications, **335**, 543-577.

LLOYD, G.E., LAW, R.D. & MAINPRICE, D.H. 2010. Predicting seismic properties from three-dimensional microstructures - a new look at an old quartzite. *In*: Law, R.D., Butler, R.W.H., Holdsworth, R., Krabbendam, M. & Strachan, R. (eds) *Continental Tectonics and Mountain Building - The Legacy of Peach and Horne*. Geological Society, London, Special Publications, **335**, 603-622.

MERCIER, J.C., ANDERSON, D.A., & CARTER, N.L. 1977. Stress in the lithosphere; inferences from steady state flow of rocks. *Pure and Applied Geophysics,* **115**, 199-226.

MOOKERJEE, M. & MITRA, G. 2008. Kinematics-Based Mathematical Model for Deforming Thrust Wedges. *Mathematical Geosciences*, **40**, 249-275.

MOOKERJEE, M. & MITRA, G. 2009. Understanding kinematic data from the Moine thrust zone in terms of a kinematics-based mathematical model of deforming thrust wedges. *Journal of Structural Geology*, **31**, 1556-1572.

ORD, A. & CHRISTIE, J.M. 1984. Flow stresses from microstructures in mylonitic quartzites of the Moine thrust zone, Assynt area, Scotland. *Journal of Structural Geology,* **6**, 639-654

PEACH, B.N., HORNE, J., GUNN, W., CLOUGH, C.T., HINXMAN, L.W. & CADELL, H.M. 1888. Report on recent work of the Geological Survey in the N.W. Highlands of Scotland, based on field notes and maps of Messers. B.N. Peach, J. Horne, W. Gunn, C.T. Clough, L. Hinxman, and H.M. Cadell. *Quarterly Journal of the Geological Society, London*, **64**, 378-441.

PEACH, B.N., HORNE, J., GUNN, W., CLOUGH, C.T., HINXMAN, L.W. & TEALL, J.J.H. 1907. *The Geological Structure of the North-West Highlands of Scotland.* Memoir of the Geological Survey of Great Britain.

READ, H.H. 1931. *The Geology of Central Sutherland Sutherland (Sheets 108 and 109).* British Geological Survey Memoir, 238pp.

STIPP, M., STUNITZ, H., HEILBRONNER, R. & SCHMID, S. 2002. Dynamic recrystallization of quartz: correlation between natural and experimental conditions. In: De Meer, S., Drury, M.R., De Bresser, J.H.P. & Pennock, G.M. (eds) *Deformation Mechanisms, Rheology and Tectonics: Current Status and Future Perspectives.* Geological Society, London, Special Publications, **200**,171-190.

STAHR, D.W., & LAW, R.D. Effect of finite strain on clast-based vorticity gauges. *Journal of Structural Geology*, in review.

STIPP, M. & TULLIS, J. 2003. The recrystallized grain size piezometer for quartz. *Geophysical Research Letters,* **30**, 5.

STRINE, M. & MITRA, G. 2004. Preliminary kinematic data from a salient-recess pair along the Moine thrust, northwest Scotland. In: Sussman, A.J. & Weil, A.B. (eds). *Orogenic Curvature: Integrating Paleomagnetic and Structural Analyses.* Geological Society of America, Special Paper, **383**, 87-107.

STRINE, M. & WOJTAL, S. 2004. Evidence for non-plane strain flattening along the Moine thrust, Loch Strath nan Aisinnin, Northwest Scotland. *Journal of Structural Geology*, **26**, 1755-1772.

THIGPEN, J.R., 2009. Regional Variation in Strain and Vorticity within Mylonites from the Moine Thrust Zone of NW Scotland. PhD thesis, Virginia Tech.

THIGPEN, J.R., LAW, R.D., LLOYD, G.E., & BROWN, S.J. 2010a. Deformation temperatures, vorticity of flow, and strain in the Moine thrust zone and Moine nappe: Reassessing the tectonic evolution of the Scandian foreland – hinterland transition zone. *Journal of Structural Geology*, **32**, 920-940.

TWISS, R.J. 1977. Theory and applicability of a recrystallized grain size paleopiezometer. *Pure and Applied Geophysics*, **115**, 227-244.

WALLIS, S.R., PLATT, J.P. & KNOTT, S.D. 1993. Recognition of syn-convergence extension in accretionary wedges with examples from the Calabrian Arc and the Eastern Alps. *American Journal of Science*, **293**, 463-495.

WEATHERS, M.S., BIRD, J.M., COOPER, R.F. & KOHLSTEDT, D.C. 1979. Differential stress determined from deformation induced microstructures of the Moine thrust zone. *Journal of Geophysical Research*, **84**, 7459-7509.